UNIVERSITÀ DEGLI STUDI DI TRIESTE

XXVII CICLO DEL DOTTORATO DI RICERCA IN

NANOTECNOLOGIE

NOVEL NANOSTRUCTURED BIOMATERIALS FOR BIOMEDICAL APPLICATIONS

Settore scientifico-disciplinare: SSD BIO/10

DOTTORANDO

LORENA TARUSHA

COORDINATORE

PROF. LUCIA PASQUATO

SUPERVISORE DI TESI

PROF. SERGIO PAOLETTI

TUTORE

DR. ANDREA TRAVAN

ANNO ACCADEMICO 2014 / 2015

UNIVERSITÀ DEGLI STUDI DI TRIESTE

XXVII CICLO DEL DOTTORATO DI RICERCA IN

NANOTECNOLOGIE

NOVEL NANOSTRUCTURED BIOMATERIALS FOR BIOMEDICAL APPLICATIONS

Settore scientifico-disciplinare: SSD BIO/10

DOTTORANDO
LORENA TARUSHA

COORDINATORE
PROF. LUCIA PASQUATO

SUPERVISORE DI TESI
PROF. SERGIO PAOLETTI

TUTORE
DR. ANDREA TRAVAN

ANNO ACCADEMICO 2014 / 2015

Acknowledgments

I would like to thank Prof. Sergio Paoletti, Dr. Eleonora Marsich, Dr. Massimiliano Borgogna, Dr. Ivan Donati, Dr. Andrea Travan and Dr. Gianluca Turco for their teaching and support during these years.

I thank my collegues Davide Porrelli, Pasquale Sacco, Francesca Scognamiglio, Dr. Michela Cok, Ilaria Geremia and all the students of the Biomat group for sharing with me this experience.

A special thanks to my family:
Marco, Samuele and Maria for teaching me the most important things in the everyday life and for making it more beautiful.
Maria Grazia and Mario for their discrete daily presence and support.

I thank Gloria and Irene for their friendship and their continuous presence.

Finally, I acknowledge all the people
I worked with and I encountered during these years.

Index:

Abstract

The wound healing process begins immediately after an injury has occurred and aims to restore the structure and function of the damaged tissue. It is a very well regulated process with a well-defined timing were four steps can be distinguished: hemostasis, inflammation, proliferation and remodeling. Defects that affect one of this steps lead to wound healing problems. Examples of such problems are keloid and hypertrophic scars, wound breakdown, chronic-wound, anastomosis wound dehiscence etc (1).

The research activity of this thesis was focused on bottom-up design, production and characterization of biomaterials in the form of medical devices (patches) for biomedical applications. More specifically, both a biomaterial for colorectal anastomosis after colorectal cancer resection, and a biomaterial for chronic non-healing wounds have been designed and developed, by exploiting the same manufacturing strategy.

In the first part of the work, the research has been mainly aimed to obtain a device for the treatment of colorectal anastomosis. This study was part of the scientific activity forecasted by the European project AnastomoSEAL (FP7, c.n.280929). The project aim was to prevent the anastomosis leakage (a defect of the intestinal wall at the anastomotic site leading to a communication between the intra- and extraluminal compartments) by wrapping the anastomosis with a patch capable to promote the healing of the wound. For this reason, specific biomolecules were chosen as biomaterial components. Alginate was selected for its ability to form gels thus providing the physical matrix; Hyaluronic Acid (HA) was chosen for its ability to stimulate wound healing (2); Butyric acid was chosen since recent data demonstrated its beneficial effect on colorectal anastomosis in rat models (3). The last two components have been also chemically combined in the Hyaluronic Acid Butyric ester (HABut) molecule (4).

Patches with alginate and HA were produced by using various polymer concentrations, HA with different molecular weights, and different alginate types (algal sources) in order to fine-tune the composition and the performances for the final application. Moreover, *in vitro* biological tests were performed on the patch components (raw materials): the effects on cell viability, proliferation and extracellular matrix production were studied on primary human fibroblasts and on a normal-derived

colonocyte cell line. Additional biological *in vitro* tests were conducted in order to study more in depth the effect of butyrate on colonocytes.

The obtained *in vitro* data enabled the selection of the best performing formulation and lead to the decision to exclude the use of HABut and butyrate from the medical device.

The second part of the work was focused on a biomaterial for chronic non-healing wounds treatment. Chronic non-healing wounds are defined as wounds that do not heal in eight weeks and are characterized by a prolonged inflammation, excess of proteolytic enzymes, reduced cell proliferation and migration, and infections which further sustains these deregulations (5,6).

For the development of a medical device for chronic non-healing wounds application alginate and HA were also chosen. Moreover, silver nanoparticles (nAgs) were chosen for their antibacterial and anti-inflammatory activity, and for their ability to inhibit proteolytic enzymes. nAgs are produced in wet conditions from silver nitrate and reducing compounds in the presence of the biopolymer Chitlac as dispersion agent, as already described by Travan *et al* (7).

A foamed biomaterial was prepared in order to increase the ratio surface/volume and therefore to enhance the bacterial exposure to nAg. The foamed membrane has been obtained by using hydroxy-methyl-2-propyl cellulose (HPMC), a cellulose water soluble derivative already employed for this purpose in many biomedical and pharmaceutical applications(8).

The HPMC-foamed membrane was characterized by structural, mechanical and biological analysis: scanning electron microscopy (SEM) and tensile strength measurement were performed. Reswelling kinetics, Water-Vapor transmition rate, and silver release were studied. The activity against bacterial biofilms, the toxicity on eukaryotic cells and the influence of the patches on wound closure in fibroblasts and keratinocytes were assessed. The inhibition properties of the Chitlac-nAgs colloidal solution on matrix metalloproteinases (MMPs) activity were tested.

The overall data confirmed that the biomaterial obtained is a promising material for the chronic non-healing wound application.

Riassunto

Il processo di guarigione della ferita inizia immediatamente dopo il verificarsi di un infortunio e mira a ripristinare la struttura e la funzione del tessuto danneggiato. Si tratta di un processo molto ben regolato e con una tempistica ben definita dove è possibile distinguere quattro fasi: l'emostasi, l'infiammazione, la proliferazione ed il rimodellamento. Difetti che interessano uno di queste fasi portano a ferite problematiche. Esempi di tali problemi sono cicatrici cheloidi e ipertrofiche, rottura della ferita, ferite croniche e deiscenza della ferita anastomotica ecc (1).

L'attività di ricerca di questa tesi è focalizzata sulla progettazione, produzione e caratterizzazione di biomateriali in forma di dispositivi medici (membrane) per applicazioni biomediche. Più specificamente, sia un biomateriale per l'anastomosi colorettale dopo resezione del cancro colorettale, e un biomateriale per ferite croniche sono stati progettati e sviluppati, sfruttando la stessa strategia di produzione.

Nella prima parte del lavoro, la ricerca è stata rivolta prevalentemente ad ottenere un dispositivo per il trattamento dell'anastomosi colorettale nell'ambito dell'attività scientifica prevista dal progetto europeo AnastomoSEAL (FP7, c.n.280929).

Lo scopo del progetto era quello di prevenire la deiscenza dell'anastomosi (un difetto della parete intestinale a livello del sito anastomotico che porta ad una comunicazione tra i compartimenti intra- ed extra-luminali) avvolgendo l'anastomosi con una membrana in grado di promuovere la guarigione della ferita. Per questo motivo, biomolecole specifiche sono state selezionate come componenti del biomateriale. L'alginato è stato scelto in quanto in grado di formare idrogeli fornendo così la matrice fisica per il biomateriale; l'acido ialuronico (HA) è stato scelto in quanto stimolante della guarigione delle ferite (2); L'acido butirrico è stato scelto in quanto recenti dati di letteratura riportano un effetto positivo di tale molecola in modelli animali di anastomosi colorettale(3). Questi ultimi due componenti sono stati anche combinati chimicamente insieme nella molecola dell'estere butirrico dell'acido ialuronico (HABut) (4).

Membrane contenenti alginato e HA sono state prodotte utilizzando diverse concentrazioni di polimero, HA con diversi pesi molecolari, e diversi tipi di alginato (da diverse fonti algali) al fine di ottimizzare la composizione e le prestazioni per l'applicazione finale. Inoltre, test biologici *in vitro* sono stati eseguiti sulle singoli componenti della membrana: gli effetti sulla vitalità cellulare, la proliferazione e la produzione di matrice extracellulare sono stati studiati su fibroblasti umani primari e su una linea cellulare derivata da colonociti normali. Ulteriori test biologici *in vitro* sono stati condotti al fine di studiare più in profondità l'effetto del butirrato sui colonociti.

I dati ottenuti dai test *in vitro* hanno permesso di selezionare la formulazione migliore e hanno portato alla decisione di escludere l'utilizzo del HABut e del butirrato all'interno del dispositivo medico.

La seconda parte del lavoro è stata rivolta al disegno e produzione di un biomateriale per il trattamento delle ferite croniche.

Le ferite croniche sono ferite che non riescono a guarire in otto settimane e sono caratterizzate da una infiammazione prolungata, eccesso di enzimi proteolitici, ridotta proliferazione e migrazione cellulare, e infezioni che ulteriormente sostengono queste complicanze(5)(6).

Per lo sviluppo di un dispositivo medico pe il trattamento delle ferite croniche, alginato e HA sono stati scelti come componenti del biomateriale. Inoltre, le nanoparticelle d'argento (nAg) sono state scelte per la loro attività antibatterica e antinfiammatoria, e per la loro capacità di inibire gli enzimi proteolitici. Le nAg sono state prodotte in condizioni umide a partire da nitrato d'argento e composti riducenti in presenza del biopolimero Chitlac come agente disperdente, come già descritto da Travan *et al* (7).

Un materiale schiumato è stato preparato in modo da aumentare il rapporto superficie / volume e quindi migliorare l'esposizione batterica delle nAg. Il biomateriale schiumato è stato ottenuto utilizzando idrossi-metil-2-propil cellulosa (HPMC), un derivato della cellulosa solubile in acqua già impiegata per questo scopo in molte applicazioni biomediche e farmaceutiche(8).

La membrana schiumata attraverso l'utilizzo dell'HPMC è stata caratterizzata mediante analisi strutturale, meccanica e biologica: la microscopia elettronica a scansione (SEM) e la misura della resistenza alla trazione sono state utilizzate. La cinetica di reidratazione, la velocità di trasmissione di vapore acqueo, e il rilascio d'argento sono stati studiati. L'attività contro biofilm batterici, la tossicità

su cellule eucariotiche e l'influenza delle membrane sulla chiusura della ferita in fibroblasti e cheratinociti sono state valutate. Le proprietà della soluzione colloidale Chitlac-nAgs di inibire l'attività delle metalloproteinasi di matrice (MMP) sono state testate.

Complessivamente, i dati ottenuti confermano che il materiale ottenuto è un materiale promettente per il trattamento delle ferite croniche.

1. Introduction

1.1. Wound healing

Wounds can occur as part of a disease process or have an accidental or intentional etiology. Immediately after the wound is established, the wound healing process begins.

Wound healing is a process that regards all tissues and consists in the restoration of structure and function of the injured tissue. There are common characteristics for the different tissues, while some others are tissue-specific and depend on the location, function and structure of the tissue. Healing depends on extension of the injury, distance from wound edges, underlying co-morbidities, and infections, or post-surgical wound dehiscence.

Generally, the wound healing process is an organic process were normally four phases are identified: hemostasis, inflammation, tissue formation or proliferation and remodeling. Disorders that affect one of these steps can lead to anomalous healing like keloid, fibrotic and chronic (non-healing) wounds (9,10).

Cell-cell interactions, cell-matrix interactions and interactions through soluble factors such as cytokines and growth factors are involved in the healing cascade. The timing of each step is finely regulated and depends on the time needed for the different biological processes (like signal transduction, production of cytokines and growth factors) to occur. For example, the activation of platelets is an immediate process, while the migration of skin keratinocytes and fibroblast has a lag face given by the necessity of changing protein expression at the adhesion level (5).

Immediately after the wound has occurred, the broken blood vessels constrict through contraction of the smooth muscle layer that is present around the vessel wall. This is followed by the formation of a fibrin-rich clot that physically protects the wound and the underlying capillaries and serves as a provisional matrix for cell migration.

Platelets are present in the blood clot and begin to degranulate, by acting as reservoir of different biological factors that give rise to the healing cascade: cytokines and chemoattractive factors that recall neutrophils and macrophages, endothelial cells, smooth muscle cells and fibroblasts. Serous fluid leak produces wound edema since at this point vessels are more permeable in order to permit migration of

monocytes into the wound site. In parallel, coagulation and complement cascade are activated by platelet degranulation (11,12).

Neutrophils and macrophages (activated monocytes) are responsible for the inflammatory stage that has the aim of preventing infections. These cells clean the wound from detriments and bacteria and produce other growth factors and cytokines that continue the wound repair signal (5).
A protracted inflammation can lead to extensive tissue damage and delayed proliferation thus resulting in the formation of a chronic wound.
During the proliferative phase, the provisional matrix is slowly replaced by a collagen-rich matrix synthesized by fibroblasts. Moreover, angiogenesis occurs together with collagen deposition, wound contraction and restoration of the epithelial barrier. The newly formed capillaries are highly permeable and thus further contribute to the edema formation.

Collagen production during the proliferative phase is very important as it correlates to tissue strength and the absence of a wound ridge given by newly formed collagen correlates with risk of dehiscence. At the same time, if the production of collagen is excessive a hypertrophic scar is formed (13).

Migration and proliferation of endothelial cells, fibroblasts and epithelial cells are important aspects of the tissue formation stage. In the ultimate phases, the excessive unnecessary cells (immune cells, fibroblasts, myofibroblasts and endothelial cells) are eliminated by apoptosis (14). A lower vascularization and a continuous remodeling of the extracellular matrix characterize this stage. Remodeling stage deficiencies can lead to wound breakdown or to keloid and hypertrophic wounds.

The result of the remodeling is a change in composition of the extracellular matrix (e.g. in the skin granulation tissue prevails collagen III while at the end of the wound healing prevails collagen I) that augments the wound tensile strength.

Adult wound healing occurs through scaring with exceptions such as the healing of the liver. In lower vertebrates and early fetal wounds, healing occurs through regeneration.

There are several known factors affecting wound healing like nutritional status, hypoxia, smoking, immunosuppression (both natural, e.g. related to HIV or drug-induced), chronic disease that affect oxygenation, immune response, age, surgical techniques, and genetics (e.g. in keloid disease) (15).

1.1.1. Healing in general surgery wounds

Wounds produced by general surgery go through the same healing steps of the spontaneous and accidental wounds, but the magnitude and temporal sequences are measurably different (16). Moreover, the site of the wound is important: for example urethral wounds go through extended duration of each phase (17).

Dehiscence of wounds is still an important adverse effect of surgery, although there have been major advances in surgical managements and approaches. Complications of wounds include failure to heal, infection, and excessive scarring or contracture, and result in prolonged hospitalizations, higher costs and increased mortality rate (18).

Surgical wounds at high risk of complications include wounds that are in proximity or in contact to bacterial reach-environments. Among this, bowel anastomosis are at high risk of dehiscence in view of the tissue function, the shear stress given by intestinal peristalsis, and the presence of bacteria that normally colonize intestinal lumen. Anastomosis is a term that describes the connection created between tubular structures, such as blood vessels or loops of intestine (19).

In gastrointestinal anastomosis, collagen is one of the most important molecules for the healing, since the tensile strength of the anastomosis derives mainly from collagen fibrils located within the submucosal layer. During the first days after the anastomosis is performed, collagen is degraded by collagenases at the wound site and consequently the anastomotic strength within the first days is dependent on the suture- or staple-holding capacity of existing collagen. Than fibroblasts and smooth muscle cells synthesize new collagen (20–23).

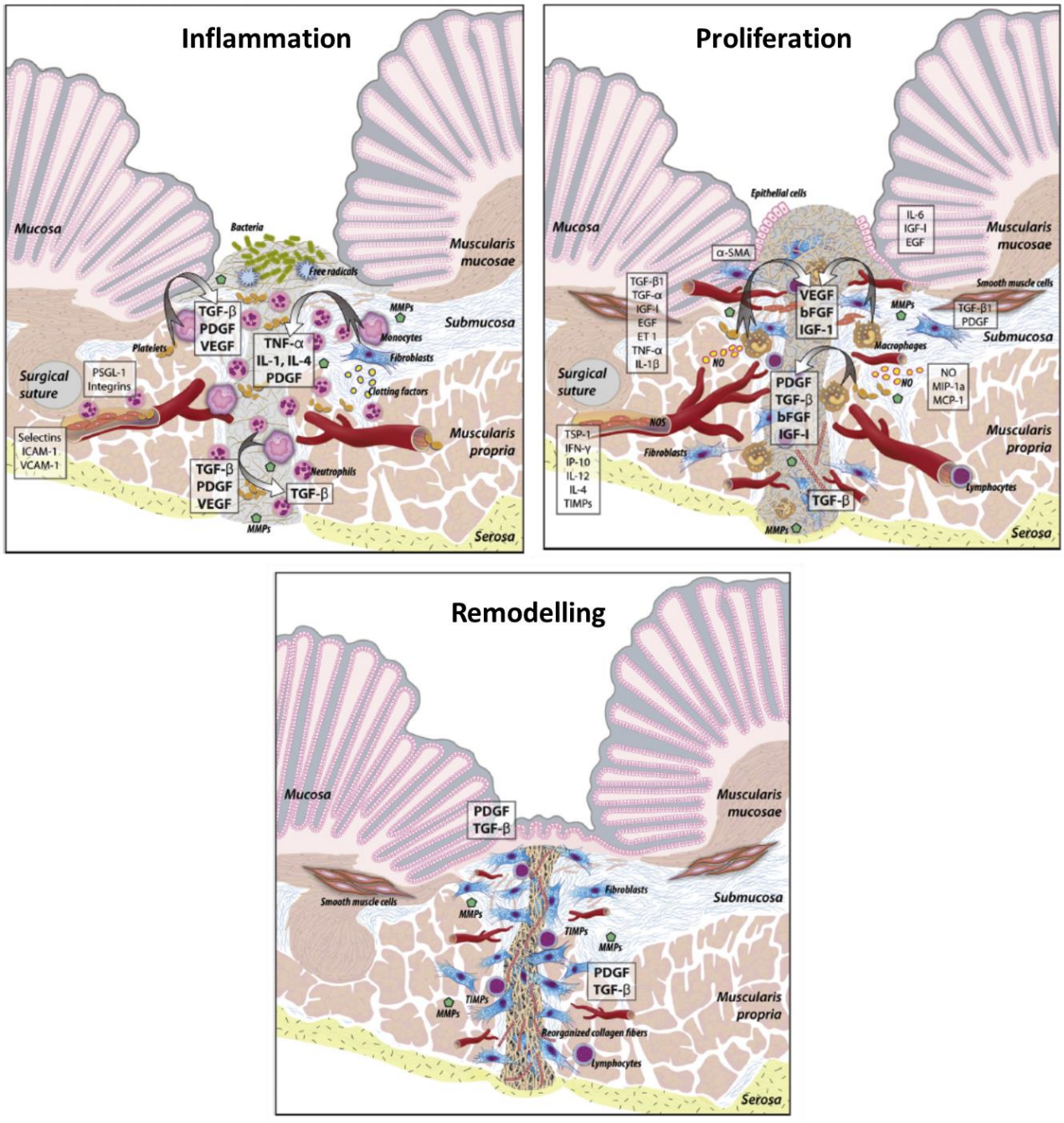

Figure 1.1*: Healing of the gastrointestinal anastomosis follows the classical steps of wound healing. Here are reported the inflammation, proliferation and remodeling phases. Reprinted from Journal of Surgical Research , Vol 187, Issue 1, Rijcken E., Sachs L., Fuchs T., Spiegel H., Neumann P., Pages No. 202-210, Copyright (2014), with permission from Elsevier.* (24).

The most frequent and severe complication of intestinal anastomosis is the anastomotic leakage (AL). AL occurs when no proper and rapid healing of the intestinal tissue takes place at the site of the anastomosis. The frequency and consequences of anastomotic failure vary according to the site within the gastrointestinal tract (25). AL after rectal surgery occurs significantly more frequently than AL in other parts of the intestinal tract and the incidence is directly related to the distance of the resection from the anal verge. There is no clear explanation for this augmented risk but it could be connected to a technically more challenging location for the surgical procedure with subsequent local tissue trauma, increased tension, or poor blood supply (26).

Bacteria that contribute to proteolytic environment can influence the outcome of the anastomosis since antibiotic therapy before surgery was demonstrated to reduce the risk of AL (27).

AL can lead to generalized peritonitis, anastomotic strictures, fecal incontinence and abdominal reoperation (28,29).

In the anastomosis performed after tumor resections, the neoadjuvant therapy is an additional risk factor for AL (30). At the same time, some studies show that AL is associated to a decrease in long-term survival (31).

1.1.2. Healing in chronic wounds

One of the major complications of the skin wounds are chronic non-healing wounds which include burn wounds, venous leg ulcers, diabetic foot ulcers, arterial insufficiency and pressure ulcers (32).

The clinical importance in terms of numbers and cost of chronic non-healing wounds is very high since this disease is correlated to other age-related pathologies, which are foreseen to increase because of the increasing life expectancy. It is also a great problem in terms of life quality since it is both a physically and psychologically debilitating disease.

Chronic non-healing wounds have been defined as wounds that do not heal in eight weeks due to impaired wound healing. Age, vascular disease, low oxygen pressure, immobility, size of wound and duration before treatment, pain and presence of infection are considered risk factors for chronic non-healing wounds (33,34).

The cascade of events that leads to a non-healing wound is not well defined, although several characteristics of the impaired healing have been described among which a prolonged inflammation (6), an inhibited proliferative activity, a defective migration of keratinocytes, and a modified fibroblasts function (35,36).

The presence of 15% of senescent fibroblasts in the wound is supposed to be the turning point from a normal healing wound to a chronic non-healing wound. Senescent fibroblasts cause defects on the extracellular matrix (ECM) because they produce higher levels of proteolytic enzymes and decreased levels of Matrix Metalloproteinases' (MMPs) inhibitors causing an uncontrolled proteolytic activity. In addition, also neutrophils and macrophages produce different proteases which are expressed at high levels in chronic wounds (37–39).

Levels of MMPs in chronic wounds are elevated 30 times the levels in acute wounds and MMPs' levels decrease when there is a progression from a non-healing to a healing phase of the wound. MMPs are very important for wound healing as they generate the way for cell migration and permit modification or remodeling of ECM. When these molecules are overexpressed, cell migration is hampered and there is excessive destruction of ECM with subsequent tissue demolition.

MMPs' inhibitors and growth factors are cleaved due to the high proteolytic activity, resulting in their inactivation. The cleavage of components of the ECM also occurs and further sustains MMPs' activity since fragments generated from ECM cleavage attract more neutrophils that in turn produce other proteolytic enzymes (40).

Often in chronic non-healing wounds, an inadequate tissue oxygenation is present, which lower the killing capacity of polymorphonuclear leukocytes (PMNs) and thus favors bacterial infection. In addition, the necrotic hypoxic tissue becomes an optimal environment for bacterial growth (41).
In chronic wounds the risk of tumor development, such as squamous cell carcinoma, is higher than in normal skin. Since MMPs have been associated to tumorigenesis, invasion and metastasis, their overexpression can partially justify the increased risk of squamous cell carcinoma in chronic leg ulcers (42). Moreover, the production of proteolytic enzymes occurs also by biofilms that can be often found in chronic-wounds.

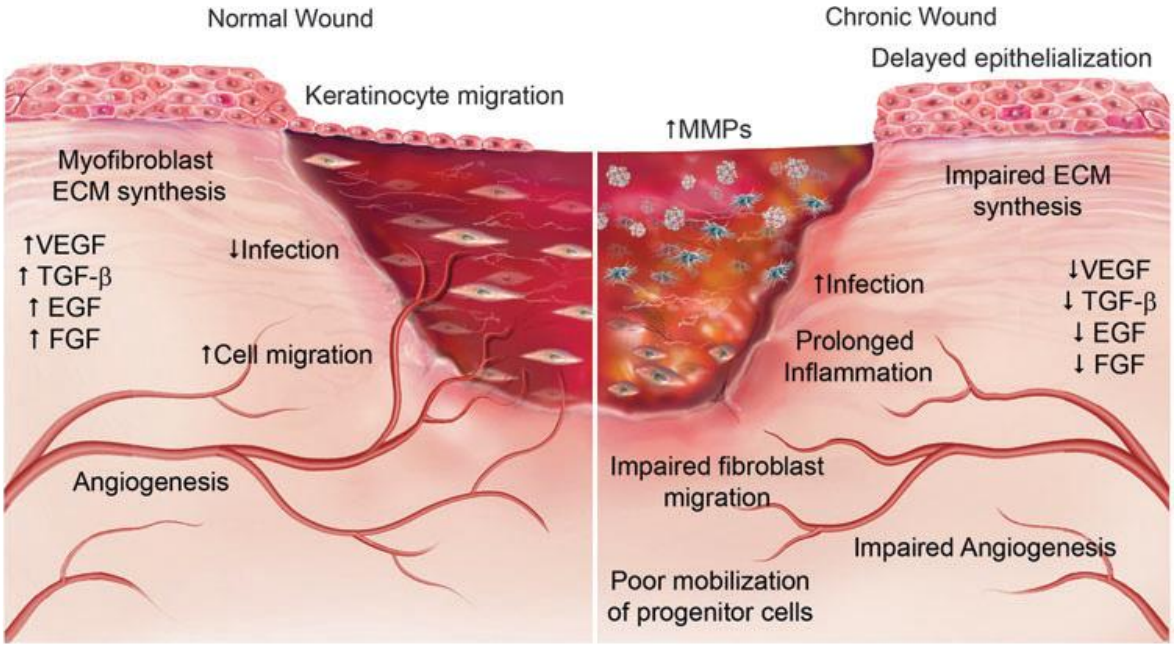

Figure 1.2: Comparing normal and chronic wounds. Chronic wounds are characterized by prolonged inflammation and infection, delayed epithelialization, impaired fibroblasts migration and synthesis of extracellular matrix, increased proteolytic activity, decreased growth factor levels, and impaired angiogenesis. Reprinted with permission from Turner and Badylak 2015 (43).

Bacteria isolated from chronic wounds are mainly *Staphylococcus*, *Enterococcus* and *Pseudomonas* (44). Planktonic bacteria are very different from bacteria present into biofilms for structure, gene expression, interaction with the host and antibiotic resistance. James et al. found that biofilms were present in 60% of chronic skin wounds and only in 6% of acute wounds. Bacterial biofilms can be constituted by a single or multiple bacterial species; normally two to five of them are present (44,45).

Bacterial biofilms are composed of bacteria immersed in a matrix composed by polysaccharides, proteins and bacterial extracellular DNA (46). Bacteria have several additional characteristics as compared to the planktonic counterparts, such as higher anti-biotic resistance, higher resistance to immune response (47–49), production of proteolytic enzymes (50), and capability to activate endogenous proteases (51).

Moreover, a study in a biofilm-inoculated diabetic mouse model showed that the presence of the biofilm avoided the wound healing process (52).

1.2. Wound care

Understanding the molecular mechanisms and the etiology of wound dehiscence is an important issue for wound treatment. Primary objectives in wound management are to reduce the risk of infection, while optimizing local conditions to help the healing process.

1.2.1. Wound care in intestinal anastomosis

After the resection of a tract of bowel, in order to join the two ends together, the surgeons can choose among hand sewing, stapling of the anastomosis or compression rings. Several studies showed no significant differences among these techniques. Moreover, any difference was proven also between laparoscopic or open approach in terms of AL incidence. Very often surgeons perform a diverting stoma as a prophylaxis for AL or a fecal diversion after AL has occurred often resulting in a permanent stoma (53,54).

Different studies on risk factors, surgical techniques and prevention, evidence that the incidence of AL over the last three decades was not reduced. The diagnosis of AL is still a problem since it is generally detected from 5 to 12 days after surgery (55,56). Moreover, no unique definition of anastomotic leakage is used (25). Thus, AL rates among the different studies are highly variable.

Management of AL depends on the clinical picture of the patient since it can go from the absence of symptoms to life-threatening septic shock (57). Antibiotic therapy is administered in presence of signs of sepsis. Some cases require reintervention with formation of a new anastomosis.

Buttressing intestinal anastomosis has shown positive effects on different animal models. Several materials, such as fibrin glue and omental pedicle grafts, were tested in clinical trials but did not show improvement on AL. (58,59)

At present, there are no efficient treatments to prevent AL.

1.2.2. The AnastomoSEAL project

The AnastomoSEAL project (FP7-NMP-2011-SMALL – c.n. 280929; http://www.anastomoseal.eu) is a European project which is focused on the prevention of the anastomotic leakage after colorectal cancer resection.

According to World Health Organization (WHO) colorectal cancer is the third most common cancer in men and the second in women (http://globocan.iarc.fr/). The therapy of colorectal cancer is surgical and consist on the removal of the affected intestine and the conjunction of the two healthy ends by an anastomosis. As mentioned in the previous paragraph, these anastomosis have a higher risk for AL than anastomosis performed in the upper parts of the gastrointestinal tract.

The AnastomoSEAL project aims to develop an engineered bioresorbable biomaterial capable of promoting a safe anastomosis during the critical period of tissue healing without causing adverse reactions. The proposed solution is to design a biomaterial in form of a patch inserted by the surgeon after the anastomotic procedure which wraps around the sutured tissue to promote physiological processes of tissue regeneration.

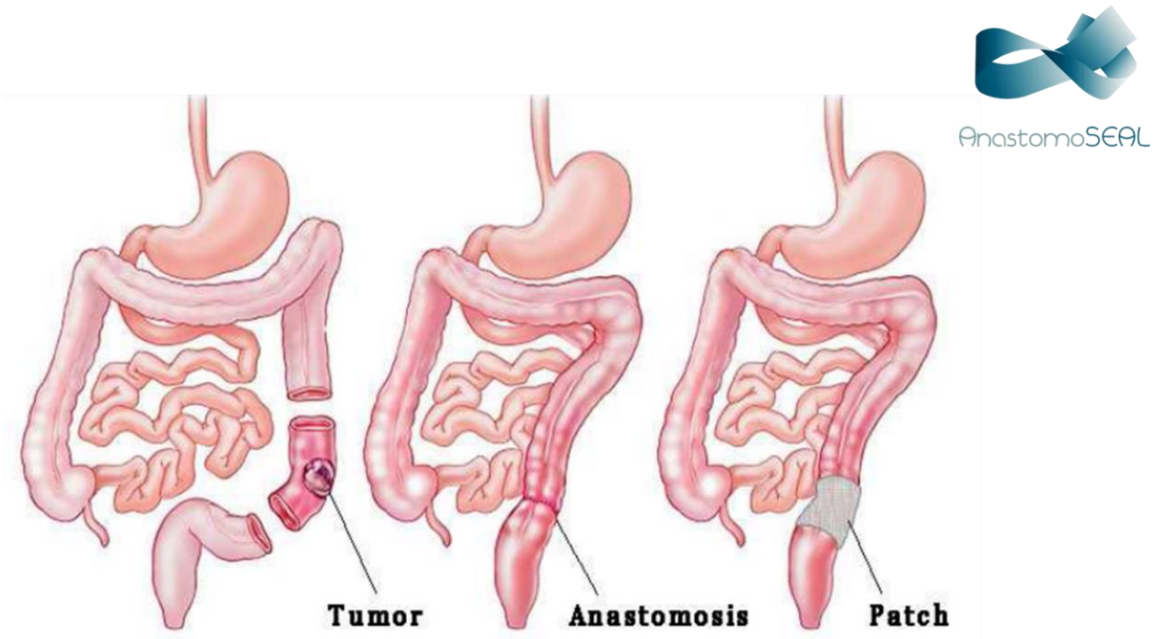

Figure 1.3: *The AnastomoSEAL project: wrapping of colorectal anastomosis with a patch that should promote healing.*

The idea for the production of the biomaterial was the use of natural polysaccharides alginate and hyaluronic acid (HA) and butyrate. Hyaluronic acid butyric ester HABut is used a a vehicle for butyrate delivery.

The project involves different partners, both from universities and companies. The components of the AnastomoSEAL consortium are listed below:

1. Univesity of Trieste (Trieste, Italy)
2. Maastricht University – Medical Center (Maastricht, The Netherlands)
3. FMC BioPolymer – NovaMatrix (Sandvika, Norway)
4. Sigea S.R.L. (Trieste, Italy)
5. Rescoll (Bordeaux, France)
6. Impuls (Gdansk, Poland)

The AnastomoSEAL project began in may 2012 and was concluded on may 2015.

1.2.3. Wound care in chronic non-healing wounds

For pathologies-associated wound dehiscence, it is important to treat directly the causes of the disease. For example, compression therapy is effectively used for venous ulcers, were chronic wounds are caused by an improper blood flow due to venous valves insufficiency. Compression counteracts the venous hypotension, and helps a correct blood flow.

Removal of damaged and necrotic tissue and management of tissue exudate, by using absorbent dressing, topical antimicrobial agents and compression therapy, and reduction of treatment-related pain associated to the dressing change are important aspects of the therapy. Antibiotic therapy is necessary when an infection is present. The selection of the best treatment has to be done for each patient, taking into account the quality of life (6,60).

The standard for wound care consists in swabbing for infection, cleaning, dressing, and debridement. Debridement of the wound aims to eliminate all avital tissue and expose the healthy perfused tissue that is required for the wound to heal. In addition, it removes most of the bacterial contamination. There are different types of debridement: the most used are surgical (by using traditional surgery) and biosurgical debridement (by using fly maggots, ultrasound plasma or laser). Negative pressure-vacuum

wound therapy is also used. It consists in applying suction to the tissue by using a pump generated negative pressure (61).

Passive debridement can be achieved with the use of hydrogels and hydrocolloids that maintain a moist environment, with consequent hydration and autodigestion of necrotic tissue by endogenous enzymes. After wound bed preparation, different approaches are used to stimulate wound healing. (60)

Skin autografting (both split-thickness autograft and cultured epithelial cell autograft) is limited by availability of donor sites and the outcome is inversely proportional to age. Moreover, the time required for preparation, the susceptibility to infection, and the necessity of an intact basal membrane limits the use of autografts. Human fibroblasts from the foreskin of neonates, bilayered tissue (keratinocytes and fibroblasts in a type I collagen matrix) were tested but this grafts cannot survive more than few weeks when placed in chronic wounds (34,62).

The moist environment created by hydrogels, hydrocolloids, polyurethane films and foams was shown to accelerate re-epithelialization, without favoring infections.

Currently there are many wound dressings available to the market. The choice is really hard and usually based on the wound stage and the exudate amount. The most common available wound dressing are made of alginate, hyaluronic acid, cellulose, collagen, chitosan, and their derivatives.

The wound dressing should avoid both desiccation of the wound and excess of exudate. A desiccated wound is painful while an excess of exudate causes maceration of the wound margins, thus slowing down the healing process. A balance between liquid absorption, Water-vapor transmition and capability to retain water is required for this function. The dressing should be permeable to oxygen, water vapor and carbon dioxide, easy to apply and remove, biocompatible, hypoallergenic, non-toxic, and available in sterile packaging. It should conform to body contours since wounds are irregular. It may be cut to size or available in a variety of shape and sizes. In addition it should give mechanical protection, create a barrier against microorganisms, and possibly control bacterial contamination and infection (33).

1.3. Biopolymers for wound healing

The International Union of Pure and Applied Chemistry (IUPAC) defines biopolymers as macromolecules formed by living organisms (63).

Biopolymers are generated from bacteria, fungi, plants, animals that are all renewable sources. They are easily biodegradable because of the oxygen and nitrogen atoms found in their structural backbone and are converted in CO_2, water, biomass, humid matter, and other natural substances (64).

In order to be used in biomedical applications biopolymers should be biocompatible, biodegradable to non-toxic products, non-immunogenic, processable to different shapes, and should have good mechanical properties and bioactivity. Moreover should be cost-effective and easy to use. Different biopolymers can be combined together to improve the wound healing properties of a medical device. The choice should be based on the location and intrinsic characteristic of the wound. For example, for chronic wounds an optimal gaseous exchange and a moist environment are necessary, while in some internal surgery procedures (e.g. liver) hemostatic properties are sought.

Biopolymers are divided in three groups: proteins, nucleic acids and polysaccharides. All of these categories are studied or in use, but nucleic acids are less used for wound healing applications. Nevertheless, there are also animal studies for their use in chronic wounds in the form of topical gene therapy based on the introduction on the wound site of the genes for growth factors (65).

Growth factors in the proteic form have been proposed and several randomized trials have been made, but only EGF (Neoderm™, Trimedicale) and PDGF (Regranex™, Janssen-Cilag) are commercially approved growth factors (66,67). Probably, the reason why growth factor have not shown to make a great difference in the treatment of chronic wounds is that they are cleaved by MMPs that have an excessive activity in chronic wounds (40)The mostly used protein-derived wound care products are based on collagen and its denatured form found in gelatin. Collagen is characterized by high tensile strength, affinity with water, can be processed in different forms and has hemostatic properties. Collagen dressings are in the form of sponges, membrane sheets, powder, and injectable gels. Their applications vary from hemostasis on liver and spleen surgery, vehicles for transportation of cultured skin cells or drug carriers for skin replacement, and bone substitutes (64). Also gelatin has good hemostatic properties and is used as tissue adhesive and for wound dressings.

Tachosil® (Nycomed) is a product used in internal surgery that is made of equine collagen, bovine thrombin, bovine aprotinin, and human fibrinogen and has very good outcome in liver open surgery but not laparoscopy (68).

Among protein biopolymers, fibrin is also used mainly as sealant systems in general surgery applications. (69).

Polysaccharides are most commonly used for wound healing products. Among the most used polysaccharides are alginate, chitosan, hyaluronic acid (HA) and cellulose derivatives, all of which have hemostatic properties.

Cellulose is obtained by both plants and bacteria, is a highly hydrophilic material that can be produced in any shape and size. There are different products made of cellulose or oxidized cellulose for skin grafts and for other wound types such as surgical wounds (70).

The polysaccharides of interest for this thesis: both natural (alginate and HA), and modified (Chitlac and HA butyric ester) will be described more in depth in the following paragraphs.

1.3.1. Alginate

Alginate is an abundant natural polysaccharide found in brown algae. Although the almost totality of alginate commercially used today is extracted from brown algae belonging to the class of *Phaeophyceae* (such as *Laminaria hyperborea* and *Macrocistis pyrifera*), it can be synthesized in large quantities also from bacteria belonging mainly to the genera *Azotobacter* and *Pseudomonas* (71,72).

Alginate is a linear binary copolymer of (1→4)-linked ß-D-mannuronic acid (M) and α-L-guluronic acid (G) residues (Figure 1.4 A). Alginate is firstly produced as a polymer composed of mannuronic acid that is than partially converted into guluronic acid by epimerases. The content in M and G units depend on the origin of the alginate (Table 1.1). Alginate is composed of a pattern of blocks where homopolymeric blocks of G residues (G-blocks), homo-polymeric blocks of M residues (M-blocks) and blocks with alternating sequence of M and G units (MG-blocks) coexist. Thus to describe the alginate molecule the monomer composition alone is not sufficient (73).

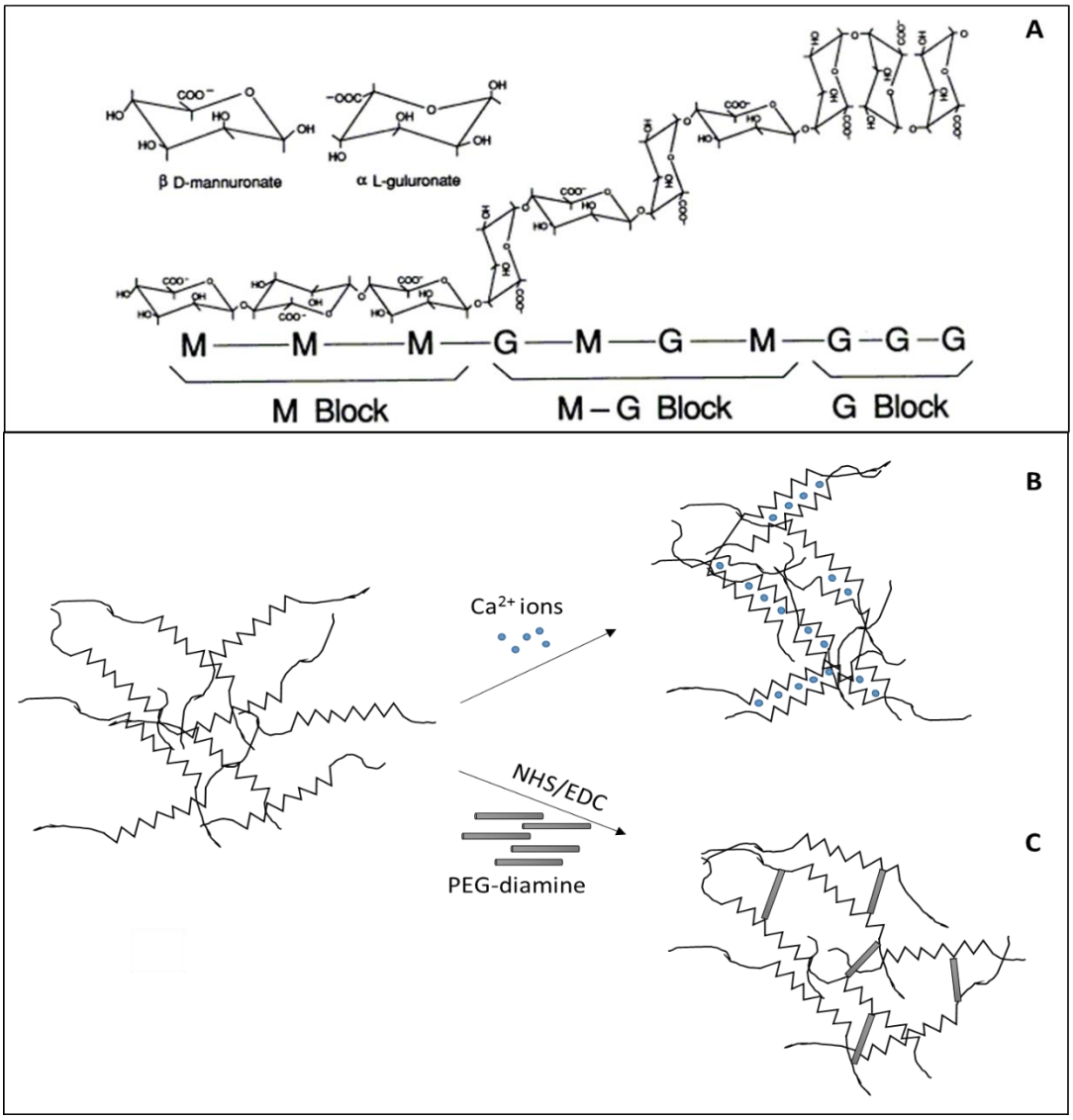

Figure 1.4*: A) ß-D-mannuronic acid (M) and α-L-guluronic acid (G) in the Alginate chemical and block structures; B) ionically crosslinked alginate and C) chemically crosslinked alginate with Poly(ethylene glycol) diamine. Adapted from* (74)*.*

NMR spectroscopy analysis of alginate has shown no regular repeating unit (75). The functional properties of alginate are primarily influenced by the G content, the G-block length and the molecular weight (MW).

Physical or chemical crosslinking strategies are used to obtain alginate hydrogels (figure 1.4 B and C). The most peculiar property of alginate, as well as the most exploited, is the ability to form temperature-

independent ionotropic gels by external or internal gelation. Ionic crosslinking is achieved in presence of divalent cations like calcium, strontium and barium.

Algal Species	F_G	F_M	F_{GG}	F_{MM}	$F_{GM,MG}$	F_{GGG}	$N_{G>1}$
Laminaria hyperborean (stipe)	0.63	0.37	0.52	0.26	0.11	0.48	15
Laminaria hyperborean (leaf)	0.49	0.51	0.31	0.32	0.19	0.25	8
Macrocystis pyrifera	0.42	0.58	0.20	0.37	0.21	0.16	6
Laminaria digitata	0.41	0.59	0.25	0.43	0.16	0.20	6
Lessonia nigrescens	0.41	0.59	0.22	0.40	0.19	0.17	6
Ascophyllum nodosum	0.41	0.59	0.22	0.38	0.21	0.13	5
Laminaria japonica	0.35	0.65	0.18	0.48	0.17	-	-
Durvillaea antarctica	0.32	0.68	0.16	0.51	0.17	0.11	4

***Table 1.1**: Alginates from different algal species and their composition in M and G residues. F_G = fraction of G residues; F_{GG} = fraction of G dimers; F_{GGG} = fraction of G trimers; F_M = fraction of M residues; F_{MM} = fraction of M dimers; $F_{GM,MG}$ = fraction of mixed sequence of G and M; $N_{G>1}$ = average length of G blocks. Data taken from* (76).

External gelation strategies are used mainly for encapsulation of cells or microbeads synthesis and consist in dropping alginate solutions or alginate drops in solutions containing bivalent cations.

Internal gelation strategies are mainly based on the use of divalent cation salts of low solubility (such as calcium carbonate and calcium sulfate), which are slowly released by mild acidic conditions formed in presence of glucone-δ-lactone (GDL). Thereby homogeneous hydrogels are obtained through internal gelation.

Unlike what was believed in the past, recent experiments suggest that the G blocks are not the only ones responsible for the formation of the junctions, but they can be formed also between MG / MG blocks and between GG / MG blocks (77).

Once in contact with tissues, an exchange between divalent cations present in the hydrogel and monovalent cations (such as Na^+) present in the environment leads to a progressive and slow degradation of the ionically crosslinked hydrogel (74).

Mechanical properties of alginate hydrogels can be modulated by changing parameters like MW, concentration, algal source, chemical modifications, and the type of the crosslinking (78).

Hydrogels, membranes, micro- and nano-spheres, microcapsules, sponges, foams, and fibers can be prepared by using alginate and are exploited in several biomedical applications: for impression making in the dental clinic, as thickener or gelling agent in food as well as in formulations for gastric reflux prevention, in drug delivery applications (79,80), and in the bone tissue engineering field (81).

In wound dressings, alginate is widely used due to its hemostatic properties, its great capability to absorb water, to provide a moist wound environment, to absorb proteinases and to reduce pain (64). Two of the main factors affecting pain at dressing change are adherent products and drying of dressings. Alginate can be removed by rinsing with saline solution, does not adhere to the tissue and remains moist. For these reasons alginate hydrogels are considered among the less painful in dressing change (82).

Alginate is used in different wound types from general surgery wounds to severe skin wounds. It is available in several forms that go from simple calcium alginate dressings such as Kaltostat® (ConvaTec) and AlgiCell® (Derma Sciences) to composite dressings such as Sorbsan Plus (calcium alginate and viscose, Aspen medical) and silver containing dressings such as Acticoat® (alginate dressing with nanocrystalline silver, Smith&Nephew).

1.3.2. Hyaluronic acid

Hyaluronic acid (HA), or hyaluronan, is a non-sulfated glycosaminoglycan (GAG) that is abundant in the human body especially into the ECM were it has structural functions.

HA was isolated for the first time in 1934 by Meyer and Palmer from the vitreous humor of the eye. It is a linear, unbranched polysaccharide composed of a repeating disaccharide unit of N-acetyl-D-glucosamine (GlcNAc) and D-glucuronic acid (GlcA). Figure 1.5. shows the structure of the HA chain were disaccharide units are linked by ß 1→3 bonds. HA has a negative charge at neutral pH due to the carboxyl group that is present at each disaccharide-repeating unit (83).

HA synthesized from the human body is characterized by high MW (more than 2 000 000). The synthesis occurs at the inner face of the plasma membrane by enzymes called HA synthases and then translocated by the same enzymes into the extracellular matrix. HA has a high turnover rate: in the local tissue it is mainly internalized by endocytosis mediated by CD44 and then subjected to enzymatic degradation by hyaluronidases which produce HA of lower MW.

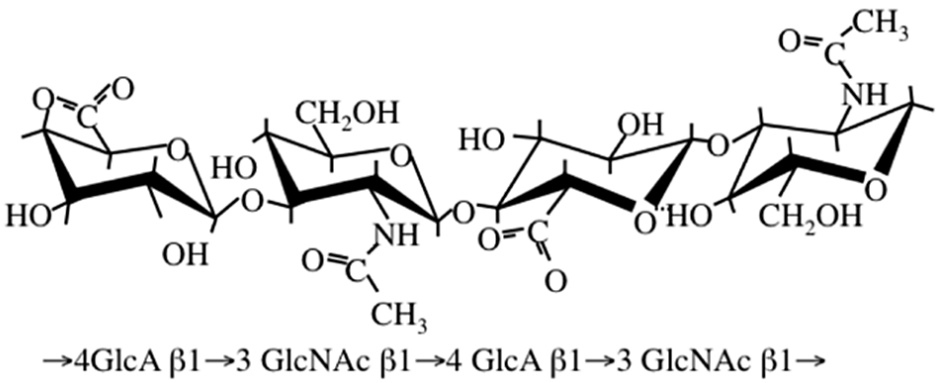

Figure 1.5*: chemical structure of hyaluronic acid and disaccharide repeat block of N-acetyl-D-glucosamine (GlcNAc) and D-glucuronic acid (GlcA).*

Several binding proteins, besides CD44, have been identified also into the intracellular environment that makes this molecule a potential signaling molecule.

HA synthesis, degradation, and signaling are regulated during the cell cycle and has important roles in this process. Lee and Spicer suggest that HA plays an important role in mitosis by maintenance of cell shape and volume or through microtubule-associated functions. Moreover, in the physiological environment HA is involved in several biological functions like cell growth, differentiation, migration, adhesion, angiogenesis and immune response.

In literature, opposite biological effects of HA are reported, and are ascribed to the dimensions in terms of MW. In general, HA of low MW stimulates angiogenesis, inflammation, and proliferation whereas HA of high MW has anti-angiogenetic and anti-inflammatory effects. However, HA used in the different studies are of different MW and with a wide distribution of MW that makes difficult to distinguish the real effect of specific molecular sizes (84).

HA has also scavenging properties given by its ability to absorb reactive oxygen species (ROS) that consequently generate HA fragments.

HA has an important role in wound healing: the inhibition of the signaling through its receptors leads to aberrant healing (85–87).

HA is widely used in the biomedical field. Viscosurgery (e.g. eye surgery for cataract), viscosupplementation (injection in synovial fluid) and esthetic medicine (wrinkle filling) exploit the capacity of HA to entrap water and its ability to maintain tissue structure.

HA is also used for drug delivery, in tissue engineering and wound repair. Dry fibers, gels, microgranules and spray of HA are available for wound healing application. The capacity of HA to induce wound healing are related to its ability to induce cell migration and proliferation, angiogenesis and his effects on inflammation. In addition HA has hemostatic ability (88).

1.3.3. Hyaluronic Acid Butyric ester

Hyaluronic acid butyric ester (HABut) is a chemically modified HA in which butyrate molecules are linked to the polysaccharide hydroxyls by means of ester bonds (4).

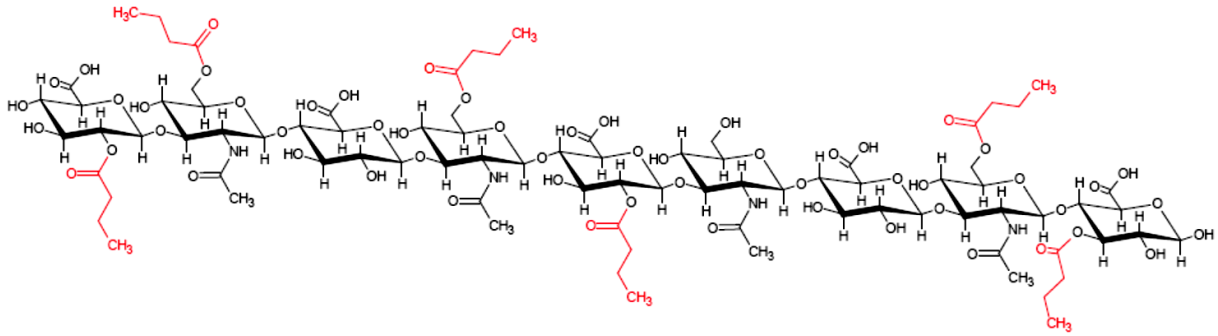

***Figure 1.6**: Schematic representation of the HABut chain.*

HABut can be synthesized by using HA with different MW and with different degree of substitutions (DS). Properties such as water solubility, chain mobility, binding on the cell membrane receptors and the enzymatic degradation kinetics by hyaluronidases are dependent on MW and DS. HABut was shown to be internalized into tumor cell lines, where butyrate can be released, through the HA receptor CD44 (4).

Previous literature work reported that HABut is an effective drug delivery system for butyrate since it was shown that HABut exhibits antiproliferative activity superior to that of the butyrate alone on different malignant cell lines derived from breast, pancreas, lung and liver tumors (4,89,90).

Butyric acid is a small chain fatty acid produced in the intestinal lumen by anaerobic bacteria fermentation of alimentary fibers and is immediately absorbed and used as a source of energy by colonocytes. It has a half-life in the range of few minutes (91,92) and this limits its use as a potential drug or alimentary supplement.

Butyrate is an inhibitor of Histone Deacetylases (HDAC) causing a hyperacetylation of histones, an aspecific mechanism of modification of gene expression. Consequently, the effects of butyrate depend on the genetic asset of cells and cell types. Several effects of butyrate have been reported and vary among the different cells.

Butyrate was shown to have several positive effects on the intestine environment. It contributes to the protective effects of dietary fiber against intestinal diseases. Butyrate was reported to control the homeostasis of colon tissue by acting on proliferation, differentiation, inflammation and apoptosis, and at the same time, it enhances intestinal defenses (mucine expression, antimicrobial peptides production, and reduces permeability of the intestinal barrier)(93). In the field of bowel surgery butyrate has shown positive effects on the intestinal anastomotic healing (3).

On the other hand, butyrate was reported to inhibit colon cancer cell growth. The opposite effects of butyrate on healthy and tumor cells (also called “butyrate paradox”) may be explained by the “Warbung effect”. The Warbung effect states that there are differential energy producing routes between healthy and cancer cells. Cancer cells produce energy mainly by glycolysis followed by anaerobic fermentation (were pyruvate is converted to lactic acid) in cytosol while normal cells have a low rate of glycolysis followed by oxidative phosphorylation (oxidation of pyruvate) in mitochondria were butyrate is metabolized. The Warbung effect leads to an accumulation of butyrate into the cancer cells but not into the healthy ones (94,95).

Several studies exist for the use of butyrate in diseases like Immune Bowel Diseases (such as Chron’s disease and Ulcerative colitis), hemoglobinopathies, genetic metabolic diseases, hypercholesterolemia, ischemic stroke, obesity and insulin resistance as well as in tumor therapy (96,97).

1.3.4. Chitosan and Chitlac

Chitosan is a linear binary copolymer of (1→4)-linked D-glucosamine and N-acetyl-D-glucosamine obtained from chitin, a hydrophobic polymer composed mainly by N-acetyl-D-glucosamine found in the

exoskeleton of crustaceans and cell wall of fungi and yeast. In the process of chitin deacetylation, typically under alkaline conditions, when the glucosamine content reaches about 50% or higher, the polymer becomes soluble in aqueous acidic medium and is called chitosan. Its properties depend on the acetylation degree (DA), the distribution of acetyl groups, MW, pH and ionic strength of the solvent (98).

The presence of the amino group and the positive charges give to the chitosan molecules fascinating properties, among these chitosan bears antibacterial, antifungine and antiviral activity, has the ability to coordinate and chelate metal ions and is able to interact with negatively charged polyelectrolytes through electrostatic interactions. In addition, chitosan is non-toxic, biocompatible, and biodegradable, has low allergenicity and is the second most abundant polysaccharide in nature behind only cellulose.

These characteristics make chitosan a very interesting molecule to use in several applications such as purification of wastewaters from heavy metals, dyes and organic compounds, as drug carries or excipient in the pharmaceutical field, as scaffold for bone tissue engineering, cartilage and nerve regeneration, and in the treatment of several diseases such as obesity and cardiovascular diseases (99).

Chitosan is used as wound dressings in emergency bleeding control and chronic wounds as it has hemostatic ability, absorbs wound exudate, enhances wound healing and has antimicrobial activity (100).

Several polymers are derived from chitosan by modification on three positions: the free amine groups on deacetylated units and the hydroxyl groups on the C3 and C6 carbons of both acetylated and deacetylated units. The scopes of these modifications are the improvement of its solubility and the widening of its applications (101).

Chemical derivatization based on the reactivity of the amine groups include acylation (102), alkylation (103), carboxymethylation (104) and quaternarization (105).

In 1984 Yalpani (106) described the modification of insoluble chitosan to soluble derivatives by chemical bonding of lactose and several other carbohydrates to the 2-amino functions of chitosan. These reactions lead to strong modifications of the physico-chemical and biological property of the polycation.

The lactitol derivative of chitosan was later named chitlac (CTL)(107). The properties of CTL depend on the properties of the chitosan used and the number of lactose moieties grafted to the NH_2 group of the polymer.

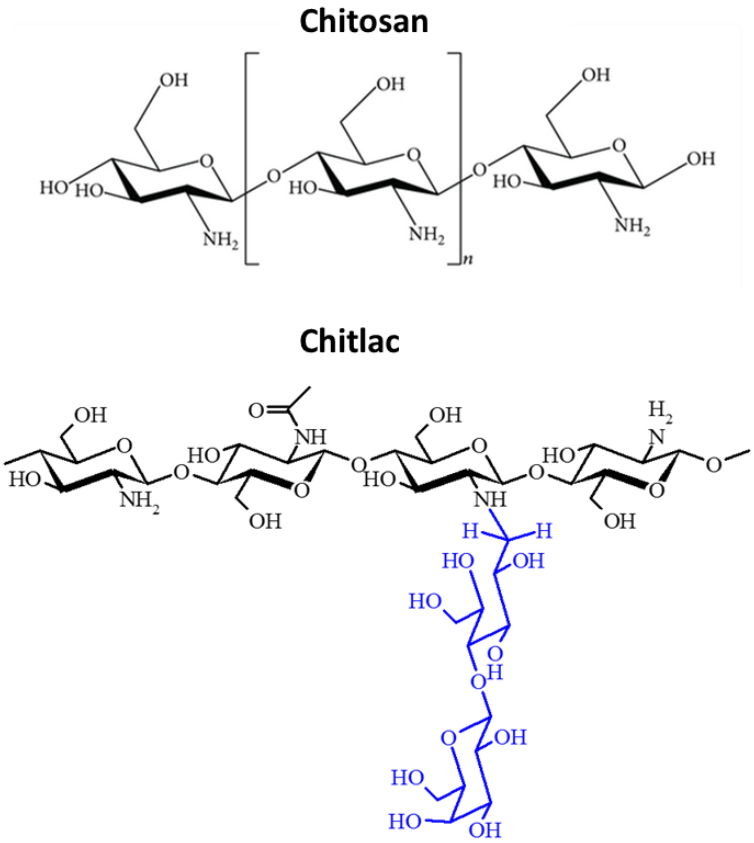

***Figure 1.7**: Chemical structure of chitosan and Chitlac*

At variance with chitosan, CTL is soluble in water at pH 7.4 and it is miscible with other negatively charged polyanions in physiological conditions. CTL, alginate and/or hyaluronan can be mixed together under proper experimental conditions and give rise to soluble complexes by interpolymer electrostatic interactions (108–110).

Chitlac bears a biologically active molecule since the galactose pendant groups are recognized by galectins, a family of soluble proteins able to recognize and bind to glycans and mediate several cellular functions (such as apoptosis, splicing, cellular adhesion)(111). CTL induces osteoblast and chondrocyte aggregation through a mechanism that involves Galectin-1 (107,112,113).

The addition of the lactitol moieties on the backbone preserves the ability of chitosan to coordinate metal ions. Chitlac was used as a stabilizing polymer for the synthesis of silver nanoparticles (nAgs) from silver nitrate in the presence of a reducing agent as reported by Travan et al. The mechanism involved in the stabilization of nAgs is due to coordination of metal ions by nitrogen atoms and a steric hindrance of the lactitol side chain that further protect the nanoparticles (7).

1.4. Biomaterials with antibacterial activity for wound healing

The loss of tissue integrity and the presence of necrotic tissue provide a favorable environment for bacterial growth. Thus, the wound is potentially at risk of infection, an important complication of all wounds. Infection originates from bacteria present in the environment, surrounding skin, and endogenous mucous membranes (gastrointestinal, oropharyngeal and genitourinary tract). Wounds that are in proximity or in contact with one of these sources as well as chronic wound, are at higher risk of infection (114).

Broad-spectrum antibiotic prophylaxis is routinely administered when surgery involves disruption of mucosal surfaces (115). Also infected chronic wounds require broad-spectrum antibiotics.

Systemic antibiotic administration has several negative effects like allergic reactions, disturbance of the normal intestinal flora, as well as induction of resistance and a reduced concentration in the site of infection. Acquisition of drug resistance occurs in a very short time since bacteria evolve rapidly, thus invalidating even the best antibiotic (116–118).

In the recent years, a lot of research has been focused on new broad-spectrum antimicrobial agents that can be efficient also into biofilms, and with low propensity to induce resistance. Several studies are focused on optimization of existing biomaterials to prevent bacterial adhesion and biofilm formation (e.g. antibacterial coatings for orthopedic biomaterials and catheters)(119), research for optimization of drug delivery, development of new antibiotic systems and biomaterials bearing antibacterial activity. Several biomaterials with antibacterial activity are already in use.

A first step of improvement in comparison to classic antibiotic therapy are biomaterials containing antibiotics for topical treatment that avoid several drawbacks of systemic administration but not acquisition of resistance from bacteria.

Many resources are focused on new antimicrobial compounds among which nanoantibiotics. Nanoantibiotics are defined as nanomaterials with intrinsic antimicrobial activity or that serve as vehicle for antimicrobial compounds by ameliorating their safety and effectiveness. The advantage of nanoantibiotics is connected to their mechanism of action, which involves multiple biological pathways thus rendering more difficult the acquisition of resistance. Moreover, they offer improved solubility, sustained and controlled release, improved patient-compliance, minimized side-effects, enhanced cellular uptake and long term stability even at high temperatures (120,121).

Nanoantibiotics are based on biopolymers (such as chitosan and antimicrobial peptides), carbon nanomaterials, surfactant-based nanoemulsions and metal or metal oxides (e.g. zinc, titanium, gold and silver)(120). In particular silver nanoparticles are very effective against microorganisms. The antibacterial activity of silver nanoparticles was shown to be shape-dependent and size-dependent (122,123).

Several wound dressings containing silver as silver nitrate, silver sulfadiazine, and nanocrystalline silver are already in commerce. Silver is a broad-range antibacterial agent that bears also anti-viral and anti-fungine activity. The use of silver into wound dressings is efficient against infections but cytotoxicity is an important drawback of these biomaterials (124).

A strategy for minimizing cytotoxicity is the entrapment of the nanoparticles into the biomaterial. Travan et al. have reported the use of non-cytotoxic round-shape and well dispersed silver nanoparticles embedded into CTL-alginate hydrogels. The production process of the silver nanoparticles (nAgs) requires the chemical reduction of silver ions to zeroth-valent metal nanoparticles in the presence of Chitlac polymer as stabilizing agent and ascorbic acid as reducing agent. The antibacterial activity against both Gram + and Gram - bacteria seems to be related to membrane damage, probably due to interaction of silver with thiol groups present at membrane level (7).

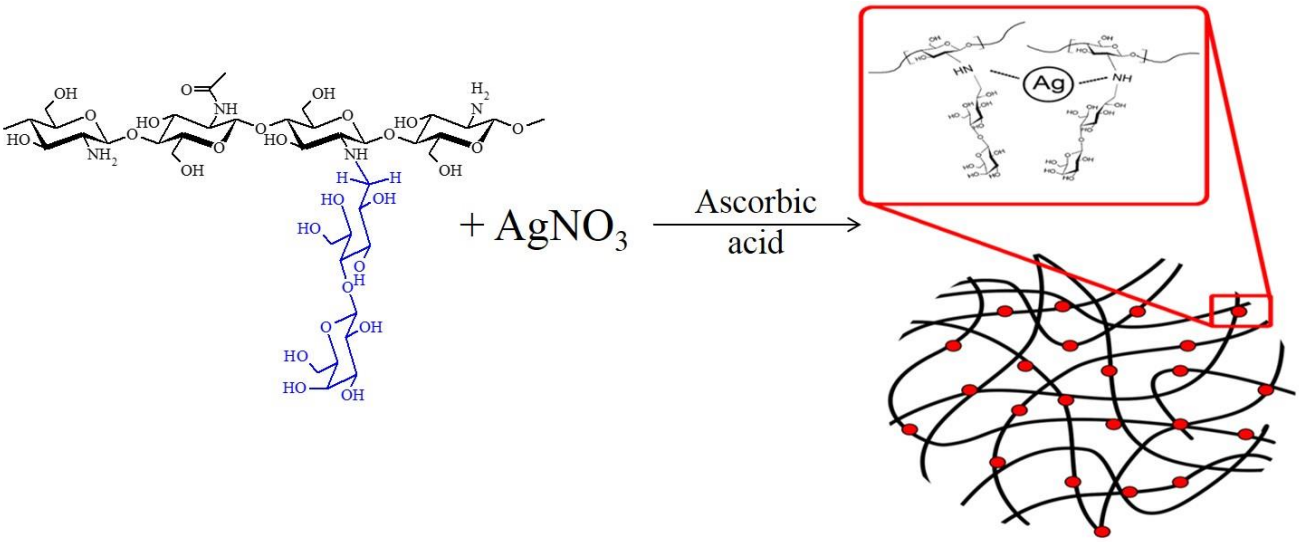

***Figure 1.8**: reaction of the synthesis of the colloidal suspension of silver nanoparticles (red) in the presence of a lactose (blue) modified Chitosan named Chitlac (CTL).*

CTL-nAg was used also as a coating for methacrylic thermosets for dental and orthopedic applications, fiber reinforced composites or nanocomposite scaffolds for bone implants and for chitosan membranes for chronic wounds. In these preparations embedded nanoparticles resulted with an efficient antibacterial activity and no cytotoxicity against eukaryotic cells (125–128).

2. Aim of the study

Although wound healing is a very finely regulated process which normally succeeds in the repair of the damages tissue, wound healing defects are still very common. Treatment of wound defects are based on the type of the defect and the site of the wound.

In this scenario, wound healing products (medical devices) that are thought specifically for the desired application are needed.

The study aims to develop and characterize novel bottom-up designed biomaterials for two biomedical applications, namely colorectal anastomosis and chronic non-healing wounds, by the use of the same manufacturing technology.

Several products are already available for wound healing. However, intestinal anastomosis healing is very difficult, and no efficient biomaterials exist for this application. In the case of chronic skin wounds, several products exist among which silver-based products. Many of these products are toxic towards eukaryotic cells, and not enough studies on their toxicity exist.

The biomaterial for colorectal anastomosis is based on the polysaccharides alginate and hyaluronic acid and will be called AnastomoSEAL patch since it was developed in the framework of the AnastomoSEAL project.

The biomaterial for the chronic non-healing wound application is based on alginate, hyaluronic acid and silver nanoparticles entrapped into a lactose –modified chitosan (Chitlac).

3. Materials and methods

3.1. Materials

Chitlac (lactose – modified chitosan, CAS registry number 85941-43-1) was synthesized starting from commercial chitosan from Sigma-Aldrich (degree of acetylation 18 %) as reported by Donati et al (107). The composition of Chitlac was determined by means of ^{1}H-NMR and resulted to be: glucosamine residues 20 %, N-acetyl-glucosamine 18 % and 2-(lactit-1-yl)-glucosamine 62 %. The relative MW of Chitlac is around 1.5×10^{6}.

HA of MW = 65 000 was obtained by degradation of HA 240 000; HA of MW= 800 000 and 1 500 000 were kindly provided by Novamatrix/FMC Biopolymer (Sandvika, Norway).

HA of MW∼240 000 (Phylcare Sodium Hyaluronate extra LW) and Hyaluronic acid butyric ester (HABut), Degree of substitution DS = 0.3, 1.0 and 1.8) were kindly provided by Sigea S.r.l. (Trieste, Italy).

Fluoresceinamine, 1-ethyl-3-[3-(dimethylamino)propyl]carbodiimide hydrochloride (EDC), N-hydroxusuccinimide (NHS) were purchased from Sigma.

Alginate from *Laminaria hyperborea* (Alginate Pronova UP LVG; MW= 120 000; fraction of guluronic residues, F_G = 0.69; fraction of guluronic diads, F_{GG} = 0.59; number average of G residues in G-blocks, N_G>1 = 16.3) was kindly provided by by Novamatrix/FMC Biopolymer (Sandvika, Norway). Alginate from Macrocystis pyrifera (M. Pyr., MW = 160 000; F_G = 0.42; F_{GG} = 0.21; N_G>1 = 5) was kindly provided by Prof. Gudmund Skjåk-Bræk, Institute of Biotechnology, University of Trondheim (NTNU) (Norway).

Calcium carbonate ($CaCO_3$), D-Gluconic acid δ-lactone (GDL), glycerol (ReagentPlus® ≥ 99.0%), sodium butyrate, C1-ethyl-3-[3-(dimethylamino)propyl]carbodiimide hydrochloride (EDC), N-hydroxusuccinimide (NHS), fluoresceinamine, 4-(2-hydroxyethyl)piperazine-1-ethanesulfonic acid (HEPES), ethylenediaminetetraacetic acid tetra sodium salt (EDTA), Mitomycin C, 2-(N-Morpholino)ethanesulfonic acid (MES), sodium chloride (NaCl), sodium bicarbonate ($NaHCO_3$), hydrochloric acid (HCl), silver nitrate ($AgNO_3$), ascorbic acid, bicinconinic acid, Copper (II) sulfate solution, MTT formazan powder [1-(4, 5-dimethylthiazol-2-yl)-3,5-diphenylformazan], glucose,

ethanol and Hanks' Balanced Salt solution (HBSS, product code H8264), phosphate buffered saline (PBS), Luria Bertani (LB) broth, LB Agar and Brain Heart Infusion (BHI) broth were purchased from Sigma-Aldrich (Chemical Co. U.S.A).

Hydroxy-methyl-2-propyl cellulose (HMPC, CAS number 9004-65-3, Pharmacoat 603, substitution type 2910) was purchased by Shin-Etsu (Tokyo, Japan).

Dulbecco's Modified Eagle's Medium high glucose and fetal bovine serum were from Euroclone (Italy). AlamarBlue® Cell Viability Reagent, Medium106 and Low serum Growth supplement were purchased from Life Technologies. MMP activity assay Kit (Fluorimetric-Green), MMP-9 and MMP-2 recombinant enzymes were from Abcam®.

All other chemicals and reagents were of the highest purity grade commercially available.

Simulated Body Fluid (SBF) was prepared according to the procedure reported by Kokubo (129).

3.2. Polysaccharide labeling

The labeling with fluoresceinamine of HA, HABut and alginate (to obtain HA-Fluo, HABut-Fluo, alginate-Fluo) was done according to the protocol reported elsewhere (130).

Briefly, NHS and EDC ([EDC]/[PolymRU] = 1.5; [NHS]/[EDC] = 1; were PolymRU refers to the polymer repeating units) were added to the polysaccharide solution (3 g/L) in MES buffer (50 mM, pH 5.5) containing 10 % ethanol. A solution of fluoresceinamine in ethanol was added to label 1/500 of the available carboxyl groups of alginate and 1/250 of the available carboxyl groups of HA or HABut.

The solutions were stirred overnight in the dark at room temperature, dialyzed against 0.05 M $NaHCO_3$ (2 shifts), 0.05 M NaCl (2 shifts) and abundantly against deionized water (until the conductivity at 4°C was below 2 µS). The pH was adjusted to 7.4; solution was filtered through 0.45 µm Millipore filters and then freeze-dried.

3.3. Production of Chitlac - coordinated silver nanoparticles

Silver nanoparticles were produced in presence of Chitlac and ascorbic acid as reported by Travan et al (7). Briefly, different quantities of CTL were dissolved in deionized water. Then $AgNO_3$ and ascorbic acid were added in different concentrations. Ascorbic acid concentration was used in a molar concentration equal to half of the concentration of $AgNO_3$. The solution was incubated overnight at room temperature in the dark and subsequently stored at 4°C. In order to select the best performing CTL-nAg, solutions with 1 g/L, 2 g/L, 4 g/L, 8 g/L and 10 g/L CTL in combination with 1 mM, 2 mM, 4 mM, 8 mM and 10 mM $AgNO_3$ were synthesized..

For the production of the CTL-nAg colloidal system to be used for patch production, the combination 4 g/L CTL, 2 mM $AgNO_3$ and 1 mM ascorbic acid was selected.

3.4. Plasmon resonance peak analysis of silver nanoparticles

The solutions were diluted 1:20 or 1:40 and UV-visible spectra was measured with scan speed of 300 nm/min using a Cary 400 spectrophotometer.

3.5. AnastomoSEAL patch production

The AnastomoSEAL patch was obtained in the form of a membrane through a multistep process.

The first step was the internal gelation of a mixture of alginate, HA and glycerol (final concentration 5% V/V) used as a plasticizing agent. The gelation was obtained by the addition of $CaCO_3$ and glucono-δ-lactone (GDL). The ratio $CaCO_3$ / GDL was 0.5 for each formulation studied; suspensions of $CaCO_3$ corresponding to $[Ca^{2+}]$ 20 mM or 50 mM were used. Immediately after GDL addition, the solution was poured into a Petri dish and incubated overnight at room temperature.

The second step consisted of a freeze-casting procedure: the hydrogel was stepwise cooled by immersion in a liquid cryostat (VWR international) containing ethyleneglycol in water 3:1 as refrigerant fluid. Temperature was decreased stepwise from +20°C to -20°C by 5°C steps with 30 min intervals for

equilibration. Subsequently the frozen hydrogels were dried under vacuum using a Single-Chamber Freeze-Dryer (Christ Alpha 1-2 LDplus).

Several membrane formulations were prepared as reported hereafter:

- Patch A: Alginate (*L. hyp.*) 15 g/L, $CaCO_3$ 20 mM, GDL 40 mM, glycerol 5% v/v;
- Patch B: Alginate (*L. hyp.*) 15 g/L, HA (800 000) 15 g/L, $CaCO_3$ 20 mM, GDL 40 mM, glycerol 5% v/v;
- Patch C: Alginate (*L. hyp.*) 20 g/L, HA (240 000) 15 g/L, $CaCO_3$ 20 mM, GDL 40 mM, glycerol 5% v/v;
- Patch D: Alginate (*L. hyp.*) 15 g/L, HA (240 000) 15 g/L, $CaCO_3$ 20 mM, GDL 40 mM, glycerol 5% v/v;
- Patch E: Alginate (*L. hyp.)* 15 g/L, HA (240 000) 15 g/L, $CaCO_3$ 50 mM, GDL 100 mM, glycerol 5% v/v.
- Patch F: Alginate (*L. hyp.*) 15 g/L, $CaCO_3$ 50 mM, GDL 100 mM, glycerol 5% v/v;
- Patch G: Alginate (*L. hyp.*) 15 g/L, HA (800 000) 15 g/L, $CaCO_3$ 50 mM, GDL 40 mM, glycerol 5% v/v;
- Patch H: Alginate (M*. pyr.*) 15 g/L, HA (240 000) 15 g/L, $CaCO_3$ 20 mM, GDL 40 mM, glycerol 5% v/v;
- Patch I: Alginate (M*. pyr.*) 15 g/L, HA (240 000) 15 g/L, $CaCO_3$ 50 mM, GDL 100 mM, glycerol 5% v/v;
- Patch J: Alginate (M*. pyr.*) 15 g/L, $CaCO_3$ 50 mM, GDL 100 mM, glycerol 5% v/v;
- Patch K: Alginate (*L. hyp.*) 15 g/L, NaCl 75 mM, $CaCO_3$ 50 mM, GDL 100 mM, glycerol 5% v/v;
- Patch L: Alginate (*L. hyp.*), HA (240 000) 10 g/L, $CaCO_3$ 50 mM, GDL 100 mM, glycerol 5% v/v;

3.6. Production of chronic non-healing wound membranes

The multistep process employed for the production of chronic non-healing wound membranes is very similar to the one used for the AnastomoSEAL patches although different Alginate / HA ratios were used and the system Chitlac-nAg was added in the formulation. HPMC was used as a foaming agent in order to obtain a foamed membrane so increasing the surface/volume ratio of the material

Alginate from *Laminaria hyperborea* and HA of MW = 240 000 were mixed in 8:4 ratio until complete dissolution. Then HEPES buffer was added to a final concentration of 0.01 M. CTL-nAg solution was then added by dripping. The CTL-nAg used for all the membranes was obtained from CTL 4 g/L, $AgNO_3$ 2 mM and 1 mM ascorbic acid.

The foaming agent (HPMC) was added to the polymer solutions and immediately after GDL was added; the solution was foamed with a foam maker for 30 seconds and then poured into a Petri dish.

Several formulations were prepared as reported hereafter:

- *Formulation A*: Alginate 8 g/L, $CaCO_3$ 20 mM, GDL 40 mM, glycerol 5 % v/v;
- *Formulation B:* Alginate 8 g/L, HPMC 4 g/L, $CaCO_3$ 20 mM, GDL 40 mM, glycerol 5 % v/v;
- *Formulation B-2*: Alginate 8 g/L, HPMC 4 g/L, $CaCO_3$ 20 mM, GDL 40 mM;
- *Formulation C*: Alginate 8 g/L, HPMC 6 g/L, $CaCO_3$ 20 mM, GDL 40 mM, glycerol 5 % v/v;
- *Formulation D*: Alginate 8 g/L, CTL-nAg, $CaCO_3$ 20 mM, GDL 40 mM, glycerol 5 % v/v;
- *Formulation E:* Alginate 8 g/L, CTL-nAg, HPMC 4 g/L, $CaCO_3$ 20 mM, GDL 100 mM, glycerol 5 % v/v;
- *Formulation E-2*: Alginate 8 g/L, CTL-nAg, HPMC 4 g/L, $CaCO_3$ 20 mM, GDL 100 mM, glycerol 5 % v/v;
- *Formulation F:* Alginate 8 g/L, CTL-nAg, HPMC 6 g/L, $CaCO_3$ 20 mM, GDL 40 mM, glycerol 5 % v/v;
- *Formulation G:* Alginate 8 g/L, HA 2 g/L, HPMC 4 g/L, $CaCO_3$ 20 mM, GDL 40 mM, glycerol 5 % v/v;
- *Formulation G-2*: Alginate 8 g/L, HA 2 g/L, HPMC 4 g/L, $CaCO_3$ 20 mM, GDL 40 mM;
- *Formulation H:* Alginate 8 g/L, HA 4 g/L, HPMC 4 g/L, $CaCO_3$ 20 mM, GDL 40 mM, glycerol 5 % v/v;
- *Formulation H-2*: Alginate 8 g/L, HA 4 g/L, HPMC 4 g/L, $CaCO_3$ 20 mM, GDL 40 mM;
- *Formulation I:* Alginate 8 g/L, HA 6 g/L, HPMC 4 g/L, $CaCO_3$ 20 mM, GDL 40 mM, glycerol 5 % v/v;
- *Formulation I-2*: Alginate 8 g/L, HA 6 g/L, HPMC 4 g/L, $CaCO_3$ 20 mM, GDL 40 mM;
- *Formulation J*: Alginate 8 g/L, HA 2 g/L, CTL-nAg, HPMC 4 g/L, $CaCO_3$ 20 mM, GDL 40 mM, glycerol 5 % v/v;
- *Formulation J-2*: Alginate 8 g/L, HA 2 g/L, CTL-nAg, HPMC 4 g/L, $CaCO_3$ 20 mM, GDL 40 mM;

- *Formulation K*: Alginate 8 g/L, HA 4 g/L, CTL-nAg, HPMC 4 g/L, $CaCO_3$ 20 mM, GDL 40 mM, glycerol 5 % v/v;
- *Formulation K-2:* Alginate 8 g/L, HA 4 g/L, CTL-nAg, HPMC 4g/L, $CaCO_3$ 20 mM, GDL 40 mM;
- *Formulation L*: Alginate 8 g/L, HA 6 g/L, CTL-nAg, HPMC 4 g/L, $CaCO_3$ 20 mM, GDL 40 mM, glycerol 5 % v/v;
- *Formulation L-2*: Alginate 8 g/L, HA 6 g/L, CTL-nAg, HPMC 4 g/L, $CaCO_3$ 20 mM, GDL 40 mM;
- *Formulation M*: Alginate 8 g/L, HA 4 g/L, CTL 4 g/L, HPMC 4 g/L, $CaCO_3$ 20 mM, GDL 40 mM, glycerol 5 % v/v;
- *Formulation M-2:* Alginate 8 g/L, HA 4 g/L, CTL 4 g/L, HPMC 4 g/L, $CaCO_3$ 20 mM, GDL 40 mM;

Alginate, $CaCO_3$ and GDL concentrations were maintained constant.

3.7. Quantification of HA and alginate release from the patch

Since both HA and alginate are chiral molecules and absorb in the UV range, circular dichroism was used for the quantification of HA and alginate released.

Simultaneous quantification of both polymers is possible since their CD spectra are different in the 230-200 nm interval of wavelength, with a maximum difference at 210 nm. Moreover, for both polymers ellipticity is directly proportional to their concentration (131). Following the Lambert-Beer law, ellipticity of the sample at a certain wavelength is proportional to its concentration:

$$\vartheta = [\vartheta] * l * c$$

Were: ϑ is reduced ellipticity in mdeg*cm^2/g,
l is the optical path in cm
c is the concentration in g/L.

The hypothesis was that the mixture ellipticity ($[\vartheta]_{rec}$) – with unknown fraction of HA and alginate but known total quantity of polymers – was equal to the sum of the ellipticity of each polymer multiplied to the fraction of the polymer (F) according to the equation:

$$[\vartheta]_{rec} = F_{alg} * [\vartheta]_{alg} + F_{HA} * [\vartheta]_{HA}$$

were $F_{HA} = 1 - F_{alg}$

This equation was solved for a range of wavelengths of 205-215 nm.

For the quantification of HA and alginate released, patches of 3.5 cm of diameter were immersed in 10 mL of MQ water or SBF for selected time intervals.

Then the supernatants were collected and dialyzed for two days against 0.1 M HCl (4 shifts) in order to remove Ca^{2+} ions. Dialysis was performed then against deionized water until the conductivity of the solution at 4°C was below 4 µS. The solution was collected and pH set at 7.2. Dialyzed supernatant was then freeze-dried and the mixture of lyophilized polymers was weighted in order to obtain the total mass of released polymers. A solution of 0.1 g/L of the mixture was prepared and the spectra were obtained by a *Jasco J-700* spectropolarimeter and a quartz cell with 1 cm optical length. The following setup was used: bandwidth, 1 nm; time constant, 2 s; scan rate, 20 nm/min. Spectra were recorded for the wavelengths in the range of 205-250 nm, at room temperature and with acquisition step of 0.2 nm. For every sample four acquisitions were performed. Raw data were normalized by the concentration of the polymeric solution, and they were expressed as percentage of released polymer.

3.8. Fluorescent microscopy of hydrogels

For the study of the distribution of the polysaccharides into the hydrogel, HA-fluo and Alginate-fluo (labelled with fluoresceinamine) were used for biomaterial production. After gelation, hydrogels were sectioned and the fluorescent signal was acquired on the cross section surfaces (xy plane) from edge to edge of the samples.

Fluorescence was acquired with a Nikon Eclipse C1 confocal microscope system on a Nikon TE-2000U inverted by the use of a 20X objective and λ_{ex} 488 nm and λ_{em} 515/30 nm. Image data analysis was done using software Image J (http://rsb.info.nih.gov/ij/index.html; NIH, Bethesda, USA) in order to measure the intensity profiles of the fluorescent sections. For each sample, fluorescence intensity was normalized on the maximum intensity recorded, while the cross section width was normalized on the hydrogel thickness in order to qualitatively compare the different samples.

Patch D and Patch E were analyzed after preparation with either labelled alginate or labelled HA. Gels containing non-labeled polymers were used as negative control.

3.9. Swelling ratio

In order to study the swelling behavior of the freeze-dried materials, they were cut into pieces of 20 mm of diameter, weighted and immersed in 10 mL of HBSS at room temperature. After 1, 2, 10, 30, 45 and 60 minutes biomaterials were blotted for 1 minute on a filter paper and weighted. The swelling ratio was calculated as the ratio between the weight at time X and the initial dry weight at time 0, following the equation:

$$Swelling\,ratio = \frac{Weight\,at\,time_x}{Weight\,at\,time_0}$$

3.10. Scanning Electron Microscopy (SEM)

For the structural analysis of the freeze-casted patches, a Leica-Stereoscan 430i Scanning electron microscope was used. Patches were sputter-coated with gold and directly visualized at the top view and cross view.

3.11. Silver release from patches

For the quantification of released silver, pieces of 60 mg of the material with Formulation K were immersed in 3 mL of HBSS for 2, 24, 72 hours and 7 days. At the defined time, the tested material was removed from HBSS and 0.5 mL of NH_4OH 1 N were added in order to solubilize silver precipitates. The sample material was washed in 3 mL HBSS for 2 minutes and, after removing, 0.5 mL NaOH 1 N were added to the solution. Both release-solution and washing-solution were used for the measurement. The sample with Formulation H (45 mg) was used as negative control.

Measurements were performed by Electro-Thermal Atomic Absorption Spectrometry (ETAAS) with Zeeman background correction. A Thermo M series AA spectrometer equipped with a GF95Z Zeeman Graphite Furnace and a FS95 Furnace Autosampler (Thermo Electron Corporation, Cambridge, UK) were used for analysis. The obtained values have been compared with a calibration curve calculated with a standard solution of silver (Silver ICP/DCP-Sigma Aldrich). The limit of detection (LOD) at the analytical wavelength of 328.1 nm was 0.5 µg/L and the precision of the measurements as repeatability (RSD%) for the analysis was always less than 5%.

Data analysis was performed by summing the silver found in the release-solution and the washing-solution. The values were express as percentage of silver released in comparison with the total amount of silver contained into the tested sample (148 µg/60 mg of patch).

3.12. Water-vapor transmission rate

For determining the ability of the patches to transmit vapor, ASTM E96 standard test method for Water-Vapor Transmission of materials was used.

Glass bottles with a top closure of 16 mm of diameter were filled with mQ water in order to have 2 cm of distance between the water and the sample, closed with a round shaped piece of sample of 17 mm of diameter and sealed laterally with parafilm. The bottle was weighted and incubated for 24 and 48 hours at 32 ± 0.4°C and 45 ± 2% humidity. At the end of the incubation time the bottle was weighted.

Commercially available dressings were used as control materials: Connettivina plus® (Fidia farmaceutici s.p.a) and Chitoderm™ (Pietrasanta Pharma). Furthermore, not capped bottles and bottles capped with parafilm were used as control for free evaporation and no evaporation.

Water-vapor transmission rate was calculated according to the formula:

$$WVTR \quad (g/m^2h) = \frac{W_{24h} - W_0}{A * 24h}$$

were:

W_{24h} = weight at 24 hours (in grams),

W_0 = initial weight of the filled and capped bottle (in grams),

A = area of the top closure of the bottle (in m^2).

Four replicates were measured per each sample and the analysis was performed by calculating the average values and the standard deviations of samples both at 24 and 48 hours.

3.13. Mechanical characterization

Mechanical characterization was done according to ASTM D638 –by using a Universal Testing Machine (Multitest Mecmesine 2.5-i) with load cell of 100 N**.** The membranes were carved with a cutter into dog-bone shape (figure 3.1) and gripped with metallic clamps.

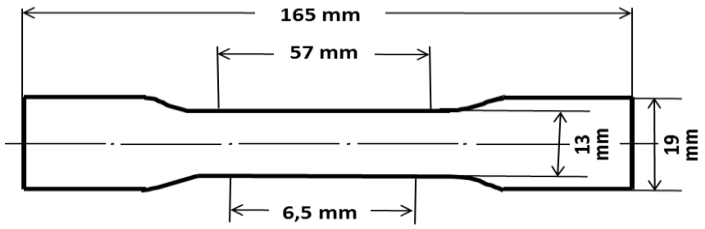

Figure 3.1: *Shape of samples for uniaxial tensile test*

Tensile tests were performed at a crosshead speed of 5 mm/min. Tensile stress was calculated dividing the load by the average original cross sectional area in the gage length segment of the specimen. Young's Modulus was calculated as the slope of the linear portion in the stress-strain curve, considering the deformation range of 1%-3%. For each formulation, 5 replicates were used and the data were averaged and standard deviations calculated.

3.14. Antimicrobial tests

To assess the antimicrobial activity of patches three different bacterial strains were used: *Staphylococcus aureus* (ATCC® 25923™), *Staphylococcus epidermidis* (ATCC® 12228™) and *Pseudomonas aeruginosa* (ATCC® 27853™). Two different protocols were employed: bacteria growth inhibition assay and biofilm formation inhibition assay.

3.14.1. Bacteria growth inhibition assay

Patch samples were cut into pieces of 40 mg and sterilized under UV rays. Bacteria were inoculated in Luria Broth medium (LB) and incubated for 16 hours at 37°C. After 16 h, 500 µL of bacterial suspension was diluted in 10 mL of broth and grown up for 120 min at 37 °C in order to restore an exponential growth phase. The optical density at 600 nm was measured in order to assess bacterial concentration. Bacteria were diluted to $5x10^6$ CFU/mL in 10% (V/V) LB in PBS and 1 mL of bacteria was added to each sample and incubated for 24 hours at 37°C. Tests were carried out in shaking condition (140 rpm) to optimize the contact between bacteria and membranes. At the end of the incubation time, bacterial solutions were diluted in PBS (from 10^{-1} to 10^{-5}) and 25 µL of each suspension was spread on LB agar. After overnight incubation at 37°C, the colony forming units (CFU) were counted. A suspension of bacteria grown in liquid medium was used as control.

3.14.2. Biofilm formation inhibition assay

Staphylococcus aureus and *Pseudomonas aeruginosa* were inoculated in Brain Heart Infusion (BHI) broth plus 3% w/V sucrose and incubated for 16 hours at 37°C. Bacteria were then diluted 1:100 in the same broth and seeded (300 µL/well) into 24-well plates for 48 hours in static conditions at 37 °C. Broth was then removed and biofilm was carefully rinsed twice with 100 µL of sterile PBS in order to remove non-adherent cells. 300 µL of PBS were added to each well and circular specimens of patches (40 mg) were deposited on the bacterial layer and incubated for 24 hours. MTT assay was performed. MTT stock solution was prepared by dissolving 5 mg/mL of MTT powder in PBS and sterilized by filtration. Membranes and PBS were gently removed from the plates and each well was carefully rinsed three times with 100 µL of PBS. 200 µL of MTT solution (prepared by mixing 0.5 mL of MTT stock solution and 4.5 mL of sterile PBS) were placed into each well and the plates were incubated for 3 h under light-proof conditions at 37°C. The MTT solution was then gently removed and formazan crystals were

dissolved by adding 200 µL of DMSO to each well. Plates were stored for an additional 1 h under light-proof conditions at room temperature and then 80 µL of the solution were transferred into the wells of a 96-well plate and absorbance was measured using a spectrophotometer (Infinite M200 PRO NanoQuant, Tecan) at a wavelength of 550 nm. Outcomes were expressed as optical density (O.D.) units.

For confocal laser scanning microscopy (LSCM) analyses of biofilm, bacteria were seeded on sterile 13 mm tissue culture coverslips (Sarstedt, U.S.A.) inside 24-well plate. After biofilm growth and treatment with membranes as described above, FilmTracer Live/Dead biofilm viability kit (Invitrogen™) was used for biofilm staining according to the manufacture's protocol. Images were acquired using a Nikon Eclipse C1si confocal laser scanning microscope with a Nikon Plan Fluor 20X as objective. Resulting stacks of images were analyzed using Image J software. The ratio between red and green signal was calculated as:

$$Normalized\ rate = \frac{Sample\left(\frac{Red}{Green}\right)}{Control\left(\frac{Red}{Green}\right)}$$

were:

Red = mean grey value of the red channel
Green = mean grey value of green channel

3.15. Cell culture

Primary human dermal fibroblasts (HDFa) were purchased from Gibco™. Cells were grown in Medium 106 supplemented with Low serum Growth supplement, 100 U/mL penicillin, 100 µg/mL streptomycin.

Human keratinocyte cell line HaCaT (kindly gifted by Dr. Chiara Florio, University of Trieste) and mouse fibroblast NIH-3T3 cell line (ATCC® CRL1658) were grown in Dulbecco's Modified Eagle's Medium high glucose, 10% heat-inactivated fetal bovine serum, 100 U/mL penicillin, 100 µg/mL streptomycin and 2 mM L-glutamine.

Human colonic epithelial cell line NCM356, derived from normal colonic mucosa, was obtained by a materials transfer agreement with INCELL Corporation, San Antonio, TX. Cells were grown in M3:BaseA^{TM} (INCELL, St. Antonio, TX) supplemented with 10% fetal bovine serum (FBS).

Cells were maintained at 37°C in a humidified, 5% CO2 environment.

3.16. Cell viability and proliferation assay

Cell viability was determined through Alamar blue assay which is based on the detection of the metabolic activity of cells. It contains resazurin, a blue non-fluorescent reduction-oxidation indicator that is reduced to resorufin in the presence of cells. Resorufin is a pink fluorescent product and its production is proportional to cell metabolism.

Cells were seeded on 96-wells plates: NCM356 cells and NIH3T3 cells were seeded 2 000 cells/well; HDFa cells and HaCaT cells were seeded 3 000 cells/well.

After adhesion, cells were treated with HA, HABut, butyrate or HPMC dissolved in complete medium and sterilized by filtration. In the case of butyrate, fresh medium containing butyrate was replaced every 24 hours since it is rapidly metabolized by cells. At defined times, medium was removed and replaced with 150 µL Alamar Blue diluted 1:10 in fresh culture medium. Cells were incubated 4 h in the dark, at 37°C in 5% CO_2. 100 µL of the Alamar Blue solution were then transferred in a black 96-well microtiter plate and fluorescence was measured in a microplate reader (Tecan) at 544/616 nm. Cell viability was expressed as growth rate (Fluorescence at Day_n / Fluorescence at Day_0).

3.17. Biocompatibility test

The biocompatibility of the silver-containing patches (Formulations B-2, E-2, G-2, H-2, I-2, J-2, K-2, L-2, M-2) was performed according to ISO10993-5:2009 International Standard specifications by direct-contact test and by extract test.

3.17.1. Direct-contact test

Patches were cut using biopsy punches into cylinders of 4 mm of diameter and sterilized under UV-rays.

HDFa and HaCaT cells were seeded in 24-well plates at a density of $2x10^4$ cells per well and 16 hours later, individual specimens of the test sample were placed directly on the cell layer for 24 and 72 hours. Samples were then removed, cells were washed in PBS and 250 µL of Alamar Blue dye diluted 1:10 in culture medium was added and incubated for 4 hours. 100 µL of Alamar solution were transferred in a 96-well microtiter plate and fluorescence was measured with a microplate reader (Tecan Infinite® M100 Pro) at λ_{ex} 544 nm / λ_{em} 616 nm. As positive control material, polyurethane films (PU) containing 0.25% zinc dibuthyldithiocarbamate (ZDBC) (6 mm disks) were used (Hatano Research Institute / Food and Drug Safety Center Reference Material Office - Japan). As negative control material, polystyrene sheets (PS, 6 mm disks) were used (Wako Pure Chemical Industries).

3.17.2. Extract test

UV-sterilized samples were placed in Dulbecco's modified Eagle's medium, 10% FBS, penicillin 100 U/mL, streptomycin 100 µg/mL and L-glutamine 2 mM for 24 h at 37 °C. The ratio between sample weight and medium volume was 10 mg/mL for the patch with Formulation B-2, 12.5 mg/mL for Formulation G-2, 15 mg/mL for Formulations E-2 and H-2, 17.5 mg/mL for Formulations I-2 and J-2, 20 mg/mL for Formulations K-2 and M-2, 22.2 mg/mL for Formulations L-2, in order to maintain constant the weight of alginate for all formulations.

HDFa and HaCaT cells were seeded in 96-well microtiter plates at a density of 3 000 cells/well and after 16 hours treated with the medium containing the components released from specimens . For HaCaT cells, the extracts containing the components released were used also diluted 1:2 and 1:10 in culture medium.

After 24 and 72 hours medium was removed and replaced with 120 µL of Alamar Blue dye diluted 1:10 in fresh culture medium. Cells were incubated 4 hours in the dark, at 37°C in 5% CO_2. 100 µL of Alamar Blue solution were then transferred in 96-well microtiter plates and fluorescence was measured in a microplate reader (Tecan Infinite® M100 Pro) at λ_{ex} 544 nm / λ_{em} 616 nm. As positive control 0,005%

(V/V) Triton X-100 in culture medium was used and cells grown in flat medium were considered for positive control. .

3.18. BCA assay for total protein quantification

For total protein quantification cells were washed and lysed with lysis buffer (0.5 mM Tris-HCl pH 6.8, 0.2% N-laurylsarcosine, 0.2 mM PMSF and 2 mM DTT), incubated for 5 minutes at room temperature, collected and frozen at -20°C.

5 µL of each sample were incubated with 200 µL of BCA mix (50 parts Bicinconinic acid and 1 part of Copper (II) sulfate solution) for 20 minutes at 65°C. Absorbance was measures at 544 nm. For the BCA calibration curve were used 0, 1, 2, 4, 6, 8, 10 µg of bovine serum albumin (BSA).

3.19. Extracellular matrix production

The effects of HA and HABut on extracellular matrix produced by fibroblasts were studied in terms of Glycosaminoglycans (GAGs) and collagen type I production.

3.19.1. Glycosaminoglycan production by fibroblasts after HA and HABut treatment

For the glycosaminoglycan quantification a colorimetric assay as previously described (132) was used . The assay is based on the ability of sulfated GAGs to bind the cationic dye 1,9-dimethylmethylene blue (DMMB)).

HDFa cells were seeded at a density of 5×10^4 cells/well on 12-wells plate and after 16 hours were treated with HA (MW=240 000) or HABut (DS=0.3) at the concentrations of 6 g/L and 0.5 g/L.

After 6 days of treatment, cells were washed twice in PBS. Then some samples were used for protein quantification by BCA method and some samples for GAGs quantification.

For GAGs quantification cells were lysed with 500 µL of lysis buffer (0.2 M sodium phosphate, 0.1 M sodium acetate, 0.01 M EDTA, 0.005 M cysteine hydrochloride, 1 U/mL papain). After overnight

incubation at 60°C, cells were collected by centrifugation for 10 minutes at 1.500 rpm. 150 µL of the supernatant or known quantities of chondroitin sulfate were incubated for 1 hour at room temperature with 250 µL of dye solution (21 mg/L DMMB, 0.005% ethanol, 2 g/L sodium formate at pH 3.0).

200 µL of mixture were transferred in 96-well plates and read at 544 nm and 620 nm with a microplate reader (Tecan Infinite® M100 Pro).

For each sample, GAGs quantity (in µg) was normalized to protein content (in µg).

3.19.2. Production of type 1 collagen from fibroblasts after HA and HABut treatment

For collagen quantification an ELISA test was used (MicroVue CICP EIA, QUIDE, USA). It measures the type I C-terminal collagen propeptide (CICP) released into the culture medium after the cleavage of collagen during its maturation process. CICP peptide can be used as an indicator of collagen production since it is proportional to the quantity of collagen produced.

HDFa cells were seeded in 96-wells microplate ($5x10^3$ per well). After 16 hours, cells were treated with HA (MW = 240 000) or HABut (DS = 0.3) at the concentrations of 6 g/L and 0.5 g/L dissolved in culture medium and sterilized by filtration. After 48 hours, the culture medium was collected and used for the quantification of the CICP peptide following the manufacturer's indications. An Alamar blue assay was performed on the adherent cells. For each sample, collagen quantity (in ng of CICP) was normalized to Alamar Blue fluorescence intensity.

3.20. Scratch test

HDFa, HaCaT and NCM356 cells were seeded in 6-well plates at a density of $2.5x10^5$, $3.5 x10^5$ and $8x10^5$ cells, respectively and incubated at 37°C until reaching a confluent monolayer.

Cells were then treated with HA (MW = 240 000) or HABut (DS = 0.3) at the concentrations 6 g/L and 0.5 g/L or with medium containing components released from the membranes prepared following the protocol described above for the cytotoxicity extract test. In order to study the contribution of cell migration on scratch closure, proliferation was blocked by treating the cells also with 1 mg/L Mitomycin (inhibitory concentration was first evaluated by Alamar blue assay).

24 hours after treatment cell layers were scratched with a 200 µl pipette tip and the scratch closure was followed over time through an Olympus CK2 Inverted Microscope (Phase Condenser ULWCD 0.3) equipped with a camera Canon PowerShot A630. The images of the scratch were acquired over time to monitor the gap closure. The analysis was performed using software Image J: the region of interest (ROI) was outlined per each scratch and the percentage of closure over time was plotted. For each sample, eight images were analyzed (133).

3.21. Flow cytometry analysis for CD44 expression

Flow cytometry was used in order to study the expression of the CD44 receptor in NCM356 cells: $5x10^5$ cells per sample were collected, washed in PBS and suspended in 0.5% BSA, 0.1%NaN_3 in PBS. Cells were then treated with a phycoerythrin-conjugated monoclonal anti-human CD44 antibody (Immunotools) or with a mouse IgG2b conjugated with phycoerythrin (Immunotools) for isotype control, incubated at 4°C for 45 minutes and washed twice in PBS (both antibodies were diluted 1:25 – 1:50). Data were collected with a Cytomics FC500 instrument (Beckman-Coulter Inc, Fullerton, CA, USA) equipped with an Argon laser (488 nm, 5 mV) and with a standard system configuration for red-filtered (610 nm, FL3) and green-filtered (525 nm, FL1) fluorescent detection. At least 10 000 events were acquired for each sample, and stored as listmode files for analysis thereafter. FL1/FL3 histograms were analyzed with the WinMDI software (Dr. J. Trotter, Scripps Research Institute, La Jolla, CA, USA). Non treated cells were used as negative control.

3.22. Flow cytometry analysis for HA and HABut binding

Binding and internalization of HA and HABut by HDFa and NCM356 cells was evaluated through cytofluorimetric analysis of cells treated with HA-Fluo and HABut-Fluo.

Cells were seeded at a density of $5x10^4$ cells/well. After 16 hours, cells were treated with HA-Fluo or HABut-Fluo 5 g/L dissolved in culture medium and sterilized by filtration. After 24 hours of treatment, cells were collected by tripsinization and washed twice in PBS.

Data collection was performed by cytofluorimetry as already described for the CD44 expression test. In particular, FL1 saved histograms were submitted for the analysis of HA-Fluo and HA-But fluo signals. Non treated cells were used as negative control.

In order to distinguish between surface binding and cellular internalization of the polymers, extracellular fluorescence was quenched with Trypan blue (0.5%).

3.23. Flow cytometry analysis of apoptosis

Annexin V/propidium iodide dual fluorescence flow cytometry assay was used to evaluate cellular apoptosis after incubation with butyrate. UV-irradiated cells were used as apoptosis positive control. Assay was performed using the Annexin V-FITC Apoptosis Detection kit by Sigma. Cells were treated with butyrate and after a defined time (48 and 72 hours) were collected by trypsinization and treated according to the manufacture's protocol

Data collection was performed by cytofluorimetry how already described for the CD44 expression assay. In particular, FL3 saved histograms were submitted for the analysis of the cell cycle, performed by MultiCycle® software.

3.24. Flow cytometry analysis of cell cycle

For cell cycle analysis, NCM356 cells were treated with different concentrations of sodium butyrate in culture medium and collected by trypsinization after 8, 24 and 48 hours.

The cells were washed with PBS and fixed in 70% ethanol for at least 4 h at 4°C. For staining, fixed cells were washed twice with PBS and allowed to balance in PBS for 2 h. Pellets were then stained overnight with a dying mixture (0.5 ml/tube) of PBS solution containing 0.01 mg/mL propidium iodide, 0.25 mg/L FITC, and 40 mg/L RNase (all from Sigma Chemicals Co.). Data collection was performed by cytofluorimetry how already described for the CD44 expression assay.

3.25. Cellular antioxidant activity (CAA) analysis

The intracellular formation of peroxide radicals was detected by the method of Wolfe and Liu (134). NCM356 cells were seeded at a density of 5×10^3 cells/well on a 96-well microplate in 100 µl of growth medium/well. The outside wells of the plate were not used. Twenty-four hours after seeding, the growth medium was removed, the wells were washed with PBS and, treated for 1 h with butyrate plus 50 µM of 2,7-dichlorodihydrofluorescein diacetate (DCFH-DA, Sigma) dissolved in culture medium without FBS. After the indicated period, cells were washed and 5 mM of 2,2'-Azobis(2-amidinopropane) dihydrochloride (ABAP) (Sigma) dissolved in HBSS was added to the cells. Fluorescence was measured (λ_{ex} = 485 nm, λ_{em} = 528 nm) every 5 min for 1 h at 37 °C in a microplate reader (Tecan Infinite® M100 Pro). Each concentration of butyrate was replicated in six wells. Each plate also included six control and six blank wells: control wells contained cells treated with the dye (DCFH-DA) and the oxidant (ABAP); blank wells contained cells treated with DCFH-DA and HBSS without the oxidant. After blank subtraction from fluorescence readings, the area under the curve of fluorescence versus time was integrated to calculate the CAA value at each concentration of butyrate as follows:

$$\text{CAA units (\%)} = 100 - (\int SA/\int CA) \times 100$$

where

$\int SA$ = the integrated area under the sample fluorescence plot versus time curve
$\int CA$ = the integrated area from the control curve.

According to this formula, CAA units for cells treated only with ABAP (control) are equal to zero, for cells non-treated with ABAP are equal to 100. Quercetin (1 and 5 µM) was used in substitution to butyrate as positive control for an anti-oxidant activity.

3.26. Treatment of NCM356 cells with sodium butyrate and hydrogen peroxide (H_2O_2)

NCM356 cells were seeded at a density of 5×10^4 cells/well on a 96-well microplate in 200 µl of growth medium/well. Eighteen hours after seeding, cells were pretreated for 2 h with butyrate and following with 100 and 300 µM of H_2O_2 for 24 hours. Culture medium was then removed, cells washed in PBS and

treated for 4 hours with 100 µL of fresh culture medium added with Alamar Blue dye. Fluorescence emission was measured at 590 nm with excitation wavelength at 530 nm. Results are expressed as percentage of live cells versus control (cells no treated with H_2O_2).

3.27. Glutathione-S-Transferase (GST, EC 2.5.1.13) activity assay

The GST activity was determined using 1-chloro-2,4-dinitrobenzene (CDNB) as the substrate as described elsewhere (135), with some modifications. Briefly, cells were seeded ($2x10^5$ cells/well) in a 12-wells plate. After twelve hours, cells were treated with butyrate for a defined time, collected by tripsinization, and lysed with 200 µl of lysis buffer [50 mM potassium phosphate (pH 7.0), 1 mM EDTA, and 250 mM sucrose].

The absorbance was read in a Tecan Infinite® M100 Pro plate reader at 340 nm immediately after preparing the reaction tests and, every minute thereafter to obtain six time points. The linearity of the reaction was determined by plotting the absorbance values against time.

The change in absorbance (ΔA340)/minute, in the linear range of the plot, was determined for the sample and for the blank using the following equation:

$$\frac{\Delta A340}{min} = \frac{A340_{\,final\ read} - A340_{initial\ \ read}}{reaction\ time_{\,min}}$$

GST specific activity was calculated with the formula:

$$\frac{\frac{\Delta A340}{\min} * V_{mL} * dil}{Venz_{mL} * \varepsilon_{mM}} = \mu mol / mL / \min$$

where:

V = reaction volume

dil = dilution factor of the original sample

V_{enz} = volume of the enzyme sample tested

ε_{mM} ($mM^{-1}cm^{-1}$) = extinction coefficient for CDNB at 340 nm

GST activity was normalized to total protein content measured using BCA method.

3.28. Catalase (EC 1.11.1.6) assay

Catalase activity was quantified using the *Amplex® Red Catalase Assay Kit* by Life Technologies. NCM cells ($2x10^5$ cells/well) were seeded in a 12-wells plate and, after adhesion treated with butyrate. After 4, 24, and 48 hours cells were collected and lysed as described for the GST activity assay. Enzyme quantification was performed following the manufacture's protocol and its activity was normalized to protein content measured using BCA method.

3.29. Glutathione reductase (GR) (EC.1.8.1.7) activity assay

NCM356 cells were seeded in 6-well plates ($2x10^5$ cells/well) and treated after 18 hours with 0.07, 0.4, and 1.4 mM of butyrate for 4 and 24 hours. Cells were lysed in PBS supplemented with 250 mM sucrose and 1 mM EDTA.

The activity of GR was measured by measuring the increase of absorbance at 412 nm caused by the reduction of DTNB (5-5'-dithiobis(2-nitrobenzoic acid)) in the presence of NADPH and GR. Reaction mixture was composed by 1 mM oxidize glutathione, 0.75 mM DTNB, 0.1 mM NADPH in 100 mM potassium phosphate pH 7.5 and 1 mM EDTA. Absorbance was measured immediately after the addition of NADPH for 120 seconds at intervals of 10 seconds.

The concentration of enzyme was calculated using the formula:

$$\frac{Units}{mL} = \frac{\Delta A_{sample} - \Delta A_{blank}}{\varepsilon mM * V_{sample_{(mL)}}}$$

where ε_{mM} ($mM^{-1}cm^{-1}$) is the extinction coefficient for TNB at 412 nm.

Data are reported as units of enzyme per mg of proteins calculated by BCA method.

3.30. Glutathione peroxidase (GPx) (EC 1.11.1.9) activity assay

For the determination of GPx intracellular activity a method based on the oxidation of glutathione (GSH) to oxidized glutathione (GSSG) catalyzed by GPx was used. In this experimental protocol, produced GSSG is then recycled to GSH utilizing glutathione reductase (GR), tert-Butyl hydroperoxide and NADPH. Reaction mixture was composed by 50 mM Tris HCl, pH 8.0, 0.5 mM EDTA, 0.25 mM NADPH, 2.1 mM GSH, 0.5 U/ml GR and 0.3 mM tert-Butyl hydroperoxide.

The decrease in absorbance at 340 nm was measure for 60 seconds at intervals of 10 seconds. Units/ml of GPx was calculated as follow:

$$\frac{\Delta A340/_{\min}}{6.22 * V} = mmol/\min/mL$$

Data was normalized on protein content (µg) calculated by BCA method.

3.31. Quantitative determination of GSH and GSSG levels

Total (GSH+GSSG), reduced (GSH) and oxidized (GSSG) glutathione was quantified using a colorimetric assay based on the reduction of 5,5'-dithiobis(2-nitrobenzoic acid) (DNTB) to 2-nitrobenzoic acid (TNB) by GSH. During the assay, the formed GSSG is recycled to GSH by glutathione reductase and NADPH. The kinetic of the formation of the yellow product TNB was measured spectrophotometrically at 405 nm at 1 minute intervals for 5 minutes in a 96-wells plate. A standard curve of reduced glutathione was used to determine the amount of glutathione in the unknown samples. Cells extracts were obtained washing the cells twice in PBS and lysing them in 5% 5-sulfosalicylic acid (SSA) by two cycles of freeze (in liquid nitrogen) and thaw (at 37°C). The extracts were then centrifuged at 10 000 x g for 10 minutes.

The reaction mixture was composed by 95 mM potassium phosphate buffer pH 7, 0.95 mM EDTA, 0.038 mg/mL NADPH, 0.031 mg/mL DNTB, 0.115 U/mL glutathione reductase and, 0.24% SSA.

For the quantification of GSSG, extracts were pre-incubated with 2-vynilpiridine for 1 hour at RT. 2-vynilpiridine was neutralized by the addition of triethanolamine and then samples processed as described above.

Cellular total GSH and GSSG were calculated using standard curve measurements performed simultaneously with the samples and expressed as nmoles of glutathione per mL of sample according to the formula:

$$Gluthation_{nmoles/mL} = \frac{A405_{sample}/\min}{\Delta A405_{1\,nmole\ \ standard}/\min * V_{sample}(mL)}$$

3.32. Superoxide dismutase (SOD) (EC 1.15.1.1) activity assay

Cell lysates were prepared as described for GST, catalase and GR. SOD activity was evaluated using the *SOD assay kit* by Sigma and the manufacture's protocol was followed.

SOD specific activity was expressed as units of enzyme per mg of total proteins. Protein concentration in the samples was determined by BCA method.

3.33. Western blot analysis

For immunoblot analysis cells were washed twice in PBS and homogenized in lysis buffer containing 45 mM Tris-HCl pH 6.8, 0.2% N-laurylsarcosine, 0.2 mM PMSF, 0.2 mM DTT and a protease inhibitor cocktail (Sigma). Cells lysates were centrifuged at maximal speed, supernatants were collected and protein concentration determined by BCA assay. Cells lysates (40 µg for each line) were separated on a 10% SDS-PAGE and transferred to a PVDF membrane. After blocking in PBS supplemented with 4%

non-fat dry milk, 0.2% BSA, 0.5 M NaCl, Tween-20 0.1%, membrane was incubated with anti-p21 and anti-p27 antibodies (mouse monoclonal IgG, BD Bioscence) and with anti-α-actin antibody (rabbit polyclonal IgG, Sigma). The primary antibodies were counterstained using HRP-conjugated anti-IgG antibodies (Sigma). Protein bands were visualized by chemioluminescence (ECL-plus, Amersham) after exposure to X-OMAT films (Eastman Kodak).

ImageJ software has been used to compare quantitatively the density of western blot bands. Adjusted density values for p21 and p27 bands were calculated by dividing the relative density of each band by the relative density of the actin-control band of the same sample.

3.34. Matrix Metalloproteinases activity assay

MMPs activity was determined through *MMP Activity Assay Kit* (Abcam). A fluorescence resonance energy transfer (FRET) peptide that is cleaved in presence of MMPs is used. The test was performed following the manufacture's protocol.

Purified MMP-2 and MMP-9 (Abcam) were first activated by treatment with 1 mM 4-Aminophenylmecuric Acetate for 1 h and 2 h respectively and used at 1 U/μL. MMP enzymes present in HDFa and HaCaT cell lysates were activated with 1 mM 4-Aminophenylmecuric Acetate for 3 hours at 37°C.

CTL (0.8 and 0.4 g/L) and CTL-nAg (0.8 and 0.4 g/L) were preincubated 20 minutes at RT with MMPs or cell lysates before addition of substrate solution supplied in the kit (containing the FRET peptide).

Endpoint measurement after 1 h of incubation at RT was performed at λ_{ex} 490 nm and λ_{em} 525 nm with a Tecan Infinite® M100 Pro plate reader.

3.35. Statistical analyses

Data are expressed as means and standard deviations (st.dv.). Statistical analyses were performed using Student's t test, and a p-value < 0.05 was considered statistically significant.

4. Results part 1: Colorectal anastomosis

4.1. AnastomoSEAL patch preparation

The aim of this part of the work was the production of a patch that could be placed to the colorectal anastomosis site through both open surgery and laparoscopy. The biomaterial should serve for the delivery of HA to the wound site and then be degraded within few weeks.

The setting up of the procedure of patch preparation was done as a first part of the work. The production process requires a two-step preparation with the first step that consists on hydrogel formation and the second step a freeze-drying procedure to obtain a membrane.

4.1.1. Hydrogel preparation and confocal analysis

The strategy of alginate reticulation by bivalent ions was chosen since it offers the advantage of a biomaterial that could be degraded in body fluids without releasing harmful substances. At the same time, alginate forms a stable hydrogel providing the structural matrix that is necessary for the bioactive component entrapment.

A macroscopically homogeneous solution is obtained when alginate and HA are mixed together in accordance with what already published (136,137). The gelation of the solution allows obtaining transparent hydrogels. The hydrogel formation is due to the presence of $CaCO_3$ and GDL which is slowly hydrolyzed to glucuronic acid once in aqueous solution. The consequent acidification of the solution causes the release of Ca^{2+} responsible for alginate hydrogel formation through an egg box structure.

The hydrogels resulted apparently homogenous as shown in figure 4.1. The molecular arrangement of the two polyanions was investigated to evaluate the distribution of the two polysaccharides after gel formation. Hydrogels produced in presence of fluorescent labelled HA or fluorescent labelled alginate were studied by confocal laser microscopy in order to spot the localization of the two polymers within the interpenetrated network. Two different concentrations of the reticulating agent Ca^{2+}, namely 20 mM and 50 mM (Patch A and F), were employed to modulate alginate crosslinking density, which increases with Ca^{2+} concentration (138). Figures 4.2 b and c show the fluorescence profiles of the two

polysaccharides. The analysis revealed that HA tends to localize preferentially on the edges of the gel, since the fluorescence intensity is higher on the gel surfaces, while the minimum intensity corresponds to the central part of the gel section (Figure 4.1 b). When the concentration of Ca^{2+} increases, this behaviour becomes more evident. At variance, there are not significant variations in alginate profiles throughout the hydrogel thickness, regardless Ca^{2+} concentration (Figure 4.1 c). This finding suggests that the higher is the crosslinking degree of alginate, the higher is the tendency of HA to segregate into larger domains that preferentially localize on the edges of the hydrogels, while alginate appears homogeneously distributed within the gel structure.

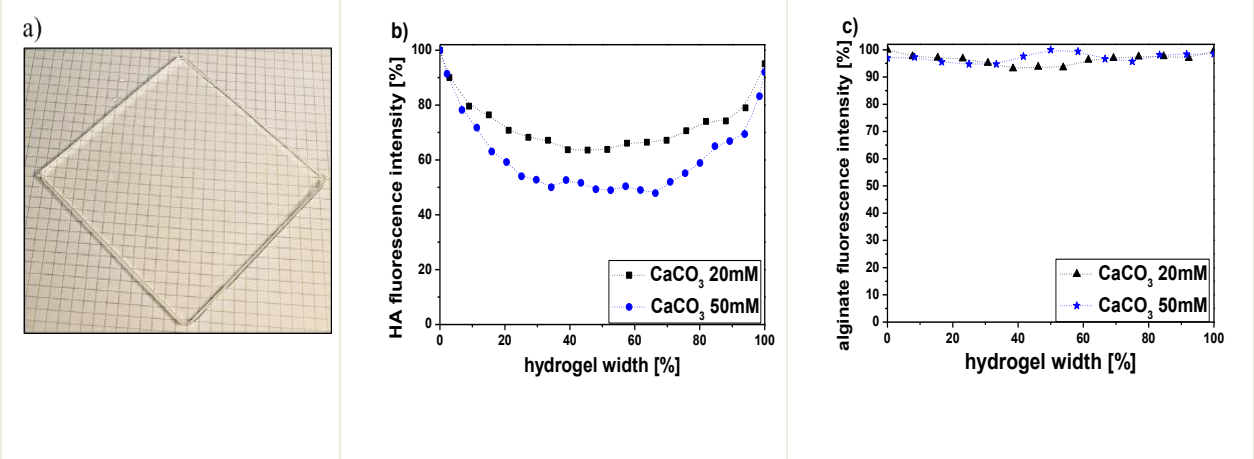

***Figure 4.1**: Alginate-HA hydrogels characterization: a) Macroscopic image of the hydrogel (Patch D); b) Profiles of HA localization in the cross-section (edge to edge) of hydrogels prepared with different $CaCO_3$ concentrations (black squares: 20 mM, Patch D); blue circles (50 mM, Patch E); c) Profiles of alginate localization in the cross-section (edge to edge) of hydrogels prepared with different $CaCO_3$ concentrations (black triangles: 20mM, Formulation D); blue stars (50 mM, Patch E). The profiles reported were chosen as representative trends among 5 replicates. Dotted lines are drawn to guide the eye.*

The homogenous distribution of the alginate macromolecules in hydrogels prepared by *in situ* reticulation was already reported by Kuo and Ma[47].

Varying the amount of Ca^{2+} results in a different arrangement of the HA chains entrapped within the polysaccharide matrix; the higher is the amount of Ca^{2+}, the higher is the amount of egg-box junctions, which results in the accumulation of HA on the surfaces of the hydrogels. The influence of calcium was confirmed also by data on release of polysaccharides from patches that will be discussed on the next paragraphs.

4.1.2. Membrane preparation and morphological analysis

To obtain the AnastomoSEAL patch, the hydrogel was freeze-dried following the protocol described in paragraph 3.5.

For the freezing of the hydrogels, two conditions were considered: one-step freezing at -80°C and a temperature controlled freezing from +20°C to -20°C by the use of a cryostat. The results of the two freezing procedures are shown in figure 4.2: the patch obtained by controlling the freezing temperature is uniform while the patch obtained by rapid freezing shows a very irregular structure with a radial pattern probably due to the ice crystals formed rapidly within the gel.

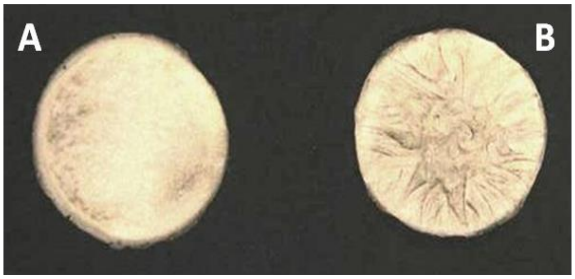

Figure 4.2*: Patches obtained by the freeze casting of the hydrogel (Patch E) by the use of a) temperature-controlled freezing and b) direct freezing at -80°C.*

The temperature controlled freezing was selected for patch preparation and, after freeze-drying, a very flexible patch was obtained (figure 4.3 a). The flexibility is due to the presence of glycerol that acts as a plasticizer and is an important issue because it permits the introduction of the patch into the site of anastomosis through laparoscopy, the procedure of choice of surgeons. In addition, the patch can be easily synthesized or cut in different forms and dimensions.

A morphological analysis of the patch at the microscopic scale was carried out by SEM microscopy (Figure 4.3 b). SEM analysis highlighted the homogeneous polymeric texture composing the membrane; the structure is compact and devoid of open pores. Cross section micrographs display an average thickness of approximately 300 µm (Figure 4.3 c); such limited thickness contributes to make the material suitable to be fold and wrapped by hand and stays within the thickness range of the main commercial surgical membranes for internal use (139).

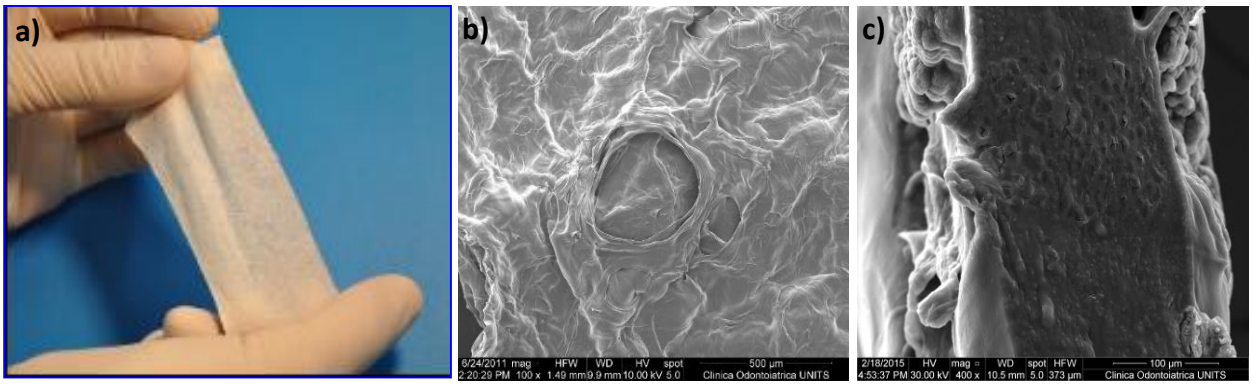

***Figure 4.3**: Images of alginate-HA freeze-dried membranes (Patch D): a) Macroscopic view; b) Top view at SEM; c) Cross section at SEM.*

4.2. Quantification of HA and alginate released from the patches

Release of polymers from the patches in the environment of the anastomosis is a very important parameter since the coordination between the time for the wound healing process and the release of the bioactive components is crucial for the functioning of the biomaterial. In literature evaluation of HA release from scaffolds with alginate/HA was done by using tritiated HA (140). In our laboratory simpler techniques were fine-tuned since tritiated HA requires a complex preparation.

For the quantification of the released HA, fluorescence spectroscopy was first used by employing HA labeled with fluoresceinamine. Fluorescence spectroscopy quantification of polymers resulted simpler and safer than the use of tritiated HA but still requires a lot of time since the reaction for the labeling of HA is very long and small amounts are produced for every preparation reaction. Moreover, the use of this technique does not permit contemporary quantification of both alginate and HA from the same patch (data not shown).

For this reason, Circular dichroism (CD) analysis was considered for polymer quantification. CD is already used for the determination of alginate composition in terms of mannuronic acid (M), guluronic acid (G) and their dyads (MM, MG, GG) (141). Since both HA and alginate are chiral molecules and absorb in the UV range, CD can be used for the quantification of HA and alginate present in a binary mixture. (131).

HA and alginate released from patches produced by the use of two $CaCO_3$ concentrations (20 and 50mM), two types of alginate (from *L. hyperborean* and *M. pyrifera*) and two HAs (with MW = 240 000 and 800 000) were measured by CD. Moreover, analysis were performed also on patches prepared with different ratio HA/alginate, different concentration of total polysaccharides and on patches produced in the presence of NaCl. The release was evaluated in both mQ water and SBF buffer.

4.2.1. Influence of calcium concentration

To study the influence of calcium concentration, the release of the polysaccharides was measured from patches synthesized with *L. hyp.* and HA with MW of 240 000 while $CaCO_3$ concentration was varied (20 mM and 50 mM; Patches A and F). The release was measured after immersion of the patch (ϕ 35 mm) for 3 hours in water.

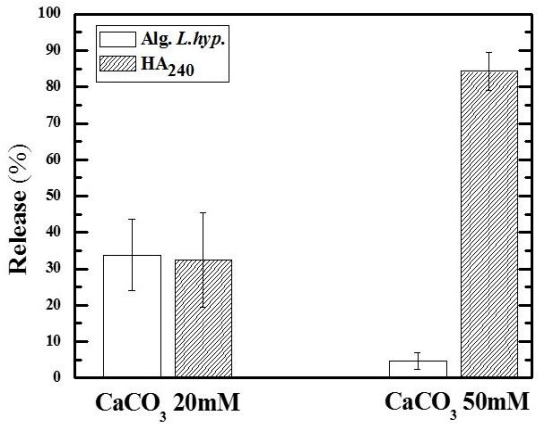

Figure 4.4*: Release of alginate and HA expressed as percentage of the total polymer from patches with $CaCO_3$ 20 mM (Patch D) and 50 mM (Patch E). The values reported in the graph are the average of three replicates. Data are mean ± st.dv.*

Figure 4.4 shows that, in the patch with $CaCO_3$ 50 mM (Patch F), HA is released in a higher percentage with respect to the patch with $CaCO_3$ 20 mM (Patch D). More specifically, there is a release of 84% and 52% for $CaCO_3$ 50 mM (Patch E) and 20 mM (Patch D) respectively. On the other hand, a higher percentage of alginate is released from the sample with $CaCO_3$ 20 mM (Patch D): more specifically 34% with respect to 4.6% released from the sample with $CaCO_3$ 50 mM (Patch E).

The data obtained here are in accordance to what observed from confocal analysis of hydrogels. The HA gradient (figure 4.1 b) explains why in patches with 50 mM $CaCO_3$ (Patch E) the release of HA is higher than the release from 20 mM $CaCO_3$ (Patch D) patches (figure 4.4).

A higher crosslinking density of hydrogels is obtained for higher calcium content. In the presence of higher calcium, the reticulum of alginate is more rapid and the negative charge of HA may interfere with the gel formation thus HA tends to be excluded and forms a gradient of distribution. In the presence of 20 mM $CaCO_3$ there is a lower crosslinking density of alginate matrix and a lower segregation of HA chain. (136,142,143)

The quantification of the alginate released was performed also on control patches without HA (data not shown): the quantity of alginate released is decreased compared to the sample with HA. Alginate released from patches with $CaCO_3$ 20 mM (Patch A) is 26.6% while from the patches with $CaCO_3$ 50 mM (Patch F) is 3.4%. This data further confirms the hypothesis of the different reticulation between gels with different calcium concentration.

4.2.2. Influence of the molecular weight of hyaluronic acid

In order to determine the effect of the MW of HA on polymer release, patches (ϕ 35 mm) containing HA 240 000 and 800 000 were used. The release was quantified for samples with $CaCO_3$ 20 mM (Patches D and B, figure 4.5 a) and 50 mM (Patches E and G, figure 4.5).

Figure 4.5 a shows that HA 800 000 (Patch B) is released in higher quantities compared to the HA 240 000 (Patch D) for the samples with $CaCO_3$ 20 mM. More specifically, 59.5% of HA 800 000 and 32.4% of HA 240 000 are released. At the same time, the quantity of alginate released from the sample with HA 800 000 (Patch B) is much lower (15.2%) than the alginate released from the sample with HA 240 000 (Patch D; 34%). The lower release of alginate and the higher release of HA 800 000 could be because of the higher hydrodynamic volume that could hamper the entrapment of the polysaccharide inside the alginate matrix. For this reason the higher exclusion of HA 800 000 from the gel matrix could facilitate the interaction between alginate chains thus forming a stronger matrix.

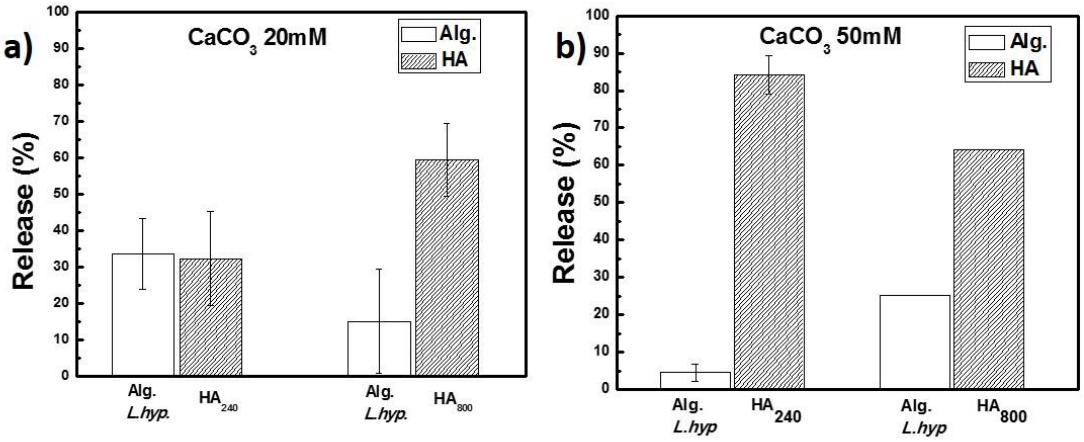

Figure 4.5*: Release of alginate (L.hyp.) and HA 240 000 and 800 000 from patches with a) $CaCO_3$ 20 mM* (Patches D and B*) and b) 50 mM* (Patches E and G*). Data are mean ± st.dv with n=3.*

There is no significant difference on polymer release when HA 800 000 is used between patches prepared with 50 mM (Patch G) and 20 mM $CaCO_3$ (Patch B). The influence of the MW of HA overrides the influence of the Ca^{2+} concentration.

Figure 4.5 b shows that for $CaCO_3$ 50 mM, HA 240 000 is released in higher quantities (84.3%; Patch E) than HA 800 000 (64.2%; Patch G). In the case of HA 240 000 and $CaCO_3$ 50 mM (Patch E) the gelation could be rapid thus resulting in a higher exclusion of HA chains from the alginate matrix while HA 800 000 (Patch G) could slower down the speed of gel formation thus having a lower exclusion of HA chains.

4.2.3. Influence of alginate composition

To study the effect of alginate composition on polymers' release, two different types of alginate were used: alginate from *Laminaria hyperborea* (*L. hyp.*) and alginate from *Macrocystis pyrifera* (*M. pyr*.). These alginates differ in the dyadic composition and for the length of G blocks and MG blocks were alginate from *L. hyp*. has higher G content and longer G blocks. The gel strength is directly related to the total content of G units and the average length of the G block in the gelling polymer (144).

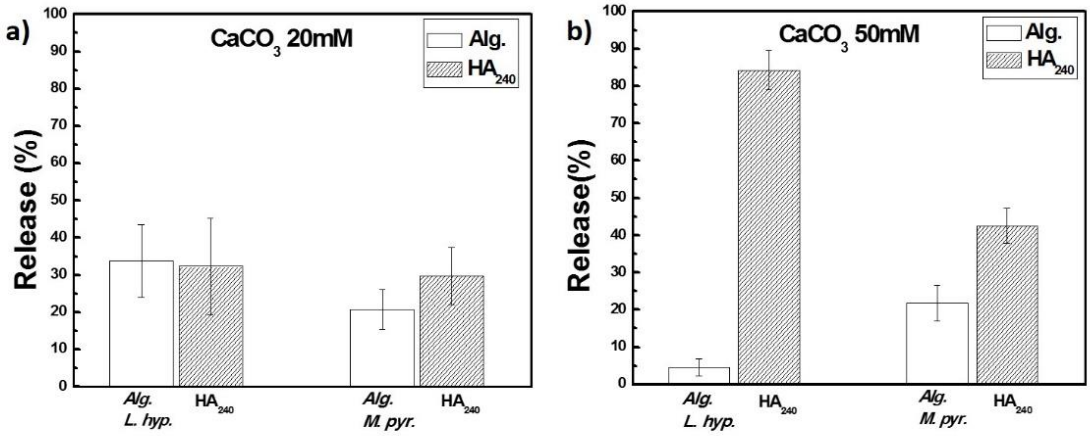

***Figure 4.6**: Release of HA (240 000; 15 g/L) and alginate from patches produced with alginate from Laminaria hyperborean (L.hyp.; Patches D and E) and Macrocystis pyrifera (M.pyr.; Patches H and I) prepared with $CaCO_3$ 20 mM (a) and $CaCO_3$ 50 mM (b). Data are mean ± st.dv with n=3.*

In figure 4.6 a can be observed that for samples prepared with $CaCO_3$ 20 mM (Patches D and H) there is no significant difference in the release of HA when different types of alginate are used but there is a lower release of alginate *M. pyr*. (20.7%) than alginate *L. hyp.* (34%).

For samples prepared with $CaCO_3$ 50 mM (Patches E and I; figure 4.6 b) there is a higher release of alginate *M.pyr.* (21.7%) than alginate *L.hyp.* (4.6%) while HA is released in higher quantities for samples with alginate *L. hyp.* (84%) than for samples with alginate *M. pyr.* (42.5%). This could be due to a stronger gel formed in the presence of alginate *L.hyp.* and high calcium content that leads to a higher exclusion of HA chains and a lower release of alginate chains. Moreover, larger gel pores are found in hydrogels formed from alginate with higher G content such as *L.hyp.* were in presence of high calcium content, lateral association occurs thus forming higher spaces in between the junction zones (76).

When alginate *M.pyr.*is used, the release of alginate does not have a significant difference for samples with $CaCO_3$ 20 mM (Patch H) and 50 mM (Patch I) while HA 240 000 is released in higher quantities in the case of $CaCO_3$ 50 mM (42.5%) than $CaCO_3$ 20 mM (29.8%). For higher calcium concentrations, formation of egg-boxes is faster thus causing a small increase on HA exclusion.

Release of alginate *M.pyr.* from a control patch (without HA; Patch J) with $CaCO_3$ 50 mM resulted in the release of 3% of total alginate (data not shown). This indicates that the addition of HA inside the alginate *M.pyr.* gel causes formation of a smaller number of alginate chain interaction.

As mentioned before, for control patch (without HA) of alginate *L.hyp.,* 3.4% of total alginate is released in presence of $CaCO_3$ 50 mM (Patch F).

Therefore, the presence of HA inside the matrix of alginate gels influences the number of chain interactions when alginate *M.pyr.* is used but does not significantly influence the number of chain interactions when alginate *L.hyp.* is used.

4.2.4. Influence of salt

In order to slow down the gelation process, NaCl was added to the polymer mix used for the patch preparation. NaCl is dissolved in water solution thus Na^+ ions could compete with Ca^{2+} ions on egg-box formation consequently influencing the kinetic of gel formation since this parameter was shown on previews experiments to strongly influence the release of HA from the patch.

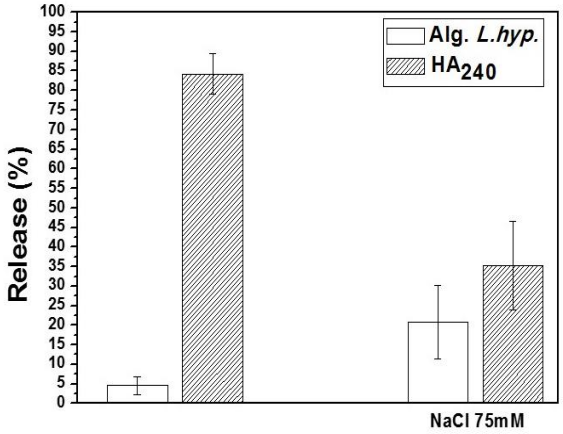

Figure 4.7*: Release of HA 240 000 and alginate from patches with $CaCO_3$ 50 mM in the presence (Patch J) and absence of NaCl 75 mM (Patch E). Data are mean ± st.dv with n=3.*

Quantification of the polymers released was performed on samples synthesized with alginate *L. hyp.*, HA 240 000 and $CaCO_3$ 50 mM with (Patch J) or without (Patch E) NaCl 75 mM. Figure 4.7 shows that NaCl addition lowers the quantity of HA released of almost 50% (from 84.3% to 35.2%) while alginate

release is increased of 16% (from 4.6% to 20.9%). These results show that the addition of NaCl succeeds in competing with Ca^{2+} ions on gel formation and that slowing down the kinetic of gel formation cause a higher release of alginate and a lower release of HA.

4.2.5. Influence of polymer concentration

In order to study the influence of polymer concentration on the release of the two polysaccharides from the patch, three different combinations of polysaccharides were used and the results are reported in figure 4.9.

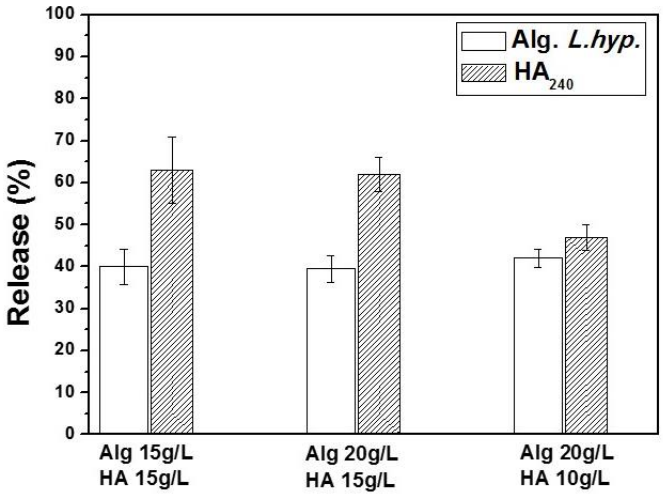

***Figure 4.8**: Release of alginate and HA from patches with different alginate and HA concentration: from left to right: Patch D, C and L. Data are mean ± st.dv with n=3.*

The difference on the release of polysaccharides from patches with different ratio between polysaccharides and different polymer concentration is very small. In fact compared to the patch used in the previous paragraphs for the quantification of released polymers (alginate 15 g/L and HA 15 g/L: Patch D), there is only a very small increase on alginate release for the patch with alginate 20 g/L and HA 10 g/L (Patch L). Also the release of HA is very similar between the patch with alginate 15 g/L (Patch D) and 20 g/L (Patch C) and HA 15 g/L while there is a decrease on the percentage of total HA released for the patch with alginate 20 g/L and HA 10 g/L (Patch L).

4.2.6. Influence of the environment

In order to evaluate the influence of the chemical environment on the patch dissolution, the release of alginate and HA in water was compared with the release in SBF, a buffer containing the same concentration of salts as the blood plasma. SBF was chosen because of the similarity with the physiological environment in which the patch will be placed since the accumulation of biological fluids is part of the normal course of the anastomosis healing.

The test was performed on samples prepared with both alginates *L. hyp.* (Patch D, figure 4.9 a) and *M. pyr.* (Patch I, figure 4.9 b) 15 g/L and HA 240 000 15 g/L.

For both types of alginates, there is an increase of the release of alginate and HA when the patch is immersed in SBF compared to the release in water. More specifically, there is an increase on alginate release of 13% from samples with alginate *L. hyp.* (Patch D) and 5% from samples with alginate *M.pyr.* (Patch I) compared to the release in water. HA release in SBF has an increase of 34% from patches with alginate *L. hyp.* (Patch D) and 19% from patches with alginate *M. pyr.* (Patch I).

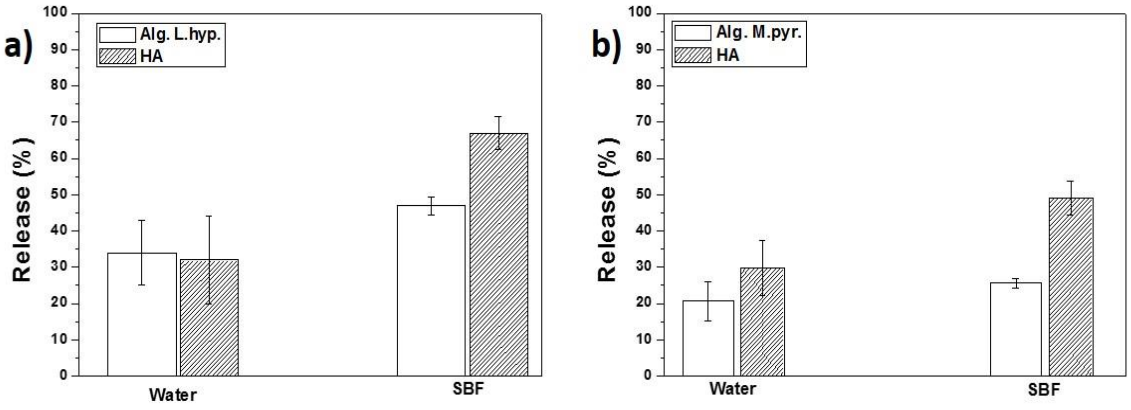

***Figure 4.9**: release of alginate (15 g/L) and HA 240 000 (15 g/L) from samples with $CaCO_3$ 20 mM immersed in water or SBF: a) Patch D and b) Patch I. Data are mean ± st.dv with n=3.*

This increase on polymer release is probably due to the presence of ions in the SBF buffer compared to water. Positively charged ions such as Na^+ could compete with Ca^{2+} ions that are present at the egg-box level weakening the structure of the patch with consequential increase of polymer release from the patch.

In summary we can say that parameters that cause a slower formation of the gel give rise to a patch were the release of alginate is higher and the HA release is lower compared to the release in patches with a faster gel formation.

4.3. In vitro tests of raw materials on fibroblasts and colonocytes

The aim of the tests that are reported below is to evaluate the biological effects of the single components of the patch on two main type of cells present in the site of the anastomosis: fibroblasts and colonocytes.

Since cell lines are very different from the primary cells, Human Dermal Fibroblasts from adult were used to represent the fibroblast component of the wound found on the outer part of the intestine were the patch should be placed.

For the other side (the inner mucosal tissue), a normal colon-derived cell line, named NCM356, was selected for the in vitro test. Primary colonocytes are very difficult to obtain and can be used for a very short time, hours till few days (145–147). NCM356 cell line was isolated from the histologically normal colonic margin of a 65 years old black male patient subjected to rectal adenocarcinoma resection (148). The cells are not tumorigenic, display normal colonic epithelial cells characteristics but mutations have been detected. Although NCM356 cells are not normal primary cells, they are a good compromise between primary and transformed cells.

4.3.1. Evaluation of the effects of HA on viability and proliferation of primary fibroblasts

Since biological effects of HA depend on its MW, HA at different MWs were considered in order to choose the best one for our application.

Effects of HA at different MWs (65 000, 240 000, 800 000, 1 500 000) were studied in terms of cell viability through an Alamar blue assay. Viability of cells treated with HA at different MWs is reported in figure 4.10 by means of growth rate (viability Day n/ viability Day 0) of cells as a function of time.

The test pointed out that for all the MWs used, HA stimulates fibroblasts proliferation since the treated cells have a higher viability than the non treated cells. However, polymers with lower MW appear to be more effective than polymers with higher MW. The best performing HA is the one with MW 240 000 at 2 g/L. For this reason, HA at 240 000 was selected for the production of patches, of HABut at different DS and for further characterization studies.

It is already known that HA at different MWs have different biological effects (84,149,150). Several studies show that HA with MW around 200 000 induces production of chemokine, cytokine, proteases, growth factors and nitric oxide from macrophages (2). At the same time *West et al* showed that polydispersed HA with a peak of 200 000 was found in fetal and adult wound fluid but in fetal wound fluid (that have a healing without scaring) it increases at day 7 and reaches a concentration of 4-5 times the HA found in adult wound fluid (151).

Thus, the selected HA could induce cell proliferation from one hand (as shown by our results) and induce the immune system to resolve tissue injury without excess of scaring.

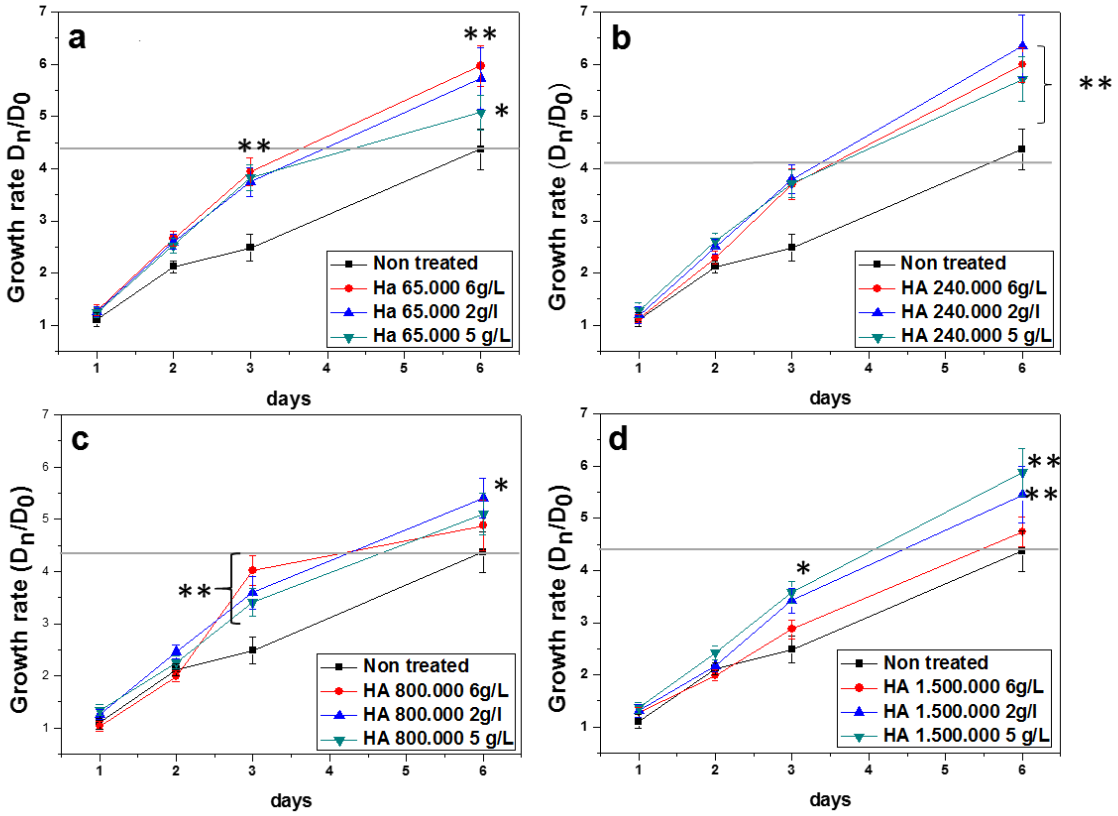

***Figure 4.10**: Viability of fibroblasts treated with HA of different molecular weights at three different concentrations. Data are mean ± st.dv.: t-student: ** indicates p<0.01, * indicates p<0.05 n=8. Grey line= maximum growth rate of non-treated cells.*

4.3.1. Evaluation of the effects of HA on viability and proliferation of colonocytes

Figure 4.11 reports the effects of HA at different MWs on colonocyte viability were grey lines indicate the maximum rate of growth reached by the cells in 6 days of culture without any treatment. The test points out that HA has a minimal effect on cellular proliferation. In particular, for all MWs of HA tested, the highest concentration (6 g/L) of polymer induces a decrement of cell replication at days 6 and 7. Lower concentrations either do not affect significantly cell growth profile or promote, only in two cases, a very slight increment of cell growth (see graphs c and d).

HA exerts a proliferative effect on several cell types, but the results are controversial and depend on cellular type and origin, as well as the size and concentration of HA. Thus is not surprising that the effect on viability and proliferation of fibroblasts and colonocytes is not the same.

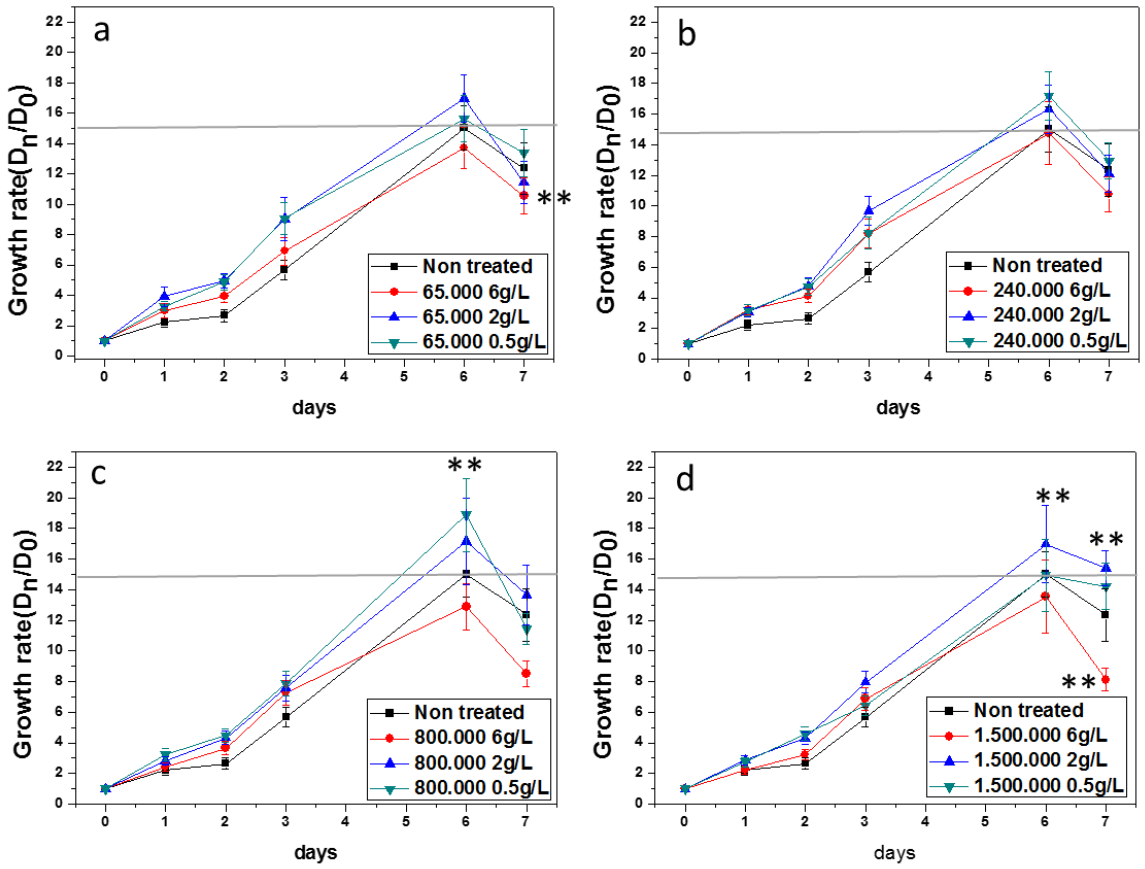

Figure 4.11*: Alamar Blue test on colonocytes treated with HA with different MWs. Data are mean ± st.dv.: t-student: **P<0.01, n=8. Grey line= maximum growth rate of non-treated cells.*

4.3.1. Evaluation of the effects of HABut and butyrate on viability and proliferation of primary fibroblasts

HABut with three DS (0.3, 1 and 1.8) at the same concentrations used for HA (0.5 g/L, 2 g/L and 6 g/L) were tested on fibroblasts (figure 4.12). These polymers are obtained from HA 240 000 to which butyrate molecules are grafted through an esterification process.

As can be seen in Figure 4.12, the cell behavior in presence of HABut is not comparable to that observed for fibroblasts treated with the corresponding HA. HABut with DS 0.3 does not affect significantly cell proliferation at any of the three concentrations of polymer used. Moreover, it can be observed that the increase of the DS of the polysaccharide induces a clear and significant decrease of cell growth. The

most consistent proliferation inhibition is observed with HABut with the highest DS and at the concentration of 2 g/L. Thus HABut inhibits fibroblasts proliferation in a dose-dependent and DS-dependent manner.

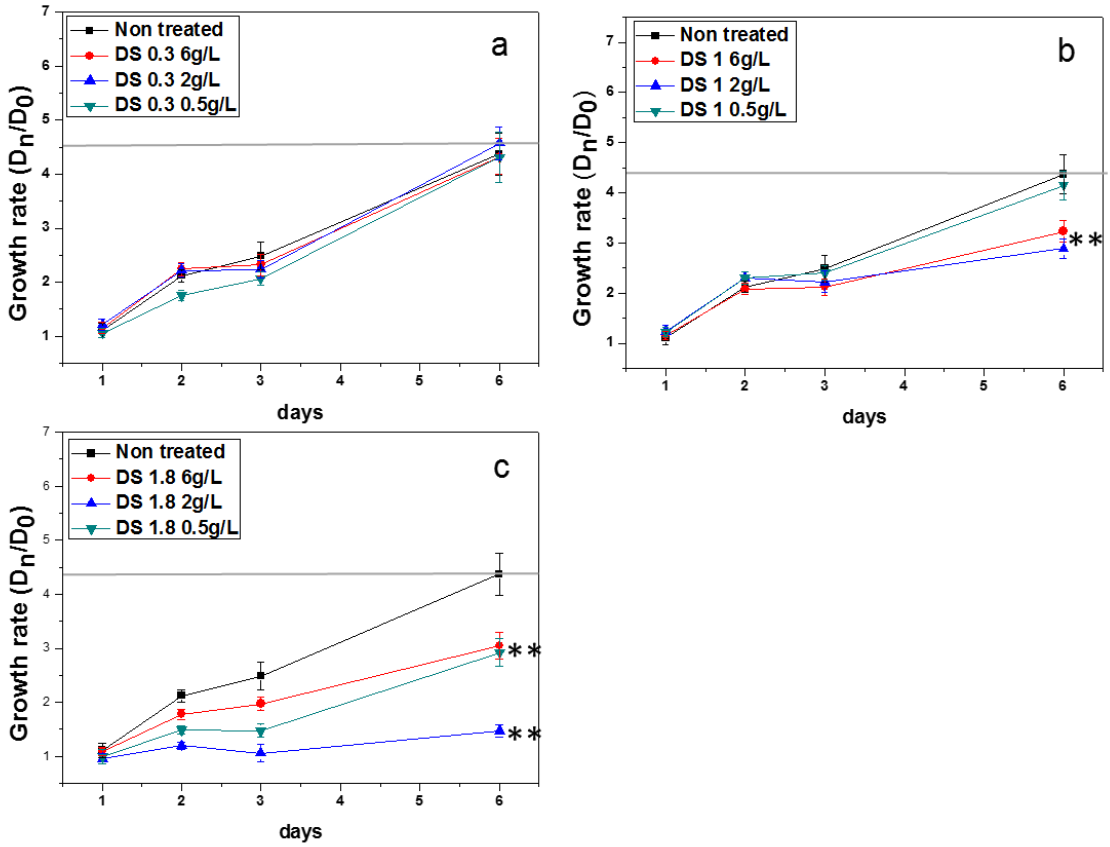

***Figure 4.12**: Viability of fibroblasts treated with HABut of different Degrees of Substitution (DS) at three different concentrations. Data are mean ± st.dv.: t-student: **indicates p<0.01, n=8. Grey line= maximum growth rate of non-treated cells.*

This effect is probably due to presence of butyrate whose effect on fibroblasts viability was also tested. Cells were treated with butyrate at different concentrations (0.07 mM, 0.4 mM, 1.4 mM). These concentrations correspond to the concentration of butyrate molecules contained into the HABut polymers. Furthermore, a ten times higher concentration (14 mM) of the one contained in HABut 6 g/L was used.

Viability of fibroblast treated with butyrate shows a dose-dependent inhibition of proliferation (figure 4.13). The lowest concentration (0.07 mM) of the short chain fatty acid does not impair growth rate in comparison with the control cells. For the intermediate concentrations, a decrease of proliferation is

evident and became significant mainly after the first two days of culture. It is interesting to note at the highest dose of butyrate (14 mM) a severe drop of the growth rate in comparison with its value at day 1, ascribable to a reduction of the number of cells in the sample and therefore to cell death.

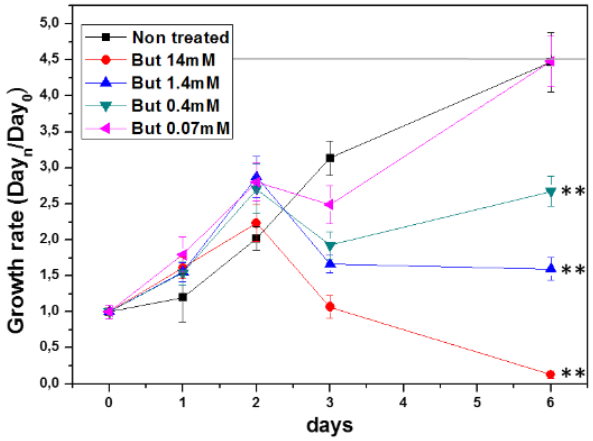

***Figure 4.13**: viability of fibroblasts treated with butyrate (But) at different concentrations. Data are mean ± st.dv.: t-student: ** indicates p<0.01, n=8. Grey line= maximum growth rate of non-treated cells.*

In order to study if the observed cell death at the highest concentration of butyrate is induced by apoptosis, in accordance with what described in literature (152–154) analysis of exposure of phosphatydilserine was done through Annexin V test. Cytofluorimetric analysis of Annexin V (figure 4.14) showed that at 72 hours of butyrate treatment, only 37.3% of cells are viable while in the control group 92% of cells are viable. Treated cells are mainly in early apoptosis (52.8% with respect to 5.4% in the non treated cells).

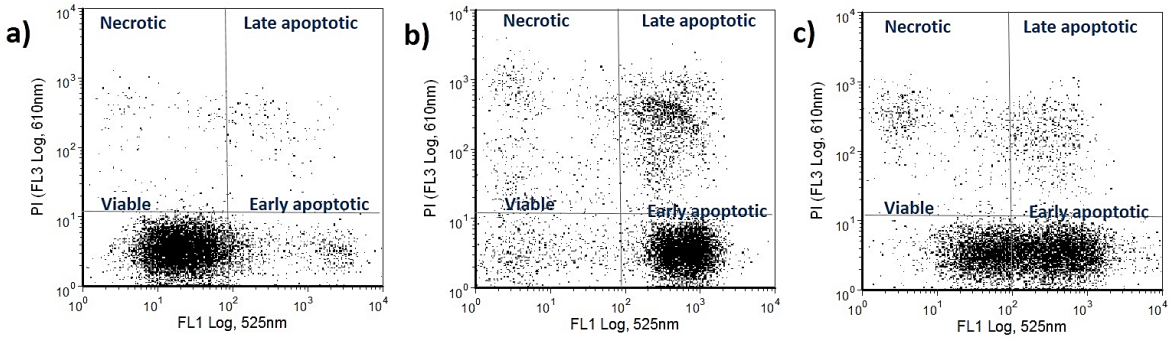

d)

	viable AnnexV -/PI-	early apo AnnexV +/PI-	late apo AnnexV +/PI+	necrotic AnnexV -/PI+
control	91,98	5,41	1,02	1,59
UV 5min	7,01	70,64	15,73	6,62
But 72h	37,3	52,76	4,61	5,33

Figure 4.14*: Cytofluorimetric analysis of the HDFa cells untreated (a) treated with UV rays for 5 minutes (b) and treated with butyrate (But) 1.4 mM for 72 h (c). FL1 indicates the green fluorescence given by Annexin V and FL3 indicates red fluorescence given by propidium iodide (PI). Table in d) shows the percentage of cells for each group.*

These results show that butyrate molecules bound on polysaccharide chain maintain the capability to be internalized into the cells and to interact with its natural intracellular targets (namely histone deacetylases)(152), so to induce biological pathways comparable to that exploited by the free molecule, in particular inhibition of cell cycle progression and induction of apoptosis.

4.3.2. Evaluation of the effects of HABut and butyrate on viability, proliferation and cell cycle progression of colonocytes

After treatment of colonocytes with HABut 0.5 g/L, 2 g/L and 6 g/L we observed that different DS do not significantly influence colonocyte growth (figure 4.15). Only the highest concentration (6 g/L) of polymer used exerts an effect on the cell growth profile when compared with non-treated cells, inducing inhibition and arrest of cell proliferation.

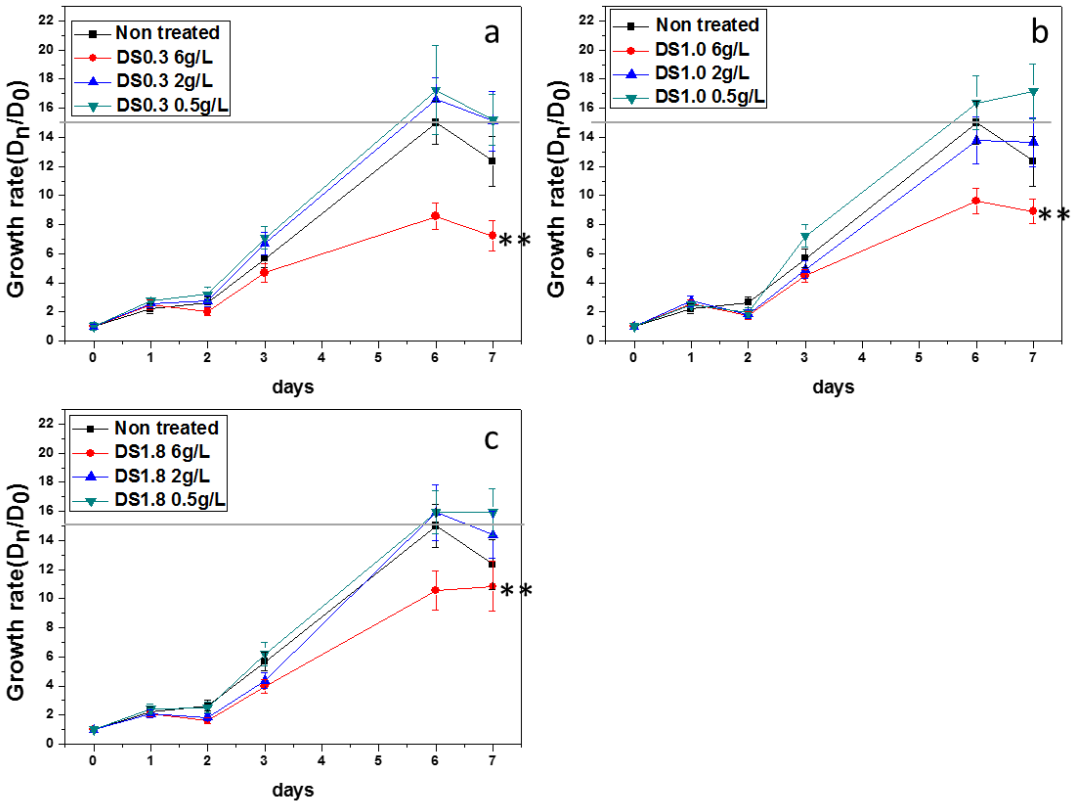

Figure 4.15*: Viability of colonocytes treated with HABut at different DS. Data are mean ± st.dv.: t-student: ** indicate p<0.01, n=8. Grey line= maximum growth rate of non-treated cells.*

We therefore tested the influence of sole butyrate on colonocytes and the results are reported in figure 4.16. As shown already for fibroblasts, butyrate causes suppression of cell proliferation and cell death at the highest concentration of the molecule.

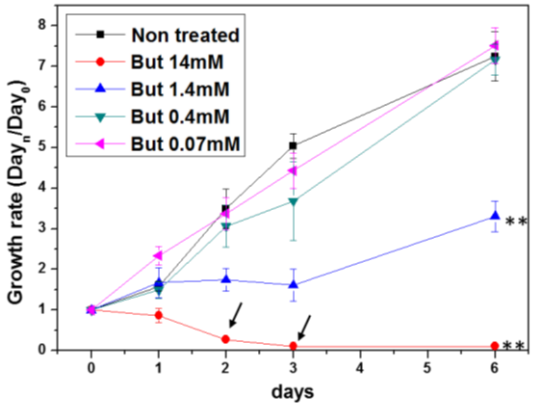

Figure 4.16*: Proliferation rate of colonocytes treated with butyrate (But) at different concentrations. Data are mean ± st.dv.: t-student: ** indicates p<0.01, n=8. Arrows indicate the time points when cytofluorimetric analysis for detection on Annexin V were performed.*

Cytofluorimetric analysis confirmed that the decreasing of colonocyte number detected after 48 hours of treatment with the highest concentration of butyrate, is due to cell death for apoptosis (figure 4.17). More in detail, after 48 hours more than 50% of the cells are in apoptotic phase (summing early and late apoptotic cells), against 8% of the non-treated cells while after 72 hours 75,7% of cells are in apoptotic phase.

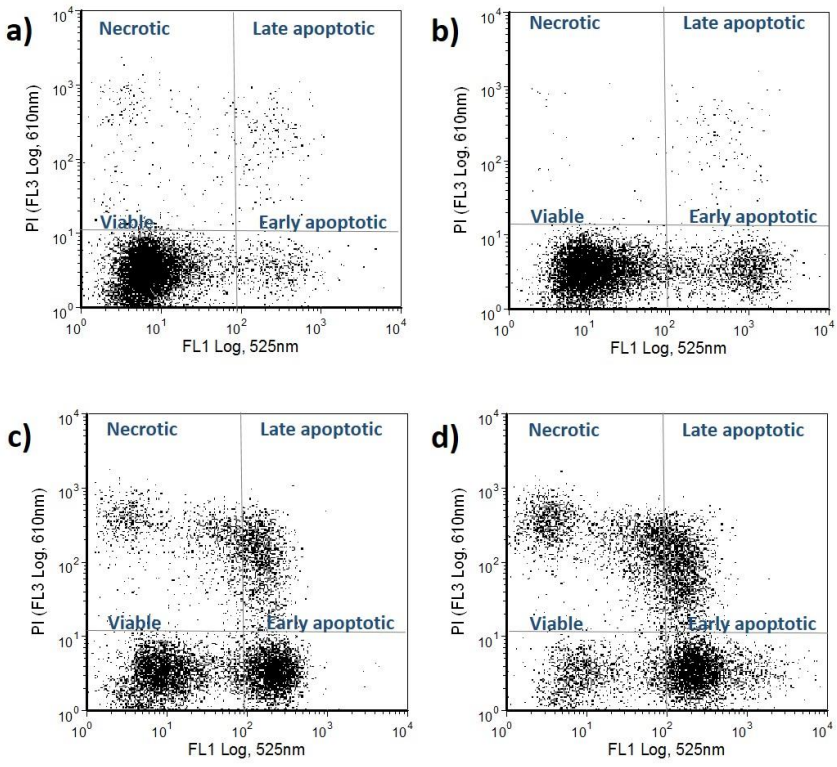

e)

		viable AnnexV -/PI-	early apo AnnexV +/PI-	late apo AnnexV +/PI+	necrotic AnnexV -/PI+
NCM	control	90,28	6,11	1,89	1,72
	UV 1mın	78,08	20,51	1,21	0,2
	But 48h	36,55	38,67	17,67	7,11
	But 72h	11,11	46,67	29	13,22

Figure 4.17*: Annexin V assay of NCM356 cells non treated (a), exposed to UV rays for 1 minute (b) and treated with butyrate (But) for 48 (c) and 72 hours (d). The percentage of cells per each sample in the different stages are reported in (e). Data shown here are obtained from a single representative experiment.*

Effects of butyrate on cell cycle progression were examined more in depth. The analysis at different time points of the cycle of cells treated with 0.4 and 1.4 mM butyrate showed an alteration of the cell cycle progression after 8, 24 and 48 hours, as reported in Table 4.1. In particular, we observed a slowing down of the replication rate in cells treated with butyrate. Moreover, the presence of sub-G1 peaks,

ascribable to cells in the apoptotic state, are observed after 24 hours in the samples treated with 1.4 mM of butyrate and after 48 hours both in cells treated with 0.4 and 1.4 mM of butyrate. We hypothesize that a small fraction of the cells are induced to block their cycle progression with further triggering of the apoptotic pathway.

But at the concentration of 0.07 mM does not influence cell cycle progression, in agreement with what observed in the proliferation test.

a)

% of cells	Non-treated	But 0,07mM	But 0,4mM	But 1,4mM
G1	83	84,7	78,1	82,8
S	11,7	11,9	13,2	10,7
G2/M	5,28	3,4	6,28	6,47

b)

% of cells	Non-treated	But 0,07mM	But 0,4mM	But 1,4mM *
G1	67,1	65,6	56	75,1
S	28	25,4	25,6	8,51
G2/M	4,91	8,98	18,4	16,4

c)

% of cells	Non-treated	But 0,07mM	But 0,4mM *	But 1,4mM *
G1	56,6	53,8	45,3	71,1
S	34,6	34,8	40,8	12,7
G2/M	8,87	11,4	13,8	16,2

Table 4.1*: Cytofluorimetric analysis of the cycle of cells untreated and treated with butyrate (But) 0.07 mM, 0.4 mM and 1.4 mM after 8 (a), 24 (b) and 48 (c) hours. The asterisk indicates the samples that show a subG1 peak (apoptotic cells). Data shown here are obtained from a single representative experiment.*

In literature there are different works supposing that butyrate induces cell death on malignant cells. It could be that, since NCM356 cells are not primary cells, the data we are seeing are due to this effect while in the intestine environment there is no or little cell death induction.

In vivo concentrations of butyrate are very difficult to be measured, several works report the fecal concentrations that do not reflect the real concentrations in the physiologic environment since most of the butyrate is rapidly absorbed from intestinal cells (155). The concentrations in vivo are probably

much lower than the ones used here since mucus is present and thus the concentration of butyrate in contact with the cells are probably lower than the one present in the intestinal lumen.

Several cyclin-dependent kinases (CDK) inhibitors, including $p21^{Cip1}$ and $p27^{Kip1}$, are reported to be under the regulation of histone acetylation/deacetylation and also involved in butyrate-mediated cell growth arrest in some colon and non-colon cancer cell lines (156–159). Thus, the protein expression levels of both p21 and p27 were investigated through western blotting analysis using specific antibodies, after 24 hours of treatment with butyrate. As shown in Figure 4.18, butyrate led to a very modest increase of the p27 expression (an average increase of 20-30% vs control), meanwhile a consistent over expression of p21 is observed mainly at the highest concentration of butyrate used.

Likely, mainly p21, and only marginally p27, seem to play a central role in butyrate-mediated cell cycle inhibition and apoptosis induction on NCM356 cells.

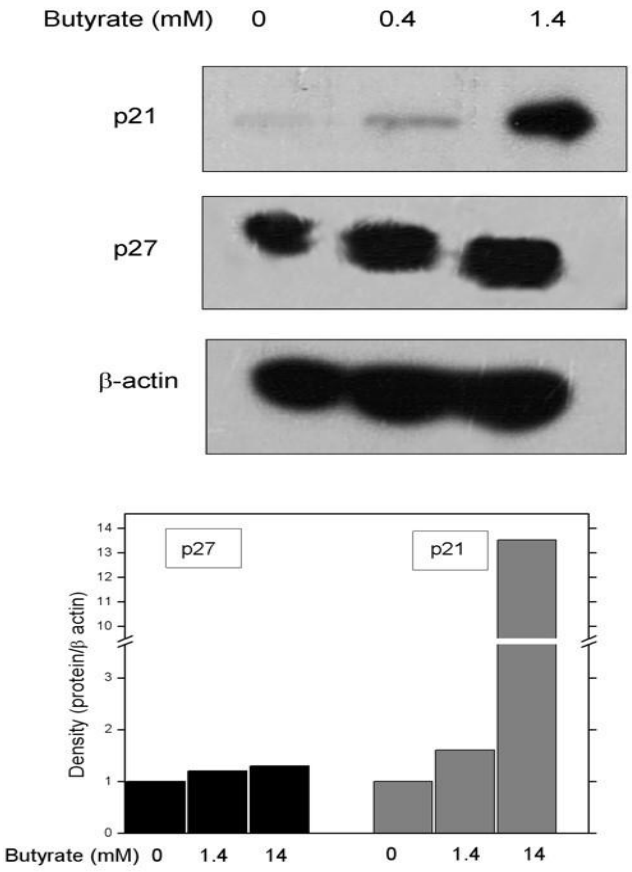

***Figure 4.18**: Effect of butyrate on the expression of cell cycle-related proteins $p21^{Cip1}$ and $p27^{Kip1}$. NCM356 cells were exposed to 1.4 and 14 mM of butyrate for 24 hours. Primary antibodies anti-p21, anti-p27 and anti-α-actin have been used for the western blotting. One representative experiment of immunoblotting is reported. Densities of western blot bands have been compared using the software ImageJ.*

Butyrate in vivo might have a dose-depend effect: at high concentrations it induces cell death while at low concentrations doesn't act at cell cycle level but on other cellular mechanisms like anti-inflammatory effects, induction of REDOX systems, production of extracellular matrix (96,135,160). For this reasons the effects of butyrate on anti-inflammatory mechanisms were studied and will be reported in paragraph 4.4.8.

4.3.3. Binding of HA and HABut on fibroblasts and colonocytes

HA is normally internalized inside the cells. Since HABut is a different molecule, assays were performed in order to verify if the HABut polymer can be internalized by the cells so to allow butyrate to interact with its intracellular targets.

A first study on the expression of CD44 receptor was performed through FACS analysis since HABut is thought to bind to HA receptor. Figure 4.19 shows that the entire population of NCM cells express CD44 receptor (gate 1) and there is no difference in expression between the less differentiated and adherent cells (gate2) and the most differentiated and suspension-growing cells (gate 3).

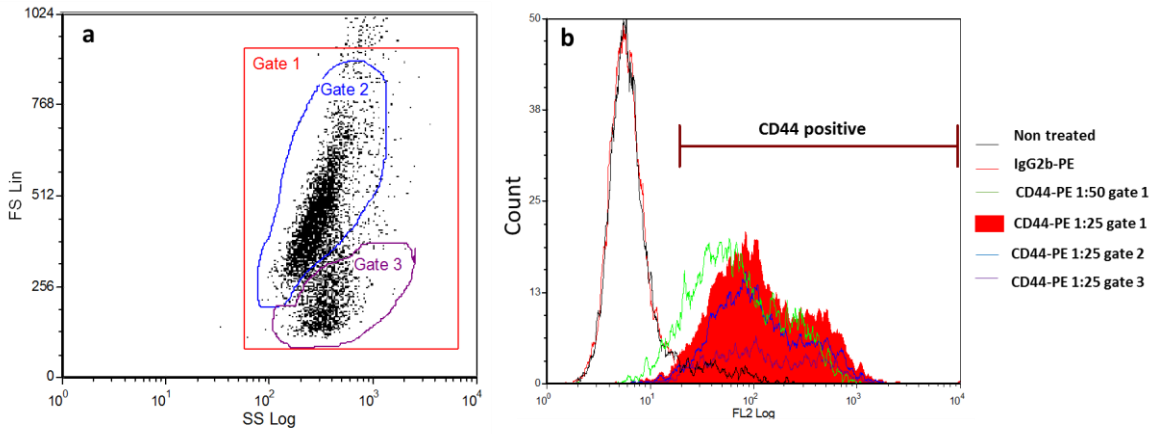

***Figure 4.19**: Cytofluorimetric analysis for CD44 expression on NCM356 cells: a) side scattering and forward scattering that show the distribution of cell population and the gated cells; b) Red fluorescence (FL2) of the cells versus cell count. A primary antibodies anti-CD44 conjugated to phycoerithrin (PE) was used; IgG2b conjugated to phycoerithrin (PE) was used as idiotypic control. One representative experiment is reported.*

Binding and internalization of HA and HABut by fibroblasts was evaluated through cytofluorimetric analysis of cells treated with HA and HABut conjugated to fluoresceinamine. In order to evaluate if the signal is due to extracellular binding or if it is due to internalization of the polymer, fluorescence was

quenched with Trypan blue. In figure 4.20 is shown that increasing quantities of Trypan blue increases fluorescence quenching of HA and HABut labeled with fluoresceinamine.

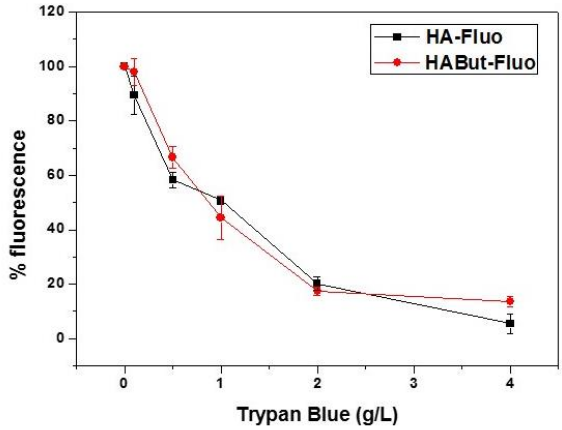

Figure 4.20*: Quenching of HA and HABut 2 g/L conjugated to fluoresceinamine (HA-Fluo and HABut-Fluo) by increasing concentrations of Trypan blue.*

In figure 4.21 a and b are reported the analyses of the cytofluorimetric data collected from fibroblasts. The grey peak represents the autofluorescence signals obtained from cells non-treated with the labeled probes. The green peak that appears shifted toward higher values of fluorescence, indicates the fraction of cells that have bound firmly the probe. After fluorescence quenching, although a slight shift of the blue peak can be noted, a consistent percentage of the fluorescence can be ascribed to probes, both HA and HABut, that have been internalized by the cells.

Similar results are obtained also from colonocytes (Figure 4.21 c and d). The graphs show that both polymers bind to NCM356 cells and treatment with Trypan blue causes a small quenching of fluorescence indicating that most of the polymer is inside the cells and only partially is outside, probably bound to the CD44 receptor. The difference in fluorescence between HA and HABut has to be ascribed to the fact that polymers are from different preparations and fluorescence cannot be compared quantitatively.

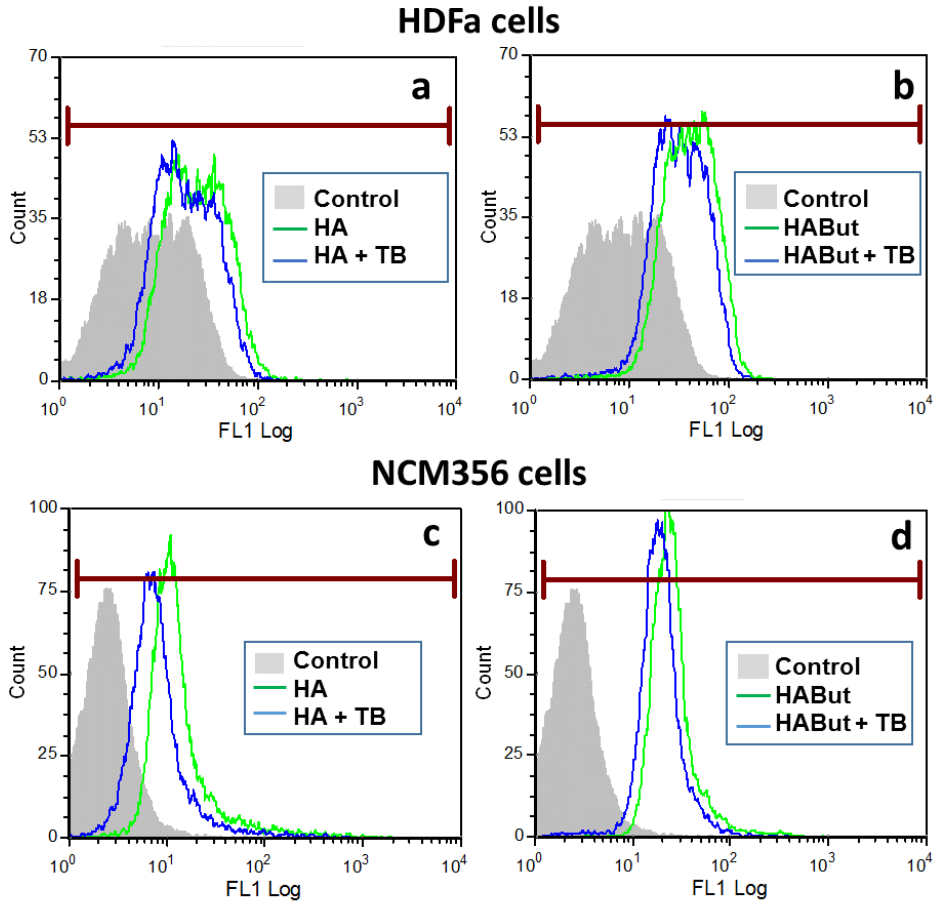

***Figure 4.21**: Green fluorescence reading (FL1) of HDFa cells (a and b) and NCM356 cells (c and d) treated with HA and HABut labeled with fluoresceinamine and with both HA and Trypan blue (TB).*

Although already published data reports that in the specific uptake of HABut by some cancer cell lines is mainly involved CD44, the major receptor for HA (4), it is not excluded that other membrane receptors, including the receptor for hyaluronate-mediated mobility, could be responsible for HABut internalization. In this respect, it remain to demonstrate whether also in cell types tested in this study, CD44 is the receptor involved in the active polymer uptake.

In figure 4.22, a schematic and hypothetic mechanism of the uptake and intracellular release of butyrate from HABut is reported.

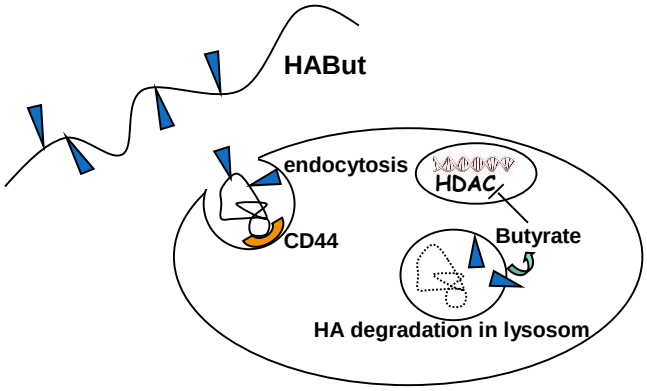

Figure 4.22: *Uptake and intracellular release of butyrate from HABut.*

4.3.4. Scratch test (wound healing assay) on fibroblasts and colonocytes

The overall influence on wound closure was evaluated by following the closure of a scratch performed on a monolayer of cells over time. Figure 4.23 a shows the results for HDFa cells treated with HA and HABut expressed as percentage of the scratch closure over time.

Scratch test on fibroblast demonstrates that the process of gap closure is efficiently promoted by HA and by HABut in a dose dependent manner (figure 4.23). As an example, after 24 hours sample treated with HA showed a complete closure of the gap whereas with non-treated cells the percentage of closure is only 50%. However, the effect of HA on gap closure is more pronounced than the effect of HABut.

In order to distinguish contributes of migration and proliferation on scratch closure, the proliferation of cells was inhibited by the use of mitomycin C. The optimal concentration was first determined by treatment of HDFa cells with mitomycin C at different concentrations (figure 4.23 b). Mitomycin C 1 mg/L was chosen for cell treatment since it maintains stable the viability of cells for 2 days.

In figure 4.23 c and d we can see in purple the healing profile of cells treated with the drug, in black the healing profile of non-treated cells. When cells are treated with Mitomycin 1 mg/L the scratch closure slows down but is not abolished meaning that proliferation gives an important contribution to the scratch closure but is not the only one. The cells cultured in presence of the polymers display an

intermediate behavior as a proof that the polymers have a role in the healing process stimulating both cell migration and cell replication.

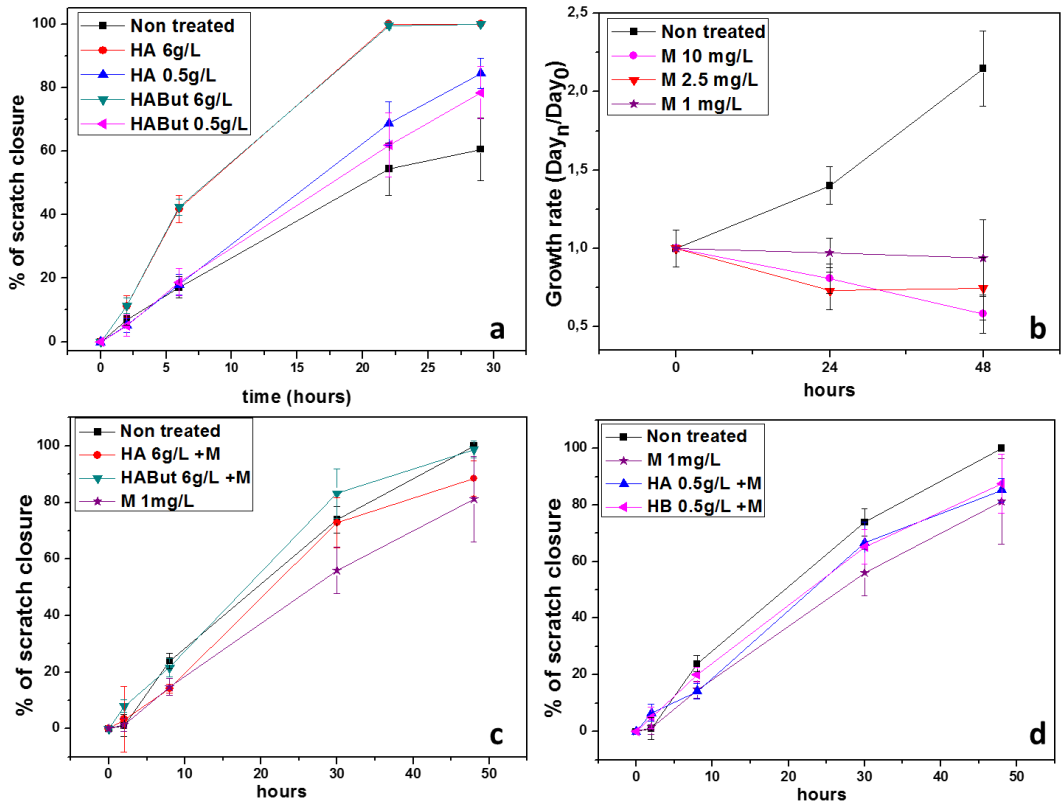

***Figure 4.23**: Scratch test on fibroblasts treated with HA (6 g/L and 0.5 g/L) and HABut (6 g/L and 0.5 g/L) and on non treated cells. In Graph a, cell response without addition of mitomycin C; in Graph b, selection of the optimal concentration of mitomycin C; in Graph c and d, cell response with addition of mitomycin C. Results are reported as percentage of closure of the gap area at time n in comparison with gap area at time 0. For each sample, data are expressed as mean ± st.dv. with n=8.*

Fibroblasts are very important to the different stages of the wound healing process: they are highly migrating cells, great contributors to the formation of the granulation tissue and of matrix remodeling and are also responsible for the wound contraction by differentiating to myofibroblasts (11,161). Data obtained from our experiments are in agreement with other studies as literature data indicate that HA induces both proliferation and migration of cells (149).

The test was performed also on colonocytes both with and without Mitomycin C. Data are reported in figure 4.24.

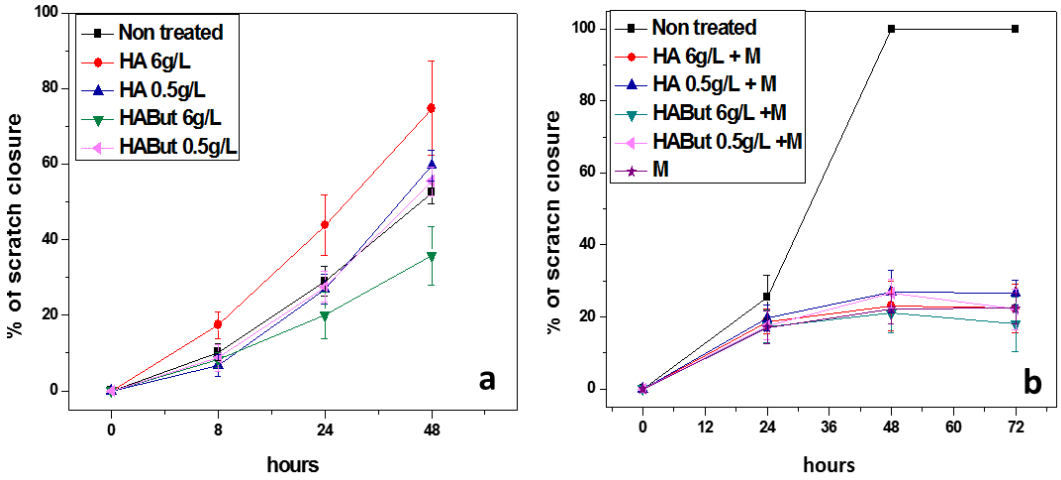

***Figure 4.24**: Scratch test performed on NCM356 cells treated with HA (6 g/L and 0.5 g/L) and HABut (6 g/L and 0.5 g/L) and on non treated cells. In Graph a, cell response without addition of Mitomycin C, in Graph b, cell response with addition of Mitomycin C. Results are reported as percentage of closure of the gap area at time n in comparison with gap area at time 0. For each sample, data are expressed as mean ± st.dv. of six scratched lines.*

Only HA (red line) at the concentration of 6 g/L promotes a significant increase in the kinetic of gap closure. HA has a dose-dependent effect on wound closure since the closure of the scratch performed on the monolayer of NCM356 cells is higher in presence of HA 6 g/L with respect to non treated cells while in the presence of HA 0.5 g/L there is a significant induction of gap closure only at 48 hours. When NCM356 cells are treated with HABut there is a dose-dependent inhibition of scratch closure since in the presence of HABut 6 g/L there is a lower closure of the scratch compared to the non treated cells. For HA 0.5 g/L there is no significative difference between treated and non-treated cells.

In NCM356 cells, Mytomicin C inhibits completely gap closure (see figure 4.24 b) suggesting that cell proliferation is the prevalent mechanism involved in the process of scratch closure .

The data obtained here are in accordance with data obtained on viability assay since HABut inhibited colonocyte proliferation. Inhibition of cell growth is the mechanism by which HABut decelerates gap closure on colonocytes.

4.3.5. Effects on extracellular matrix production

ECM production is important in wound healing since this component has to be restored when an injury occurs. Moreover, the ECM plays an active role on wound healing since it serves for cell adhesion and migration, reservoir of growth factors and MMPs.

ECM production on human primary fibroblasts after treatment with HA 240 000 or HABut DS 0.3 was studied in terms of glycosaminoglycan (GAG) production and collagen production and is shown in figure 4.25.

Figure 4.25 a shows the quantity of GAGs (in µg) normalized over micrograms of total protein content and figure 4.25 b shows the results for collagen production in terms of CICP peptide quantity normalized on number of cells (measured by Alamar Blue Assay).

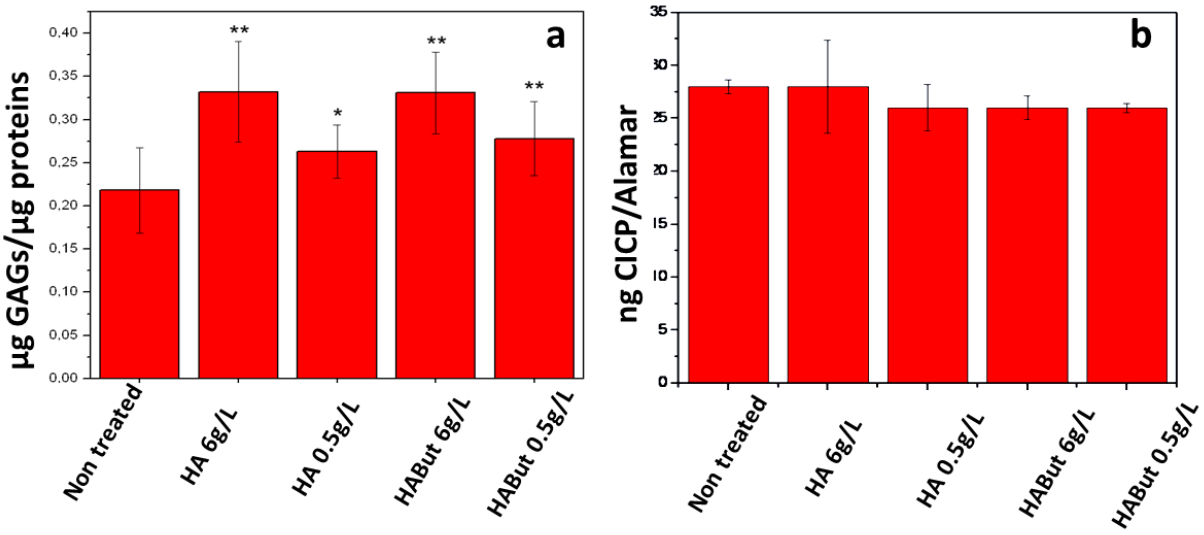

***Figure 4.25**: ECM production after treatment with HA and HABut. a) Glycosaminoglycan quantification after 6 days of treatment; b) CICP peptide quantification in culture medium after 48 hours of treatment. Data are mean ± st.dv. and are from a single representative experiment with n=3. t-student is indicated in the figure with ** for p-value <0.01 and * for p-value <0.05.*

Treatment of fibroblasts with both HA and HABut increment GAGs production from fibroblasts in a dose-dependent manner. Since the assay is based on DMMB which reacts with the sulfate group of the GAG chain, HA is not detected and thus there is no interference of the HA used for the treatment.

Production of collagen type I is not influenced by the treatment with HA and HABut for 48 hours.

Collagen is an important molecule in the anastomosis healing process since it influences the strength of the anastomosis (58). The submucosa contains mainly collagen type I.

Literature data report an augmented collagen deposition both by native and oligo-HA (162–164) while other studies show a decreased collagen production (165). Studies are performed on different types of fibroblast (fetal, adult, dermal or lung) and different treatment times. This could justify the difference on the response.

Data in literature report that treatment with butyrate 4 mM for 48 hours promotes collagen biosynthesis in human dermal fibroblast by over-expression of insulin growth factor I, the most potent stimulator of collagen biosynthesis in the skin (160). The concentrations of HABut used in the test shown in figure 4.25 b correspond to lower butyrate concentrations and this may be the reason why data obtained in our expriments with HABut do not have a significant effect on collagen synthesis.

This assay measures the production of collagen I but also the overall quantity of collagen is important and is given by the equilibrium between degradation and production.

Collagen type III and V are also present in the intestine environment but the influence of HA and HABut on these molecules was not evaluated.

4.3.6. Evaluation of the effects of butyrate on the antioxidant mechanisms of colonocytes

The aim of the test reported hereafter was to verify the effects of butyrate at low and physiologic concentrations on the antioxidant cellular processes (135,166). The antioxidant properties of butyrate were assessed for concentrations of 0.07, 0.4 and 1.4 mM.

Cellular Antioxidant Assay (CAA; (134)) was used to determine the ability of butyrate to detoxify from reactive oxygen species formed by the addition of ABAP with consequent formation of oxidating peroxyl radicals. The presence of an antioxidant agent inhibits oxidation of the probe DCFH-DA to the fluorescent 2',7'-dichlorofluorescein (DCF). Therefore, in the presence of an antioxidant agent a reduction of fluorescence with respect to the control cells is observed. Figure 4.26 a shows that pre-

treatment of NCM356 cells with butyrate causes a significant decrease of fluorescence intensity. The antioxidant capacity of butyrate is comparable to the one exploited by a potent well-known antioxidant, quercetin (used as positive control at 1 and 5 μM).

Butyrate-induced anti-oxidant effect was expressed also as CAA units (percentage of the antioxidant activity) calculated as described in Material and Methods paragraph 3.25 and compared to the CAA values of the positive control (figure 4.26 b).

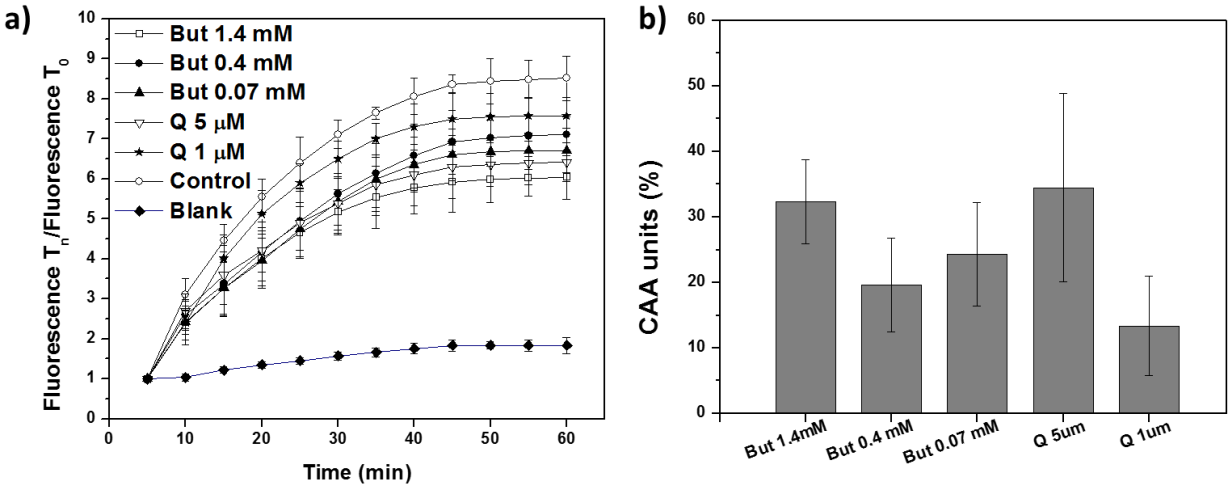

***Figure 4.26**: Antioxidant properties of butyrate (But) a) Time-dependent fluorescence increase induced by ABAP in NCM356 cells pre-treated with DCFH. The plots represent the data obtained from a single representative experiment and are expressed as mean ± st.dv. with n = 6. Cells were pre-treated with the indicated concentrations of butyrate (But) and Quercetin (Q). Control is a cell sample treated with ABAP and DCFH without anti-oxidant agents, blank are cells pre-loaded with DCFH alone. b) Calculated values for cellular antioxidant activity (CAA) of sodium butyrate (But) and quercetin (Q) in NCM356 cells. The results are reported as the average of four independent experiments.*

To confirm the effectiveness of butyrate on protection of cells from damages induced by a strong oxidating agent, NCM356 cells were treated with hydrogen peroxide (H_2O_2) and cellular viability was evaluated in presence and absence of butyrate. Cells were pre-treated with butyrate for 12 hours then H_2O_2 was added for additional 24 hours. Figure 4.27 reports viability of cells treated with butyrate and H_2O_2 and shows a significant effect of butyrate on inhibiting the decrease of viability given by H_2O_2. This effect is dependent on the concentration of butyrate since higher concentrations have a higher effect on the inhibition of viability decrease caused by H_2O_2.

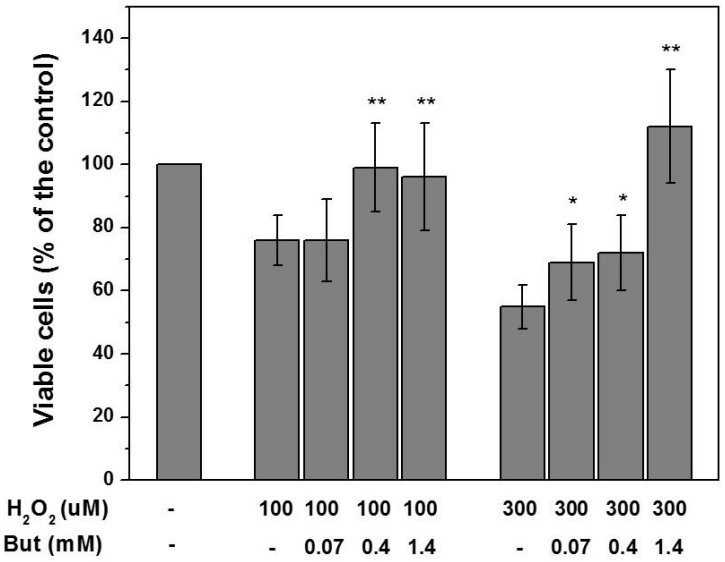

***Figure 4.28**: Effect of butyrate (But) on viability of NCM356 cells exposed to H_2O_2. Cells were treated with H_2O_2 (100 and 300 µM) for 24 h after pretreatment with sodium butyrate for 12 hours (0.07, 0.4 and 1.4 mM). Cells treated with plain medium served as a control that was set equal to 100%. Data are expressed as mean ± st.dv.. For statistical analysis, samples exposed to butyrate and H_2O_2 were compared with samples treated only with H_2O_2 at the same concentration (n = 6): *p < 0.1; **p < 0.05 by t-test.*

In order to identify the molecular mechanism through which butyrate displays its antioxidant ability, several enzymes involved in the protection of cells from oxidant molecules were investigated. The effect of butyrate on activity of Catalase (CAT), Superoxide Dismutase (SOD), Glutathione reductase (GR), Glutathione peroxidase (GPx) and Glutathione-S-Transferase (GST) is shown in figure 4.28.

CAT activity shown in figure 4.28 a undergoes a time and dose-dependent increase after butyrate treatment for all the concentration used. The maximum variation is achieved at 48 hours of treatment while at 24 hours a significant increase is detected only for the highest concentration used. CAT activity was also studied for shorter time of treatment but no difference was seen between treated and not treated cells (data not shown).

Since Catalase is one of the key defense systems against oxidative stress by converting H_2O_2 to H_2O and O_2, the increased levels after butyrate treatment could explain the significant protection from H_2O_2 toxicity in pre-treated NCM356 cells.

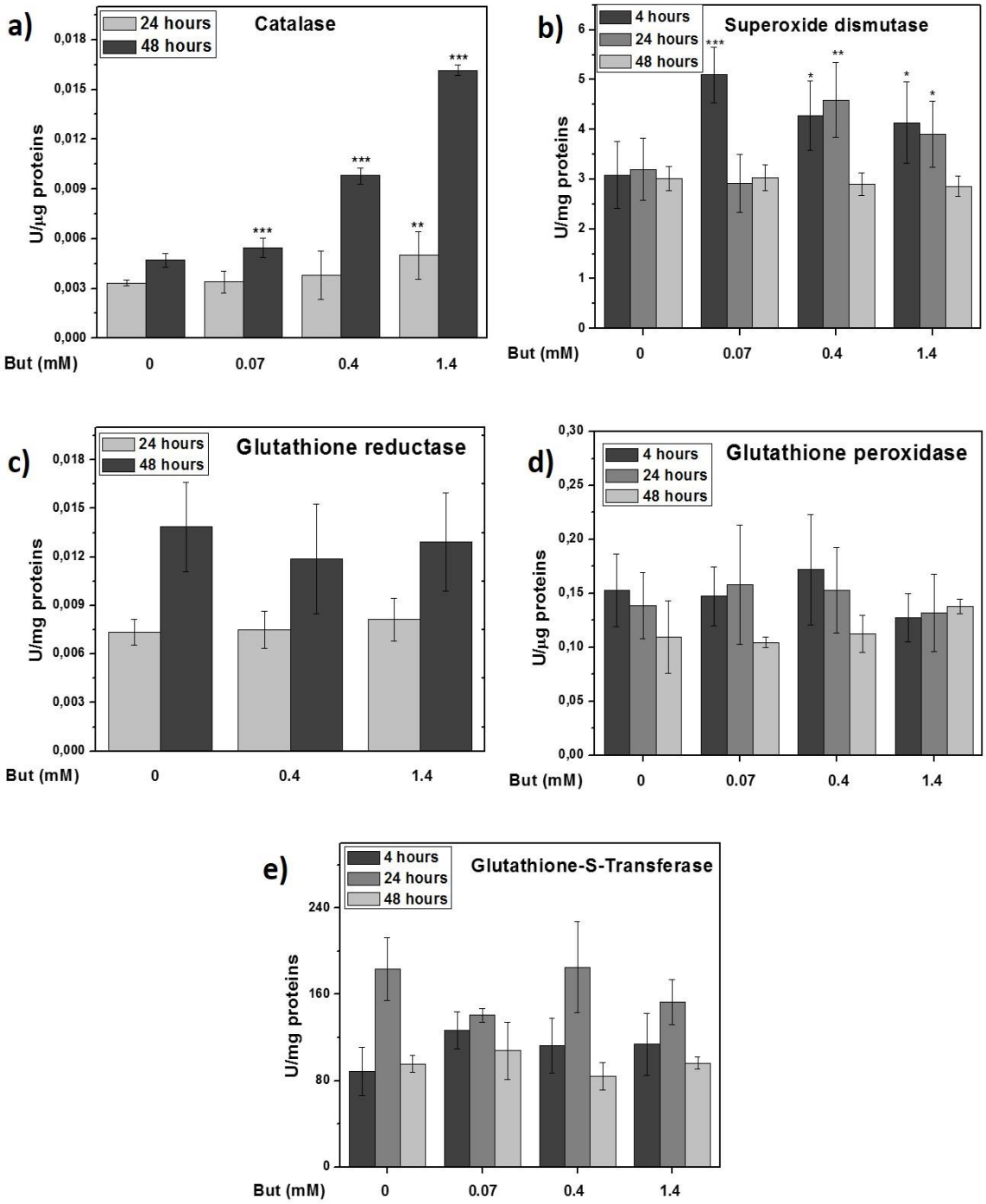

Figure 4.28**: Effects of various concentrations of butyrate (But) on the activity of: a) Catalase; b) Superoxide dismutase; c) Glutathione reductase; d) Glutathione peroxidase; e) Glutathione-S-Transferase. Data are expressed as mean ± st.dv.. For statistical analysis, samples exposed to butyrate were compared with samples treated with plain medium (n = 3). In the Student's t test, p = 0.1 was considered as the limit of significance. In detail *p < 0.1; **p < 0.05;p<0.01 by t-test.*

A transient increase in SOD activity is seen within the first four hours of treatment butyrate at 48 hours no significant increase is observed (figure 4.28 b).

No significant difference in enzyme activity is seen between treated and non treated cells for the other enzymes studied, namely GR, GPx and GST (figure 4.28 c, d and e).

Since glutathione is a very important molecule for protection against oxidants and a decrease in the GSH-to-GSSG ratio is considered an oxidative stress marker, quantification of this ratio after 24 and 48 hours of butyrate treatment was carried out. Figure 4.29 shows the behavior of this ratio at 24 (a) and 48 (b) hours of butyrate treatment.

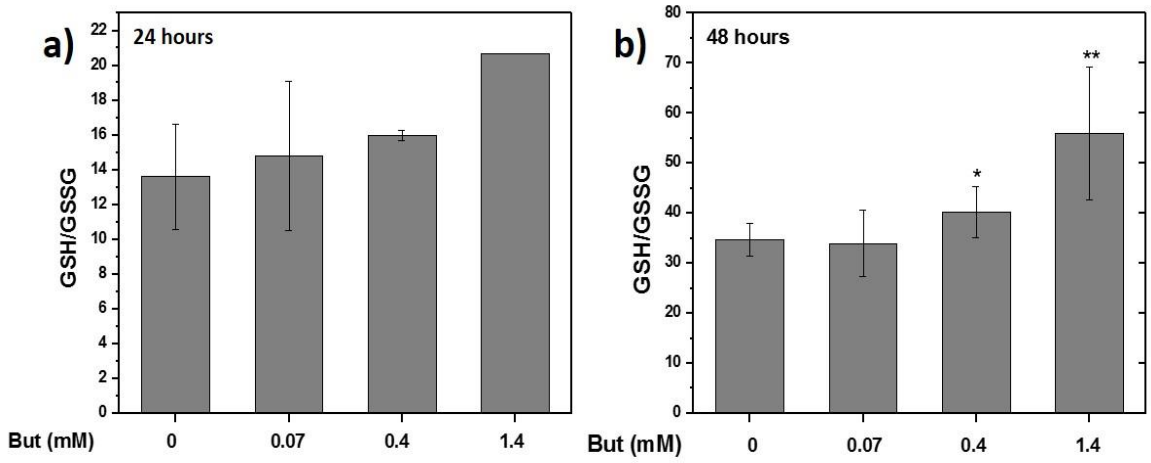

***Figure 4.29**: Ratio between reduced (GSH) and oxidized (GSSG) glutathione in non-treated and cells treated with butyrate (But) after 24 (a) and 48 hours (b). The reported data are the mean of three independent experiments. Student's t test: *p < 0.1; **p<0.01.*

The effects of butyrate on enzymatic and non-enzymatic molecules involved in protection against ROS are schematized in figure 4.30.

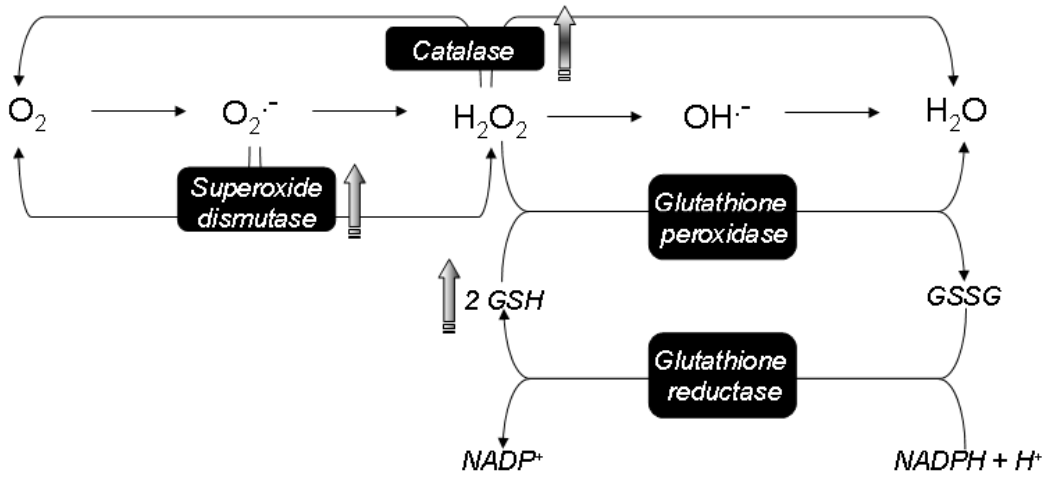

***Figure 4.30**: Schematic representation of the main antioxidant cellular pathways. The arrows indicate the network points affected by butyrate cell treatment*.

5. Conclusions of part 1

Wound repair is achieved by sophisticated interaction of different factors and cell types like fibroblasts, keratinocytes, immune cells (like macrophages and lymphocytes) and endothelial cells. All this cells are equipped with HA receptors therefore interact with HA. In fact, biomaterials containing HA are widely used for wound repair.

A biomaterial based on alginate and HA was successfully produced as described in the first part of the work. Different parameters that influence the HA and alginate release from the membranes in an aqueous environment were studied. The results led to the hypothesis that the polymers' release depend on the kinetic of hydrogel formation. Since HA and alginate are both negatively charged, when the alginate matrix is formed rapidly (high calcium concentrations, HA of lower molecular weight) HA is more segregated from the alginate matrix while the crosslinking density of the matrix itself is higher. This leads to higher release of HA and lower release of alginate (thus gel degradation).

Our tests showed that HABut is able to bind to both fibroblasts and colonocytes and to be internalized. Butyrate is probably released from HABut and exerts its biological functions inside the cell. It is released from the HABut molecules once it is internalized into the cell probably by CD44 interaction.

The use of butyrate in the form of HABut inside the patch for anastomosis healing was justified by data in literature showing that butyrate enemas had a positive effect on colonic anastomotic strength (3). However, *in vitro* tests with these molecules demonstrated that both butyrate and HABut inhibit fibroblasts and colonocytes proliferations in a dose-dependent manner. Moreover, cells treated with butyrate at high concentrations are induced to block their cycle progression with further triggering of the apoptotic pathway.

Thus, these results led us to exclude the use of HABut inside the AnastomoSEAL patch since it would be applied at the outer face of the intestine were mainly fibroblasts of the serosa are present. Instead, based on literature data, the possibility to sinergically combine the use of a patch loading HA to the use of HABut or butyrate enemas was considered. *In vivo* colonocytes are not exposed to high butyrate concentrations since the presence of the mucus and the structure of the intestine surely create a

gradient of butyrate concentration. Moreover, butyrate half-life causes a low concentration of butyrate at the final part of the intestine compared to the first part.

Thus cells of the crypt that are located in the highest part of the intestinal crypt are exposed to higher butyrate concentrations while the cells located at the lowest part of the crypt are exposed to lower butyrate concentrations. In this scheme an apoptotic effect of butyrate could be looked-for since the most exposed cells are those in contact with stress given by food and pathogens ingested with air, liquid and food. Thus these cells are at high risk of mutagenesis and a rapid turnover is a mechanism by which butyrate could protect the intestine from tumor development. The cells at the bottom of the crypts could have benefic effect from low concentration butyrate exposure thanks to other mechanisms (see Figure 5.1).

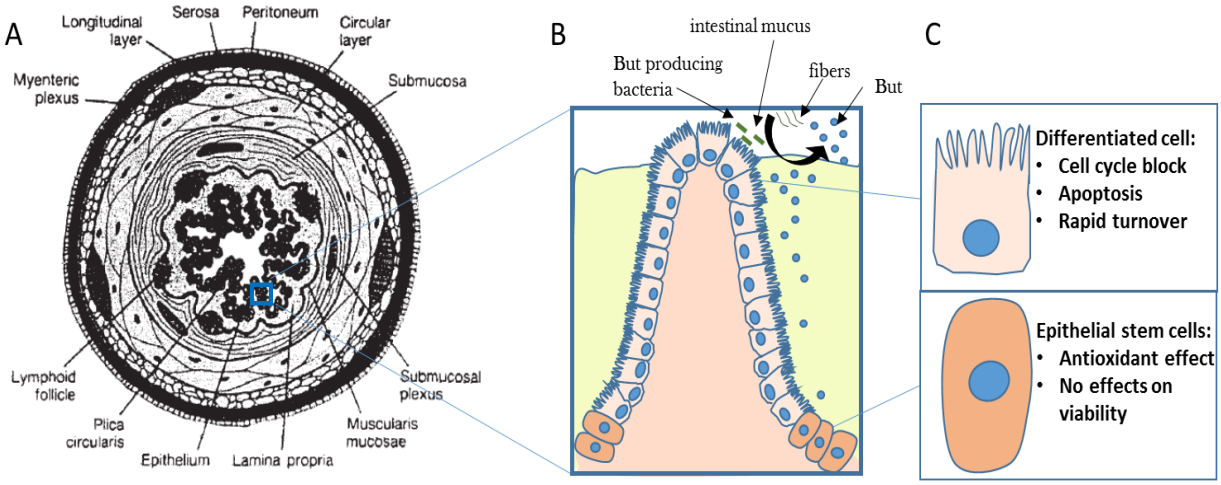

Figure 5.1: Possible mechanism of butyrate (But) in its physiologic environment: A) the structure of the intestine; B) an intestinal crypt were butyrate is produced by bacteria from mainly undigested dietary fibers and creates a gradient of concentration; C) butyrate effects on differentiated cells that are located in the top of the crypt and on epithelial stem cells located on the bottom of the crypt.

In accordance with what already published in literature, butyrate at low concentrations had positive effects on antioxidant mechanisms of the cells. Butyrate at 0.4 and 1.4 mM showed a protection against H_2O_2 induced cell damage and had cellular antioxidant activity comparable to the activity of quercetin, a potent natural antioxidant. These effects were connected to induction of catalase activity and an induction of higher GSH/GSSG ratio.

Nevertheless this was retained not enough for the use of butyrate enemas together with alginate-HA patches at the outer side of the intestine. The AnastomoSEAL consortium decided to further develop Alginate-HA patches excluding the use of both HABut and butyrate from the patch. HA displays, mainly on fibroblasts, biological properties that are highly beneficial and useful in promoting tissue healing. These results justify the rationale of its use as bioactive component of the patch.

The biomaterial composed of alginate and HA was further characterized in our laboratory and also in other laboratories of the AnastomoSEAL consortium.

6. Results part 2: Chronic non-healing wounds

This part of the work was focused on the bottom-up design, production and characterization of a polymeric biomaterial that should fasten healing of chronic non-healing wounds.

6.1. Selection of best performing Chitlac-nanosilver colloidal suspension

Since silver nanoparticles have a very high antibacterial capacity (122,167) but free nAgs are toxic for eukaryotic cells due to endocytosis (168), the system chosen for the incorporation of nAgs was their synthesis in wet conditions in the presence of the Chitlac polymer (CTL) as previously described by Travan et al (7).

With the purpose of finding the best combination between the concentrations of CTL and $AgNO_3$, UV-Vis spectroscopy of different CTL-nAg suspensions was performed and the results are shown in Figure 6.1. The plasmon resonance peak of each solution can qualitatively evaluate the dispersion, number and size of nanoparticles: a symmetric and narrow peak of the solution is associated to a good dispersion of nanoparticles, high absorbance with a higher number of nanoparticles. Moreover, in order to have a good stabilization of the nanoparticles within the polysaccharide solution used for the gel synthesis, a low CTL concentration is required.

$AgNO_3$ 1 mM is not sufficient to generate good nanoparticles (Figure 6.1 a) since the height of the peaks that are formed are low for all the CTL concentrations used. When $AgNO_3$ 2 mM is used, there are high peaks for concentrations of CTL equal or higher than 2 g/L while a concentration of 1 g/L is not enough to coordinate the silver ions in the solution, as the peak of this formulation is very broad and low.

Increasing $AgNO_3$ concentrations require higher CTL concentrations in order to have good plasmon resonance peaks of nanoparticles (Figure 6.1 c and d). Highest and narrower peaks are formed in presence of $AgNO_3$ 8 mM (Figure 6.1 d) and 10 mM (Figure 6.1 e) in presence of CTL 8 or 10 g/L but the viscosity of these suspensions is very high. It should be considered that this solution will be mixed with

other polysaccharides that further increase viscosity. Based on these criteria, the best performing suspension was selected as CTL 4 g/L and $AgNO_3$ 2 mM (red arrow).

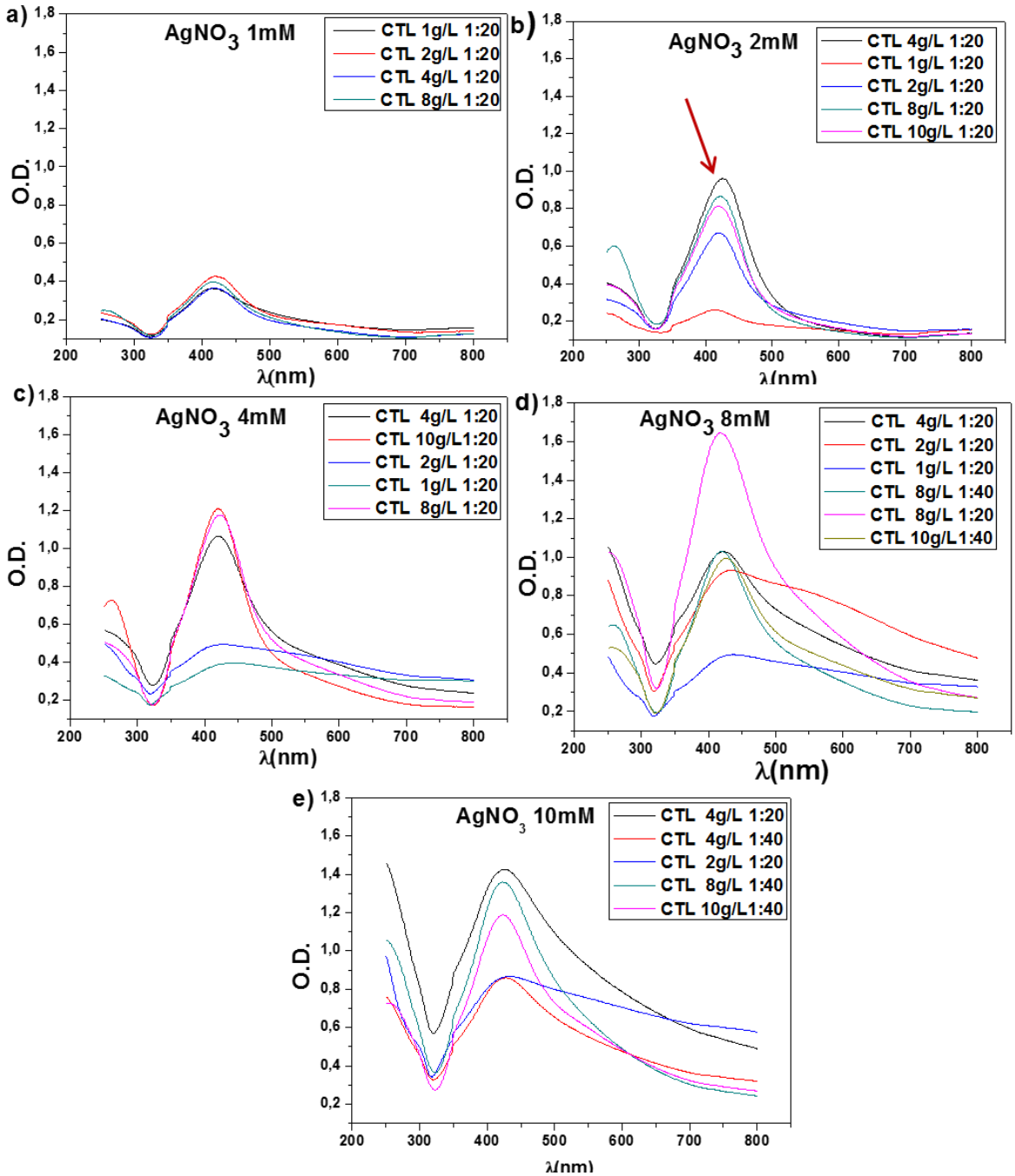

***Figure 6.1**: UV-Visible spectra of different solutions of CTL-nAg with different concentrations of CTL and a) $AgNO_3$ 1 mM; b) $AgNO_3$ 2 mM; c) $AgNO_3$ 4 mM; d) $AgNO_3$ 8 mM and e) $AgNO_3$ 10 mM. The solutions are diluted 1:20 or 1:40 as indicated in the legend of each picture.*

6.2. Biomaterial manufacturing

The production process used for the biomaterial production is the same of the production process for the AnastomoSEAL patch with only small variations.

For the manufacturing of the patch, HA at different concentrations was dissolved in water together with alginate. The selected CTL-nAg suspension was added dropwise under stirring to the polysaccharide solution. Before mixing the two solutions, HEPES buffer 10 mM was added in order to maintain a physiologic pH. In these conditions no precipitation of polymers was observed (130). Then the polymers solution was subjected to gelation in presence of $CaCO_3$ and GDL as described for the patch preparation of the colorectal anastomosis (paragraph 4.1).

The foaming agent was added to the polysaccharide solution just before adding GDL. Immediately after GDL addition, a foam maker was used for 30 seconds and the solution was poured into the dish. Then the foamed hydrogel was subjected to freeze-casting.

Previously, Tween 20-foamed membranes were prepared. The membranes produced by foaming with Tween 20 seem to have good properties in terms of flexibility and manageability. During foaming of the polysaccharide solution and the subsequent gelation the structure is highly porous but during the freeze-drying process there is a small collapse of the structure which becomes less porous (data not shown).

Subsequently, Hydroxy-methyl-2-propyl cellulose (HPMC) was chosen as foaming agent due to its biocompatibility and its role in the preparation of porous alginate-based matrices (169); HPMC finds already application in the biomedical field for artificial tears, orbital surgery and gastro-soluble coatings for drugs (8).

The production process of this membrane is described in Figure 6.2. A brown soft, flexible and spongy biomaterial is obtained as shown in the same figure. The membrane can be produced in different sizes and can be easily cut in the needed shape.

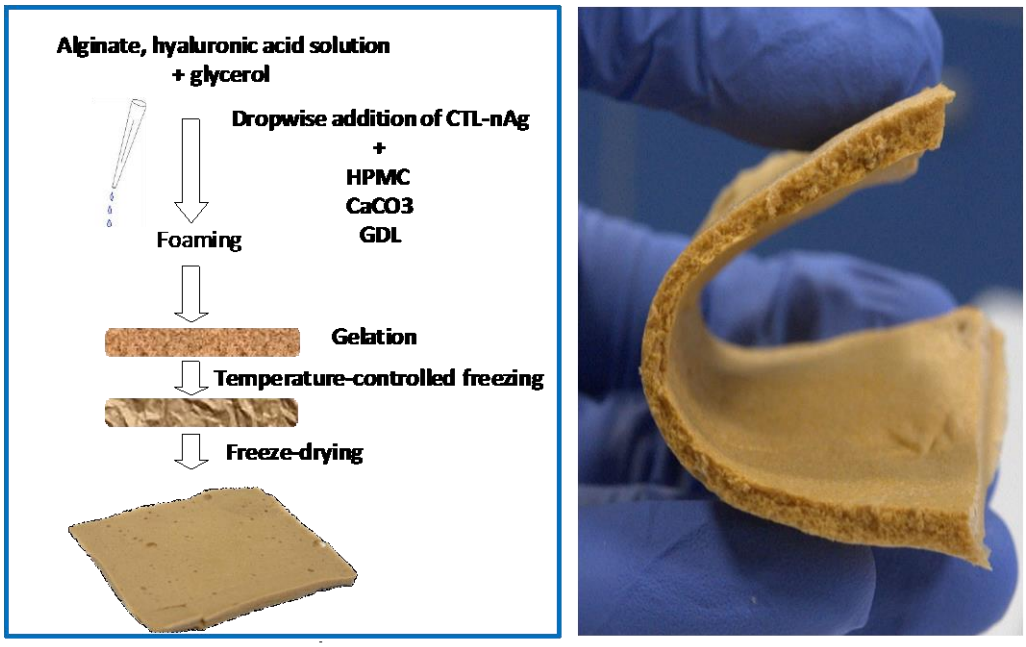

***Figure 6.2**: Scheme of the manufacturing process of the membrane with alginate and CTL-nAg and a picture of the membrane (Formulation K) cut on one side to show the highly porous structure.*

6.3. Selection of best HPMC concentration

In order to select the best HPMC concentration for the biomaterial, different quantities of HPMC were incorporated into the membrane. The selection was based on the results given by antibacterial tests and in vitro biocompatibility test.

6.3.1. Biocompatibility assay

In order to evaluate the in vitro biocompatibility of HPMC, the compound was tested on a murine fibroblast NIH-3T3 cell line and on human adult primary fibroblasts (HDFa); Alamar blue assays were performed and Figure 6.3 shows the effect of HPMC at different concentrations. High concentrations of HPMC (15-20 g/L) slow down proliferation of NIH-3T3 cells while lower concentrations are not toxic for both NIH-3T3 and HDFa cells.

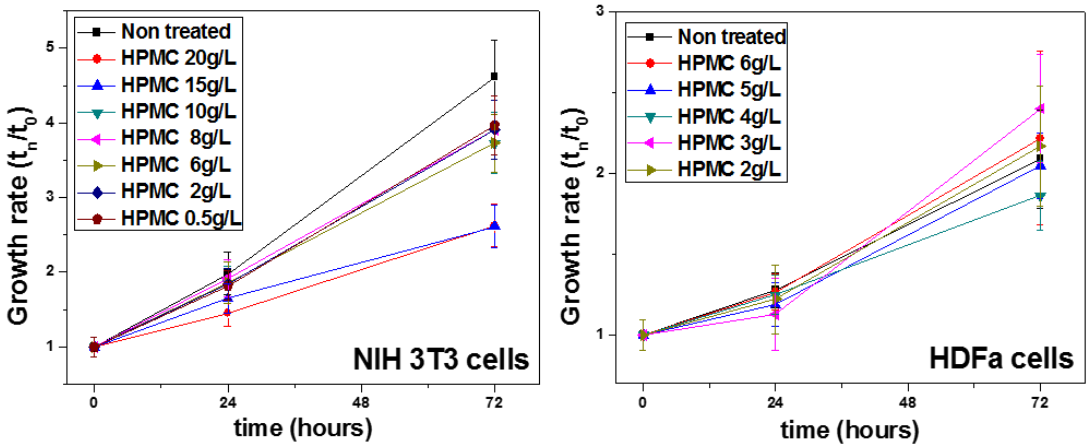

***Figure 6.3**: In vitro proliferation of cells treated with HPMC at different concentration (Alamar blue assay). Data are obtained from a single representative experiment and are expressed as mean ± st.dv. with n=6.*

6.3.2. Antibacterial activity of membranes with different HPMC concentrations

In order to evaluate the effect of HPMC concentration inside the membranes (which affects the foamed structure), HPMC at concentrations 4 g/L and 6 g/L was used for the membrane preparation. The antibacterial activity of the membranes (Formulations A, B, C, D, E and F) was tested on three different bacterial strains that commonly infect chronic non-healing wounds.

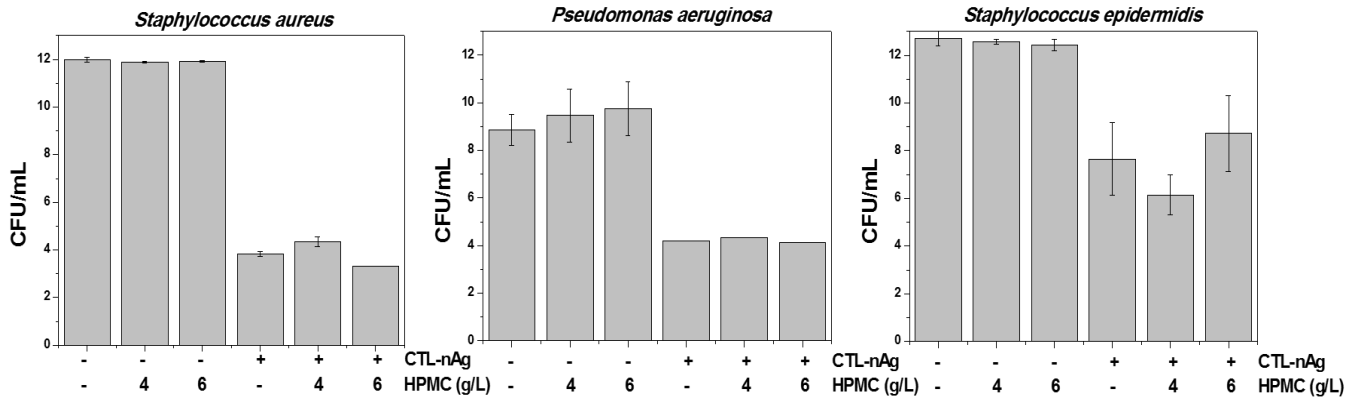

***Figure 6.4**: Antimicrobial efficacy of membranes with different content of HPMC in the presence or absence of CTL-nAg. Plus (+) indicates presence of CTL-nAg and minus (-) indicates absence of CTL-nAg. Data obtained from a single representative experiment and are expressed as mean ± st.dv. with n=3.*

Overall, the antibacterial tests against planktonic *S.aureus*, *P.aeruginosa* and *S. epidermidis* showed a very good antibacterial activity of the biomaterial. These data agree with other data obtained for hydrogels, membranes, scaffolds and coatings containing CTL-nAg (Travan 2009, Travan 2010, Sacco 2015, Marsich 2013).

The membrane containing 4 g/L HPMC was chosen for further experiments since no big difference was seen on antibacterial activity between the two tested HPMC concentrations.

6.4. Selection of best HA concentration

In order to select the best HA concentration for the biomaterial, different quantities of HA were incorporated into the membrane. The selection was based on the results given by antibacterial tests and in vitro biocompatibility test.

6.4.1. Antibacterial activity of membranes with different HA concentrations

The antimicrobial activity was tested on *Staphylococcus aureus, Staphylococcus epidermidis* and *Pseudomonas aeruginosa;* no difference in antibacterial activity was observed in the CTL-nAg membranes with HA (Formulations J, K and L) with respect to those without HA (Formulation E) as shown in Figure 6.5. Membranes without CTL-nAg were used as controls (Formulations B, G, H and I).

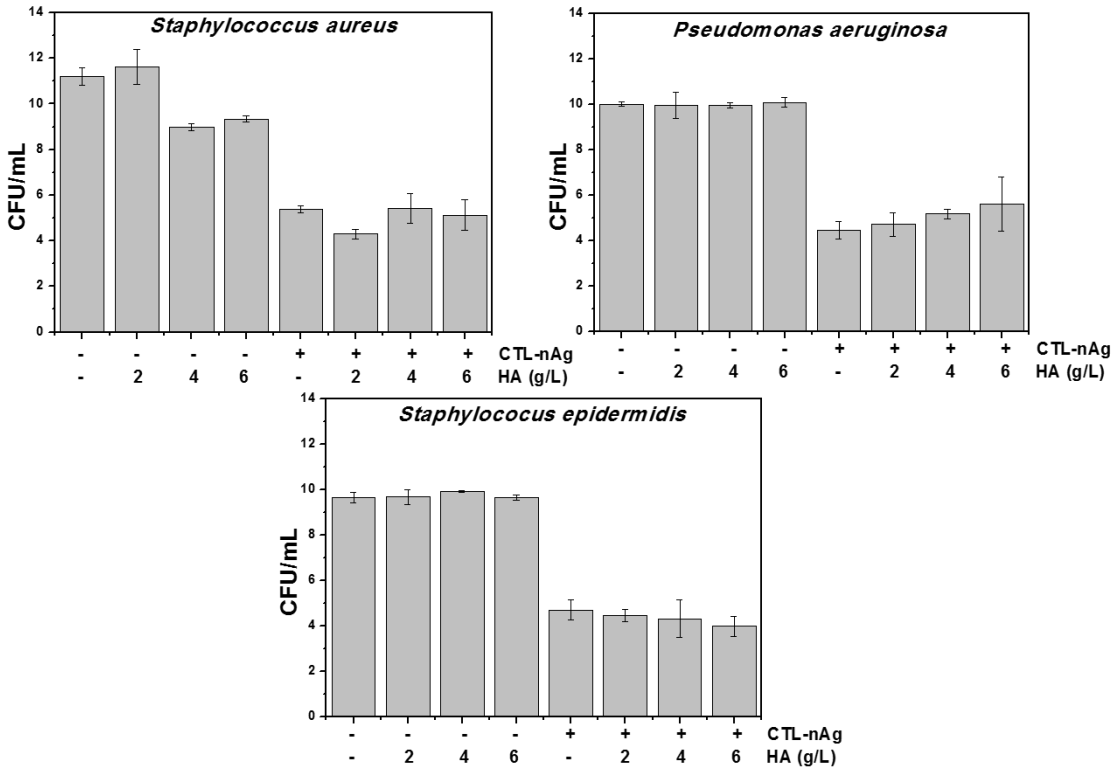

Figure 6.5*: Antibacterial tests of membranes containing CTL-nAg and HA at different concentrations. Data obtained from a single representative experiment and are expressed as mean ± st.dv. with n=3.*

6.4.2. Biocompatibility assay of membranes with different HA concentrations

Cellular toxicity of membranes (Formulations B-2, E-2, G-2, H-2, I-2, J-2, K-2 and L-2) with different concentrations of HA and 4 g/L HMPC was tested on human primary fibroblasts. Two modalities of testing were used: direct contact of the materials with the cells and treatment of the cells with components released by the membranes incubated in culture medium.

Figure 6.6 a shows the results of the contact test: there is no difference between the different materials and the non-treated cells.

Figure 6.6 b shows the results of the release test: membranes without HA (Formulation E-2) and with 2 g/L HA (Formulation J-2) are only slightly toxic while the material with 6 g/L HA (Formulation L-2) is highly toxic. This could be ascribed to the fact that the high content of HA may interfere with the alginate matrix stability, resulting in a loose structure that is prone to release a high amount of nanoparticles. Although mechanical tests were not performed for the evaluation of the mechanical

properties of these patches, the poor resistance of the material with the highest HA concentration was qualitatively pointed out. Conversely, the membrane containing 4 g/L HA (Formulation K-2) is not toxic.

This difference in the results of the two employed toxicity tests could be ascribed to the difference of the ratio between the mass of the material and the volume of the medium where the sample is soaked. In the case of the release test, the concentration of the components released is higher because greater is the ratio mass of the material/volume of extraction medium.

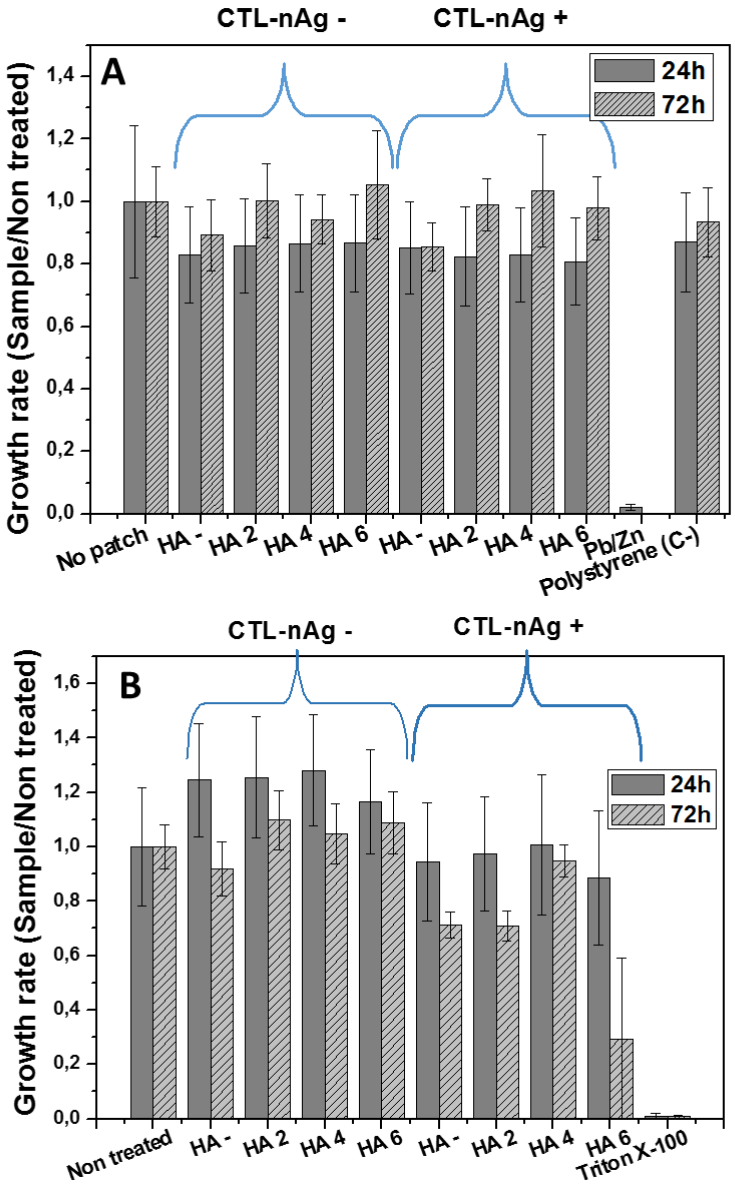

***Figure 6.5**: In vitro biocompatibility tests on fibroblasts A) for direct contact with membranes and B) on components released from membranes with HA. Data are shown as mean ± st.dv. with n = 4 in A and n= 6 in B.*

In literature, the cytotoxicity of silver in form of nanoparticles is discussed (167,170,171). Different works show that silver can be cytotoxic for eukaryotic cells since it interferes with mitochondrial function leading to apoptosis (168,172–174). Nanoparticles have to be available for cellular uptake in order to exert cytotoxicity. CTL-nAg suspensions entrapped into hydrogels, membranes and coatings were previously shown to be not cytotoxic on eukaryotic cells (7,127,175). The data obtained here confirm the biocompatibility of CTL-nAg when entrapped into membranes.

6.5. Structural and mechanical analysis

On the basis of previous tests, the membrane containing alginate 8 g/L, HA 4 g/L, CTL-nAg (CTL 4 g/L, $AgNO_3$ 2 mM, Ascorbic acid 1 mM) HPMC 4 g/L, $CaCO_3$ 20 mM, GDL 40 mM, 5% v/v glycerol (Formulation K) was selected for further physico-chemical and mechanical analysis characterizations.

The foamed membrane was analyzed by means of electron microscopy in dry conditions both at top view and at cross-section. Figure 6.6 reports the SEM images of samples with and without nanoparticles. In both cases, the cross section shows a highly porous structure while the top view shows a smooth surface.

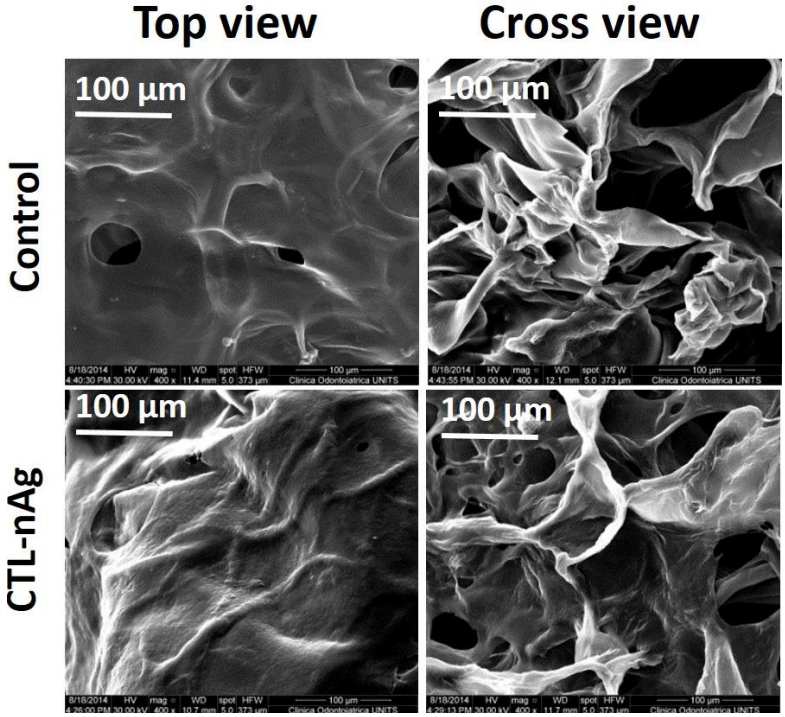

Figure 6.6*: SEM images of membranes with Formulation H (without nanoparticles; upper figures) and Formulation K (with nanoparticles; lower figures).*

An ideal wound dressing material must have good tensile strength because the dressing should not be damaged by handling procedures and must withstand the stress resulting from skin movements without rupturing.

The stiffness (Young's Modulus), the resistance (stress at break) and the deformation (strain at break) of the material were then studied by uniaxial tensile tests and results are reported in Figure 6.7.

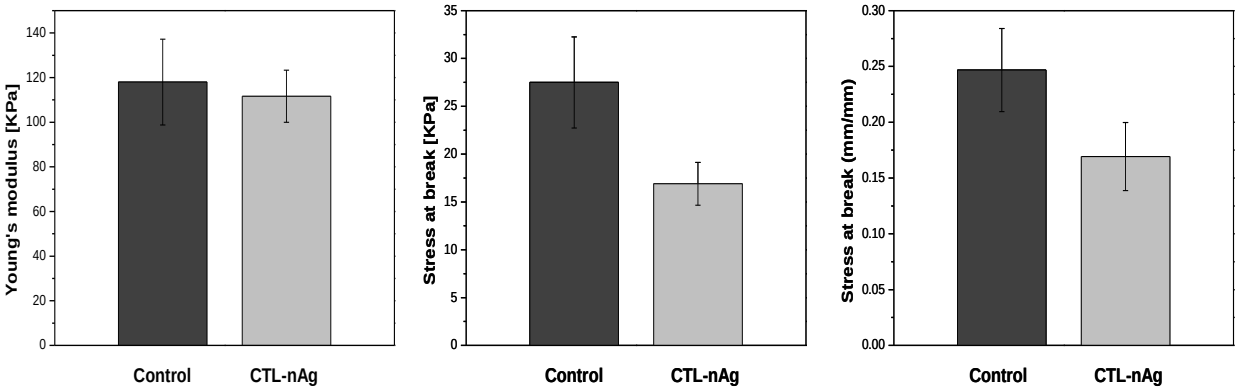

Figure 6.7*: Mechanical properties of the foamed membranes: Young's modulus (left), stress at break (center) and strain at break (right). Data are expressed as mean± st.dv. with n=5. Control represents the membrane with Formulation H and CTL-nAg the membrane with Formulation K.*

Mechanical properties of alginate matrices depend on several parameters such as type of alginate (molecular weight distribution and chemical composition) and alginate concentration (142,169). The results pointed out that, in the presence of CTL-nAg, the membranes display lower strength and deformation at break compared to the control: this could be ascribed to the destabilizing role of the polycation with respect to the alginate cross-linked matrix. However, the stiffness of the membranes (Young's modulus) is comparable in the two cases.

6.6. Reswelling kinetics

The reswelling behavior of the materials with CTL (Formulation M) or with CTL-nAg (Formulation K) was studied in HBSS buffer. Figure 6.8 reports the swelling behavior, expressed as a variation over time of the weight rate (weight of the membrane at t_x over weight of the dry patch). An immediate increase of

the weight is observed within the first minute, which is followed by a small decrease of weight of samples containing CTL-nAg (Formulation K). This behavior can be explained by ascribing the initial weight increase to water absorption and the following decrease to release of HA. In fact, HA is embedded inside the alginate matrix and when immersed in solution HA is extruded from the alginate matrix since both polymers are negatively charged. For this reason a ^{1}H-NMR was performed on the components released after 30 minutes and confirmed the release of HA (data not shown).

The material containing CTL (Formulation M), absorbs less water than the one containing CTL-nAg (Formulation K).

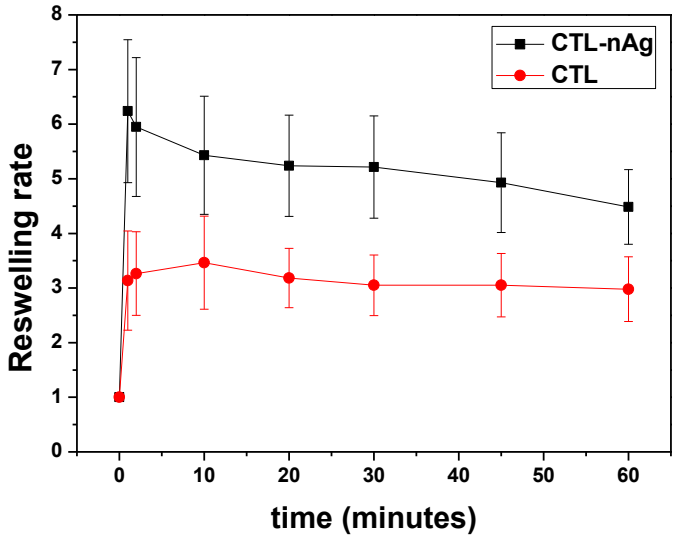

***Figure 6.8**: Swelling behavior of membranes with (red, Formulation K) and without (black, Formulation M) CTL-nAg. CTL represents the membrane with Formulation M while CTL-nAg the membrane with Formulation K. Data are expressed as mean ± st.dv. with n=4.*

Since an excess of exudate characterizes chronic wounds, the reswelling kinetics of the biomaterial is important. A good biomaterial for this application should keep the wound wet and at the same time should absorb the excess of exudate (6).

Alginate membranes are already known to have a great absorbency (169) which was confirmed also for the alginate membrane produced in this work. As other alginate dressings, the membrane obtained here should be used in wounds with high exudate amount.

6.7. Water-vapor transmission rate

Besides a good water swellable nature, an important requisite for a wound dressing to maintain a moist environment, without risking dehydration or exudates accumulation, is a suitable water vapor transmission rate (WVTR). WVTR is defined as the transmission of the water vapor per unit time through a unit area of the tested material. The biomaterial should keep a balance between presence of liquid and water evaporation.

WVTR was measured for the foamed membrane with Formulation K (containing CTL-nAg). Membranes with CTL (Formulation M), membranes without CTL nor CTL-nAg (Formulation H) and two commercially available membranes were used as control samples. *Connettivina plus®* (Fidia Farmaceutici, Italy) is a highly permeable membrane since it is hyaluronan-impregnated perforated gauze while *Chitoderm™* (Trusetal Verbandstoffwerk GMBH, Germany) is a chitosan containing pad with a polyurethane film of 20 µm which makes it less water permeable. Moreover, bottles sealed with parafilm and non-sealed bottles were used as controls since in the first case, there is no evaporation and in the second case, there is a maximum evaporation. The results are reported in Figure 6.9.

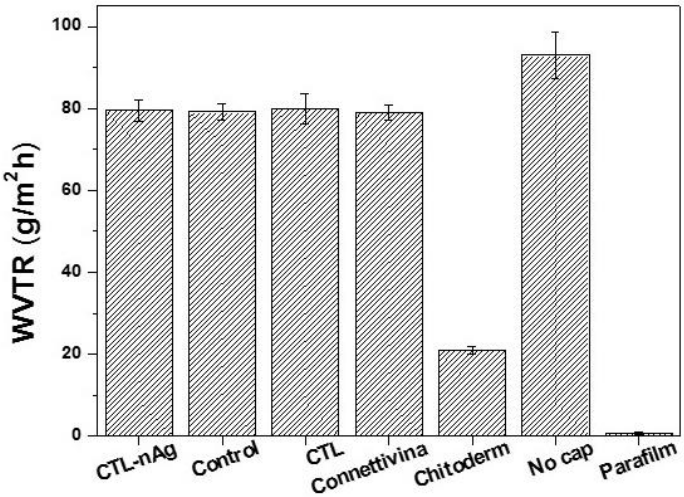

Figure 6.9*: WVTR of alginate membranes and commercial samples. Not capped bottles and bottles capped with parafilm were used as control for free evaporation and no evaporation. Control represents the membrane with Formulation H, CTL represents the membrane with formulation M and CTL-nAg the membrane with formulation K. Data are expressed as mean ± st.dv. with n=6.*

The membrane containing CTL-nAg (Formulation K) has a WVTR (78.5 ± 2.6 g/m^{2}h) comparable to that of the membrane with only CTL (Formulation M) and the control membrane that does not contain CTL nor silver (Formulation H). Moreover the rate of water loss in the form of vapor of this membranes are comparable to the WVTR of *Connettivina plus®*. As expected the WVTR of *Chitoderm™* is much lower (20.8 ± 1.2 g/m^{2}h) than the other samples.

6.8. Silver release

Silver release of the membrane with Formulation K was studied by ETAAS as described in paragraph 3.11. A progressive release of silver can be seen over time (Figure 6.10). However, silver released is only a minimal fraction of the total content of silver: at one week only 0.9% of the total silver is released thus achieving the goal of entrapping silver inside the patch. Similar results were obtained also by Travan et al for CTL-nAg and alginate hydrogels (7).

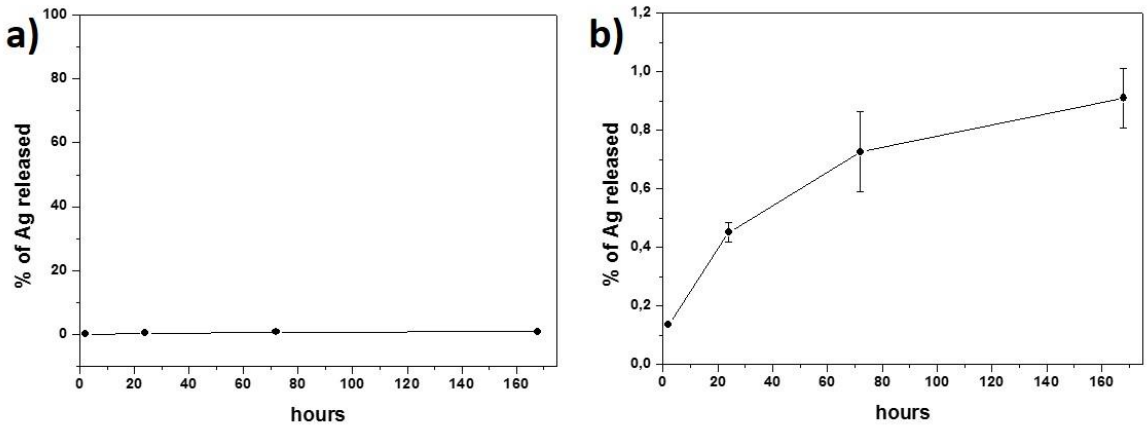

Figure 6.10*: Release of silver from membrane with CTL-nAg (Formulation K) expressed as percentage of total silver content. Zooming on the lowest values were the release is present can be appreciated in b. Data are expressed as mean ± st.dv. with n=3.*

The data obtained here are in agreement with biocompatibility assay since silver has to be available for cellular uptake in order to be cytotoxic.

6.9. Antibacterial activity of the membrane versus biofilms

The antibacterial activity versus planktonic bacteria of alginate membranes was already measured in paragraph 5.4.1. Although the biomaterial showed a very high antibacterial performance with respect to growth inhibition, the activity versus mature biofilms is very important since bacteria growing into biofilms are very different from planktonic bacteria and have a high antibiotic resistance (46). Moreover biofilms are found in 60% of chronic non-healing wounds and only 6% of acute wounds (44). Antibacterial tests on mature biofilms have been then performed.

Figure 6.11 shows the results of the antibacterial test of the membranes (Formulations H and K) versus *Pseudomonas aeruginosa* and *Staphylococcus aureus* biofilm. In both cases, the antibacterial activity against the two bacterial strains is preserved even when bacteria are grown into biofilms. The optical density after MTT assay is twice lower for biofilms treated with the CTL-nAg membrane compared to the control samples.

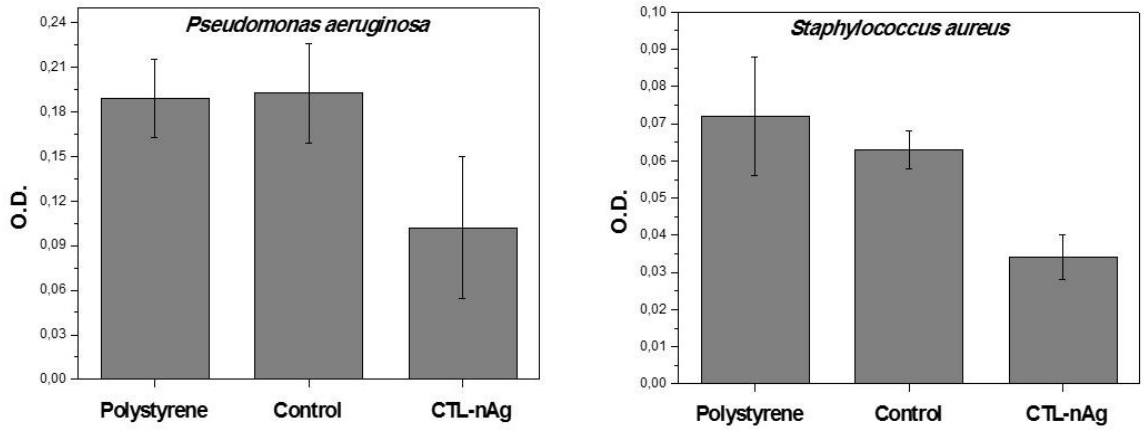

Figure 6.11*: Antibacterial tests of membranes on Pseudomonas aeruginosa and Staphylococcus aureus biofilm. Control represents the membrane with Formulation H and CTL-nAg the membrane with Formulation K. Data are expressed as mean ± st.dv. and n=3.*

To confirm the data obtained through MTT assay, biofilms were studied at the fluorescence confocal microscope after Live/Dead assay. Biofilms were grown into glass coverslips and treated for 24 hours with the material. After Live/Dead cell labelling, images were acquired and were than analyzed calculating the ratio between the red signal (dead cells) and the green signal (alive cells) for the treated sample and the control as shown in Figure 6.12.

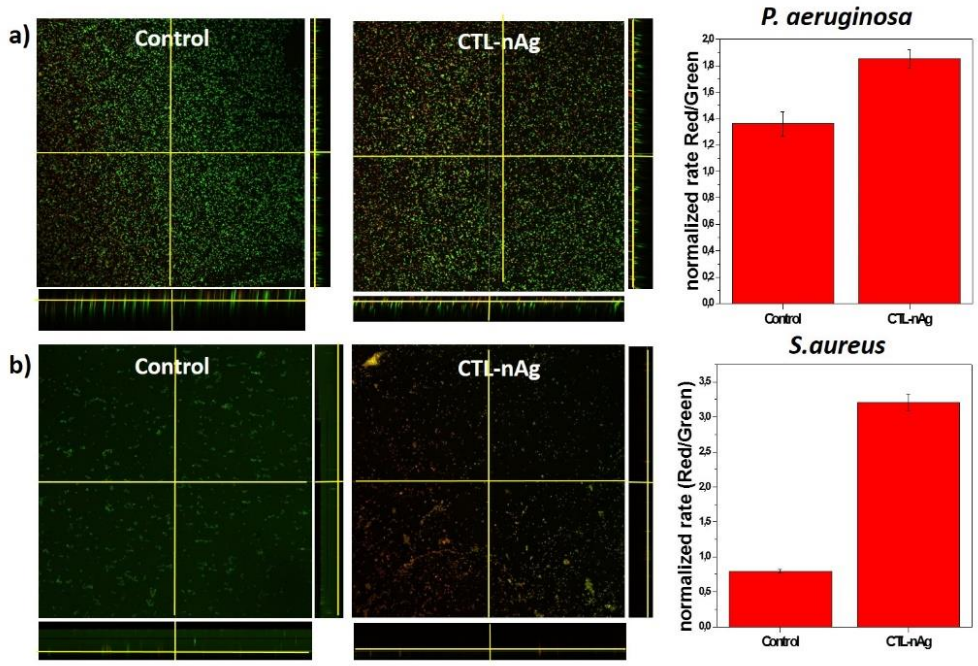

***Figure 6.12**: Live/Dead assay for P. aeruginosa (a) and S. aureus (b) biofilms treated with CTL-nAg patches: images of the biofilms treated with the control and the CTL-nAg patch. Control represents the material with Formulation H and CTL-nAg the membrane with Formulation K. The graphs show the ratio between the red (given by propidium iodide) and the green signal (given by Syto9) normalized over the control sample consisting in non treated bacteria.*

The Live/Dead assay confirmed data from MTT assay: in the biofilm treated with the CTL-nAg membranes there is a significant increase of the ratio between red and green signal for the biofilms treated with CTL-nAg compared to the non treated biofilms. The difference is higher for *S. aureus* biofilms (3.2 times) than for *P.aeruginosa* (1.85 times). This could be because of the ability of *P. aeruginosa* to produce alginate that probably protects him from direct exposure to silver.

6.10. Viability of keratinocytes treated with membranes

Cellular biocompatibility of membranes with Formulation H-2 and K-2 on human primary fibroblasts is shown in paragraph 6.4.2. The effects on cell viability of these membranes were tested also on a

keratinocyte cell line. Two modalities of testing were used as described in paragraph 3.15. Figure 6.13 A shows the results of the contact test while Figure 6.13 B reports the results of the release test.

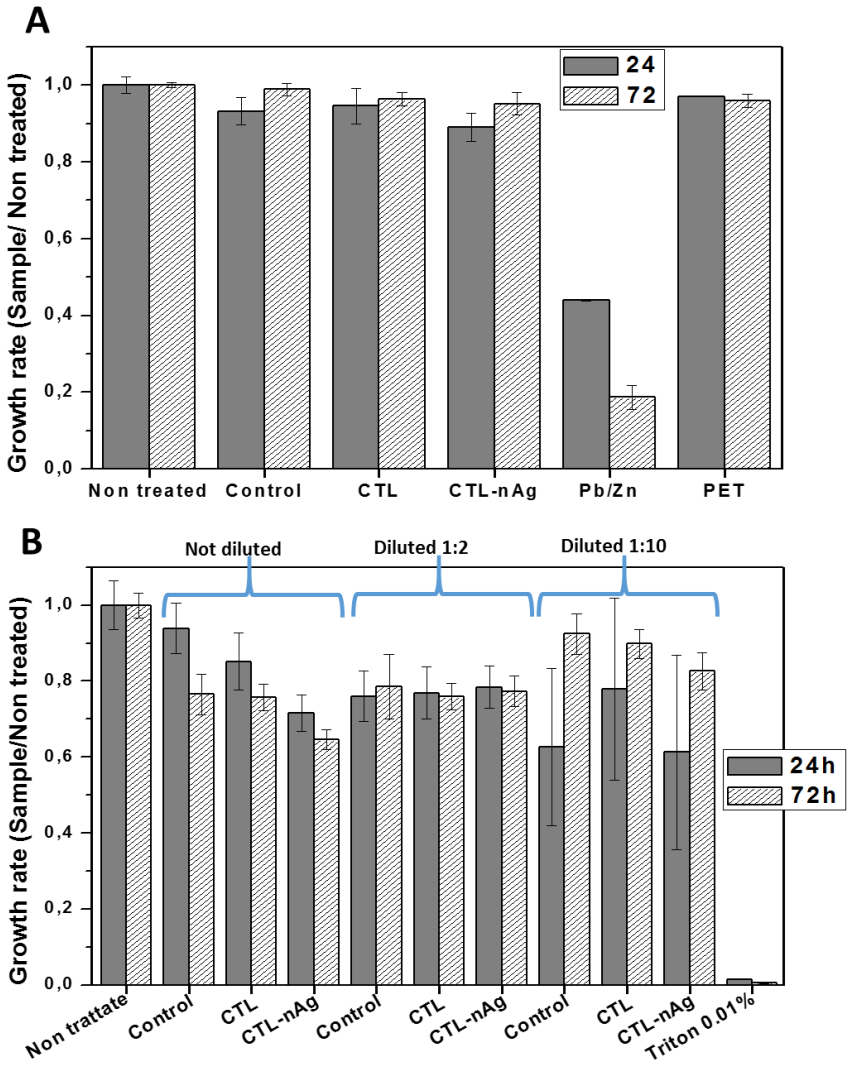

***Figure 6.13**: In vitro biocompatibility tests on HaCaT cells treated with membranes (Control = Formulation H-2; CTL-nAg = Formulation K-2, CTL = Formulation M-2) (A) by direct contact modality and (B) with components released from membranes. Data are mean ± st.dv. with n = 6.*

The test points out that there is no difference between the cells treated with the membranes and the non treated cells.

The proportion of the membrane used was chosen as the maximum quantity of the membrane that could be immersed in the medium. The medium containing the components released from membranes

was then further diluted 1:2 and 1:10. The treatment of HaCaT cells with the non-diluted components released from membranes results in a slight decrease of the cell viability with respect to the non treated cells and cells treated with membranes with CTL but not nAg and membranes without CTL and nAg (control patch). When cells are treated with the diluted medium, containing components released from membranes the viability of cells treated with the membrane containing CTL-nAg is comparable to the viability of cells treated with membranes with CTL but not nAg and membranes without CTL and nAg.

As described in paragraph 5.4.2, in the case of the release test the concentration of the material released is higher because a greater membrane mass is used for the test.

6.11. Scratch test on cells treated with components released from membranes

In vitro scratch tests (which consist in monitoring the closure of a scratch in a monolayer of cells when treated with the material) was performed on both keratinocytes (HaCaT) and fibroblasts (HDFa) since this cell types are important for the wound healing. Cells were treated before performing the scratch with the components released from the membranes (Formulations H-2 and K-2) in culture medium. The percentage of scratch closure over time is shown in Figure 6.14 for both HDFa cells and HaCaT cells.

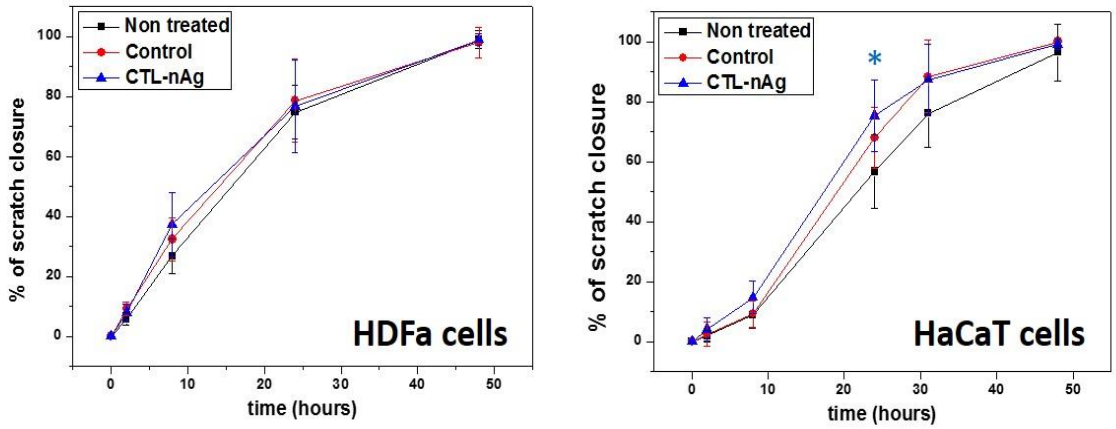

***Figure 6.14**: Scratch test on HDFa cells (left) and HaCaT cells treated with components released from membranes and (Formulation K-2) with CTL-nAg and control membranes without CTL-nAg (Formulation H-2) . Data shown here are from a single representative experiment with n= 8. t-student is indicated in the figure with * for p-value <0.05.*

No difference in the time of closure was observed between treated and non treated cells for HDFa cells. For HaCaT cells, the only point at which there is a significant difference (p-value < 0.05) is at 24 hours for cells treated with the membrane containing CTL-nAg compared to the non treated cells.

Although this result seems to show that the material does not influence wound closure, the model of this assay is based on normal wounds while chronic non-healing wounds are very different from normal ones. Thus, the application of the membrane to chronic non-healing wounds might positively influence a chronic non-healing wound but not a normal wound.

6.12. MMPs activity assay

Excess of proteolytic enzymes is one of the major issues of the chronic non-healing wound; for this reason the effect of the CTL and CTL-nAg suspentions on MMPs activity was studied both on total MMPs extract from cultured cells and on isolated MMP-2 and MMP-9.

Elevated levels of MMP-2 and MMP-9 were found in chronic wounds (40,176,177). Figure 6.15 shows that both CTL-nAg and CTL reduce MMP-2 and MMP-9 activity and also the overall activity of MMPs extracted from fibroblasts and keratinocytes.

The inhibiting activity that CTL exerts on MMPs is not surprising since also Chitosan was found to inhibit MMPs. A possible mechanism for the inhibition of the activity of MMPs is the chelation of Zn ions (178). An hypothesis of the modality by which silver reduces MMPs activity is by binding close to the active site which contains Zn^{2+} (179).

MMPs activity in chronic wounds is 30 times higher than the MMPs activity in acute wounds. Elevated levels of MMP-9 correlate to clinical severity of the wound (176). Inhibition of MMPs activity is a very good result for a biomaterial for chronic non-healing wounds.

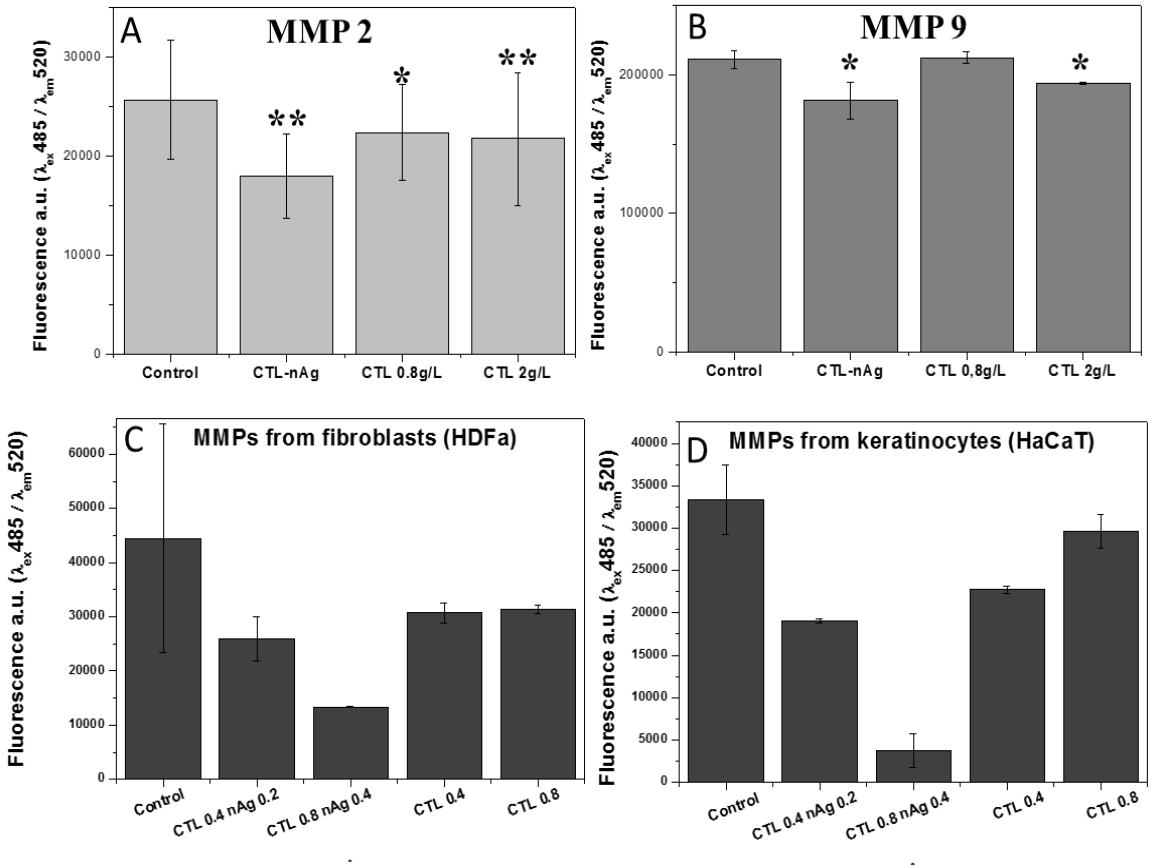

***Figure 6.15**: MMPs activity in presence of a CTL-nAg or CTL: (A) effects on MMP-2; (B) Effects on MMP-9; (C) Effects on MMPs' extract from fibroblasts (HDFa); and (D) Effects on MMPs' extract from keratinocytes (HaCaT cells). Data are expressed as mean ± st.dv. with n=3.*

7. Conclusions of part 2

Chronic-non healing wounds are a great clinical problem which is expected to become more serious due to the increasing duration of life and thus the increasing number of people affected by diseases correlated to chronic non-healing wounds.

In concomitance to the treatment of the causes that led to the chronic wound, the treatment of the wound itself is important. At the moment, a number of products in form of membranes, gels and pomades are available in the market (33) but there is continuous need of biocompatible biomaterials with a wide range efficacy and the capability to prevent biofilm formation while at the same time stimulating wound closure.

In this work a novel bioactive material was synthesized which exploits the properties of HA and nanosilver that were shown to contrast different characteristics of the chronic non-healing wounds.

Maintaining a moist environment into the wound is expected to accelerate reepithelization and to limit infection (180). Thus, a hydrophilic biomaterial like the material developed within this project may represent a good solution. Moreover, the treatment should absorb the wound exudate and be permeable to oxygen. The great capacity of the CTL-nAg membrane to absorb water (as shown by the swelling ratio test) is another good characteristic of our membrane that can prevent also dehydration. The membrane is flexible and simple to apply, and can be cut easily into the desired shape.

CTL-nAg membranes were shown to be effective against various planktonic bacteria and against bacterial biofilms, which makes them appealing for the prevention of bacterial infection and for treatment of infected wounds.

Keratinocytes and fibroblasts are a very important cell types in the healing of wounds. Studies of the toxicity of the membrane on a keratinocyte cell line and on primary fibroblasts showed that the membrane was non cytotoxic on this cells. Moreover, quantification of the release of silver over time from the membrane showed a very low release of silver.

In vitro scratch tests (181) performed on both keratinocytes and fibroblasts showed no significant amelioration of the wound closure but this test mimics a normal wound while chronic non-healing wounds are very different from normal ones.

Excess of proteolytic enzymes is one of the major issues of the chronic non-healing wound; CTL showed an inhibiting activity on MMP-2, MMP-9 and on total extracts of MMPs.

Overall, the research activity led to the production of a non-toxic, foamed and flexible biomaterial with a considerable high antibacterial activity.

In order to be applied to chronic wounds biomaterials should be available in sterile packaging. Thereafter studies on sterilization are needed and afterward in vivo tests on animals should be done (182).

8. References:

1. Diegelmann RF, Evans MC. Wound healing: an overview of acute, fibrotic and delayed healing. Front Biosci J Virtual Libr. 2004 Jan 1;9:283–9.

2. Jiang D, Liang J, Noble PW. Hyaluronan in tissue injury and repair. Annu Rev Cell Dev Biol. 2007;23:435–61.

3. Bloemen JG, Schreinemacher MH, de Bruine AP, Buurman WA, Bouvy ND, Dejong CH. Butyrate enemas improve intestinal anastomotic strength in a rat model. Dis Colon Rectum. 2010 Jul;53(7):1069–75.

4. Coradini D, Pellizzaro C, Miglierini G, Daidone MG, Perbellini A. Hyaluronic acid as drug delivery for sodium butyrate: Improvement of the anti-proliferative activity on a breast-cancer cell line. Int J Cancer. 1999;81(3):411–6.

5. Eming SA, Krieg T, Davidson JM. Inflammation in wound repair: molecular and cellular mechanisms. J Invest Dermatol. 2007 Mar;127(3):514–25.

6. Bowler PG. Wound pathophysiology, infection and therapeutic options. Ann Med. 2002;34(6):419–27.

7. Travan A, Pelillo C, Donati I, Marsich E, Benincasa M, Scarpa T, et al. Non-cytotoxic Silver Nanoparticle-Polysaccharide Nanocomposites with Antimicrobial Activity. Biomacromolecules. 2009 Jun 8;10(6):1429–35.

8. Li CL, Martini LG, Ford JL, Roberts M. The use of hypromellose in oral drug delivery. J Pharm Pharmacol. 2005 May;57(5):533–46.

9. Erfurt-Berge C, Renner R. Chronic wounds - Recommendations for diagnostics and therapy. Rev Vasc Med. 2015;3(1):5–9.

10. Yordanov YP, Shef A. Hypertrophic scars and keloids - Contemporary concepts and treatment options. Acta Medica Bulg. 2014;41(1):57–74.

11. Aukhil I. Biology of wound healing. Periodontol 2000. 2000 Feb;22:44–50.

12. Beldon P. Basic science of wound healing. Surg Oxf. 2010 Sep;28(9):409–12.

13. Young A, McNaught C-E. The physiology of wound healing. Surg Oxf. 2011 Oct;29(10):475–9.

14. Greenhalgh DG. The role of apoptosis in wound healing. Int J Biochem Cell Biol. 1998 Sep;30(9):1019–30.

15. Guo S, DiPietro LA. Factors Affecting Wound Healing. J Dent Res. 2010 Jan 3;89(3):219–29.

16. Schaffer CJ, Reinisch L, Polis SL, Stricklin GP, Nanney LB. Comparisons of wound healing among excisional, laser-created, and standard thermal burns in porcine wounds of equal depth. Wound Repair Regen. 1997 Jan 1;5(1):52–61.

17. Hofer MD, Cheng EY, Bury MI, Park E, Xu W, Hong SJ, et al. Analysis of Primary Urethral Wound Healing in the Rat. Urology. 2014 Jul;84(1):246.e1–246.e7.

18. Ueno C, Hunt TK, Hopf HW. Using physiology to improve surgical wound outcomes. Plast Reconstr Surg. 2006 Jun;117(7 Suppl):59S – 71S.

19. Anastomosis: MedlinePlus Medical Encyclopedia [Internet]. [cited 2015 Oct 5]. Available from: https://www.nlm.nih.gov/medlineplus/ency/article/002231.htm

20. Renvall S, Grönroos I, Laato M. Burst abdomen. Local synthesis of nucleic acids, glycosaminoglycans, proteins and collagen in wounds. Ann Chir Gynaecol. 2001;90 Suppl 215:33–7.

21. Stumpf M, Klinge U, Wilms A, Zabrocki R, Rosch R, Junge K, et al. Changes of the extracellular matrix as a risk factor for anastomotic leakage after large bowel surgery. Surgery. 2005;137(2):229–34.

22. Stumpf M, Cao W, Klinge U, Klosterhalfen B, Kasperk R, Schumpelick V. Collagen distribution and expression of matrix metalloproteinases 1 and 13 in patients with anastomotic leakage after large-bowel surgery. Langenbecks Arch Surg. 2002;386(7):502–6.

23. Thompson SK, Chang EY, Jobe BA. Clinical review: Healing in gastrointestinal anastomoses, Part I. Microsurgery. 2006 Jan 1;26(3):131–6.

24. Rijcken E, Sachs L, Fuchs T, Spiegel H-U, Neumann P-A. Growth factors and gastrointestinal anastomotic healing. J Surg Res. 2014 Mar;187(1):202–10.

25. Bruce J, Krukowski ZH, Al-Khairy G, Russell EM, Park KGM. Systematic review of the definition and measurement of anastomotic leak after gastrointestinal surgery. Br J Surg. 2001 Sep 1;88(9):1157–68.

26. Shogan BD, Carlisle EM, Alverdy JC, Umanskiy K. Do we really know why colorectal anastomoses leak? J Gastrointest Surg Off J Soc Surg Aliment Tract. 2013 Sep;17(9):1698–707.

27. Shogan BD, Belogortseva N, Luong PM, Zaborin A, Lax S, Bethel C, et al. Collagen degradation and MMP9 activation by Enterococcus faecalis contribute to intestinal anastomotic leak. Sci Transl Med. 2015 May 6;7(286):286ra68.

28. Lange MM, den Dulk M, Bossema ER, Maas CP, Peeters KCMJ, Rutten HJ, et al. Risk factors for faecal incontinence after rectal cancer treatment. Br J Surg. 2007 Oct;94(10):1278–84.

29. Tuson JR, Everett WG. A retrospective study of colostomies, leaks and strictures after colorectal anastomosis. Int J Colorectal Dis. 1990 Feb;5(1):44–8.

30. Kanellos D, Pramateftakis M-G, Demetriades H, Zacharakis E, Angelopoulos S, Mantzoros I, et al. Healing of colonic anastomoses after immediate postoperative intraperitoneal administration of oxaliplatin. Int J Colorectal Dis. 2008;23(12):1185–91.

31. Den Dulk M, Marijnen CAM, Collette L. Multicentre analysis of oncological and survival outcomes following anastomotic leakage after rectal cancer surgery. Dis Colon Rectum. 2010;53(4):508–9.

32. Gould L, Abadir P, Brem H, Carter M, Conner-Kerr T, Davidson J, et al. Chronic wound repair and healing in older adults: Current status and future research. J Am Geriatr Soc. 2015;63(3):427–38.

33. Dissemond J, Augustin M, Eming SA, Goerge T, Horn T, Karrer S, et al. Modern wound care – practical aspects of non-interventional topical treatment of patients with chronic wounds. JDDG J Dtsch Dermatol Ges. 2014 Jul 1;12(7):541–54.

34. Dreifke MB, Jayasuriya AA, Jayasuriya AC. Current wound healing procedures and potential care. Mater Sci Eng C. 2015 Mar 1;48:651–62.

35. Katz MH, Alvarez AF, Kirsner RS, Eaglstein WH, Falanga V. Human wound fluid from acute wounds stimulates fibroblast and endothelial cell growth. J Am Acad Dermatol. 1991;25(6 I):1054–8.

36. Thamm OC, Koenen P, Bader N, Schneider A, Wutzler S, Neugebauer EA, et al. Acute and chronic wound fluids influence keratinocyte function differently. Int Wound J. 2015;12(2):143–9.

37. Harding KG, Moore K, Phillips TJ. Wound chronicity and fibroblast senescence--implications for treatment. Int Wound J. 2005 Dec;2(4):364–8.

38. Lobmann R, Ambrosch A, Schultz G, Waldmann K, Schiweck S, Lehnert H. Expression of matrix-metalloproteinases and their inhibitors in the wounds of diabetic and non-diabetic patients. Diabetologia. 2002;45(7):1011–6.

39. Moor AN, Vachon DJ, Gould LJ. Proteolytic activity in wound fluids and tissues derived from chronic venous leg ulcers. Wound Repair Regen. 2009;17(6):832–9.

40. Trengove NJ, Stacey MC, MacAuley S, Bennett N, Gibson J, Burslem F, et al. Analysis of the acute and chronic wound environments: the role of proteases and their inhibitors. Wound Repair Regen Off Publ Wound Heal Soc Eur Tissue Repair Soc. 1999 Dec;7(6):442–52.

41. Bowler PG. Wound pathophysiology, infection and therapeutic options. Ann Med. 2002;34(6):419–27.

42. Impola U, Jeskanen L, Ravanti L, Syrjänen S, Baldursson B, Kähäri V-M, et al. Expression of matrix metalloproteinase (MMP)-7 and MMP-13 and loss of MMP-19 and p16 are associated with malignant progression in chronic wounds. Br J Dermatol. 2005 Apr;152(4):720–6.

43. Turner NJ, Badylak SF. The Use of Biologic Scaffolds in the Treatment of Chronic Nonhealing Wounds. Adv Wound Care. 2015 Aug 1;4(8):490–500.

44. James GA, Swogger E, Wolcott R, Pulcini E deLancey, Secor P, Sestrich J, et al. Biofilms in chronic wounds. Wound Repair Regen Off Publ Wound Heal Soc Eur Tissue Repair Soc. 2008 Feb;16(1):37–44.

45. Zhao G, Usui ML, Lippman SI, James GA, Stewart PS, Fleckman P, et al. Biofilms and Inflammation in Chronic Wounds. Adv Wound Care. 2013 Sep;2(7):389–99.

46. Høiby N, Ciofu O, Johansen HK, Song Z, Moser C, Jensen PØ, et al. The clinical impact of bacterial biofilms. Int J Oral Sci. 2011 Apr;3(2):55–65.

47. Hanke ML, Kielian T. Deciphering mechanisms of staphylococcal biofilm evasion of host immunity. Front Cell Infect Microbiol. 2012;2:62.

48. Schommer NN, Christner M, Hentschke M, Ruckdeschel K, Aepfelbacher M, Rohde H. Staphylococcus epidermidis uses distinct mechanisms of biofilm formation to interfere with phagocytosis and activation of mouse macrophage-like cells 774A.1. Infect Immun. 2011;79(6):2267–76.

49. Thurlow LR, Hanke ML, Fritz T, Angle A, Aldrich A, Williams SH, et al. Staphylococcus aureus biofilms prevent macrophage phagocytosis and attenuate inflammation in vivo. J Immunol. 2011;186(11):6585–96.

50. S Cosgrove, N Guyot, CM Greene, NG McElvaney. The Effects of Differential Protease Secretion by Pseudomonas aeruginosa under Aerobic and Anaerobic Conditions In Vitro. In: A50 CYSTIC FIBROSIS BASIC, CLINICAL AND TRANSLATIONAL STUDIES [Internet]. American Thoracic Society; 2009 [cited 2015 Oct 7]. p. A1772. (American Thoracic Society International Conference Abstracts). Available from: http://www.atsjournals.org/doi/abs/10.1164/ajrccm-conference.2009.179.1_MeetingAbstracts.A1772

51. Matsumoto K, Shams NBK, Hanninen LA, Kenyon KR. Proteolytic activation of corneal matrix metalloproteinase by pseudomonas aeruginosa elastase. Curr Eye Res. 1992;11(11):1105–9.

52. Zhao G, Hochwalt PC, Usui ML, Underwood RA, Singh PK, James GA, et al. Delayed wound healing in diabetic (db/db) mice with Pseudomonas aeruginosa biofilm challenge: a model for the study of chronic wounds. Wound Repair Regen Off Publ Wound Heal Soc Eur Tissue Repair Soc. 2010 Oct;18(5):467–77.

53. Boccola MA, Lin J, Rozen WM, Ho Y-H. Reducing anastomotic leakage in oncologic colorectal surgery: An evidence-based review. Anticancer Res. 2010;30(2):601–7.

54. Ulrich AB, Seiler C, Rahbari N, Weitz J, Büchler MW. Diverting stoma after low anterior resection: more arguments in favor. Dis Colon Rectum. 2009 Mar;52(3):412–8.

55. Daams F, Luyer M, Lange JF. Colorectal anastomotic leakage: Aspects of prevention, detection and treatment. World J Gastroenterol WJG. 2013 Apr 21;19(15):2293–7.

56. Hyman N, Manchester TL, Osler T, Burns B, Cataldo PA. Anastomotic Leaks After Intestinal Anastomosis. Ann Surg. 2007 Feb;245(2):254–8.

57. Girard E, Messager M, Sauvanet A, Benoist S, Piessen G, Mabrut J-Y, et al. Anastomotic leakage after gastrointestinal surgery: Diagnosis and management. J Visc Surg. 2014 Dec;151(6):441–50.

58. Ho Y-H, Ashour MAT. Techniques for colorectal anastomosis. World J Gastroenterol. 2010;16(13):1610–21.

59. Pommergaard H-C, Achiam MP, Rosenberg J. External coating of colonic anastomoses: A systematic review. Int J Colorectal Dis. 2012;27(10):1247–58.

60. Lawall H. Treatment of chronic wounds. VASA Z Für Gefässkrankh. 2012 Nov;41(6):396–409.

61. Werdin F, Tenenhaus M, Rennekampff H-O. Chronic wound care. The Lancet. 2008 Dec 5;372(9653):1860–2.

62. Falanga V. The chronic wound: impaired healing and solutions in the context of wound bed preparation. Blood Cells Mol Dis. 2004 Feb;32(1):88–94.

63. Nič M, Jirát J, Košata B, Jenkins A, McNaught A, editors. IUPAC Compendium of Chemical Terminology: Gold Book [Internet]. 2.1.0 ed. Research Triagle Park, NC: IUPAC; 2009 [cited 2015 Oct 20]. Available from: http://goldbook.iupac.org

64. Yadav P, Yadav H, Shah VG, Shah G, Dhaka G. Biomedical biopolymers, their origin and evolution in biomedical sciences: A systematic review. J Clin Diagn Res. 2015;9(9):21–5.

65. Yao F, Eriksson E. Gene therapy in wound repair and regeneration. Wound Repair Regen. 2000 Nov 1;8(6):443–51.

66. Ma C, Hernandez MA, Kirkpatrick VE, Liang L-J, Nouvong AL, Gordon IL. Topical platelet-derived growth factor vs placebo therapy of diabetic foot ulcers offloaded with windowed casts: A randomized, controlled trial. Wounds. 2015;27(4):83–91.

67. Tsang MW, Wong WKR, Hung CS, Lai K-M, Tang W, Cheung EYN, et al. Human epidermal growth factor enhances healing of diabetic foot ulcers. Diabetes Care. 2003;26(6):1856–61.

68. Toro A, Mannino M, Reale G, Di Carlo I. TachoSil use in abdominal surgery: a review. J Blood Med. 2011 Mar 14;2:31–6.

69. Scognamiglio F, Travan A, Rustighi I, Tarchi P, Palmisano S, Marsich E, et al. Adhesive and sealant interfaces for general surgery applications. J Biomed Mater Res B Appl Biomater. 2015 Apr 17;

70. Mohite BV, Patil SV. A novel biomaterial: bacterial cellulose and its new era applications. Biotechnol Appl Biochem. 2014 Apr;61(2):101–10.

71. Gacesa P. Bacterial alginate biosynthesis - recent progress and future prospects. Microbiology. 1998;144(5):1133–43.

72. Remminghorst U, Rehm BHA. Bacterial alginates: from biosynthesis to applications. Biotechnol Lett. 2006 Nov;28(21):1701–12.

73. Smidsrød O. Molecular basis for some physical properties of alginates in the gel state. Faraday Discuss Chem Soc. 1974 Jan 1;57(0):263–74.

74. Bidarra SJ, Barrias CC, Granja PL. Injectable alginate hydrogels for cell delivery in tissue engineering. Acta Biomater. 2014 Apr;10(4):1646–62.

75. Grasdalen H. High-field, 1H-n.m.r. spectroscopy of alginate: sequential structure and linkage conformations. Carbohydr Res. 1983;118(C):255–60.

76. Skjåk-Bræk G, Donati I, Paoletti S. Alginate Hydrogels: Properties and Applications. In: Matricardi P, Alhaique F, Coviello T, editors. Polysaccharide hydrogels. Pan Stanford Publishing. 2016. p. 449–89.

77. Donati I, Holtan S, Mørch YA, Borgogna M, Dentini M, Skjåk-Braek G. New hypothesis on the role of alternating sequences in calcium-alginate gels. Biomacromolecules. 2005 Apr;6(2):1031–40.

78. Augst AD, Kong HJ, Mooney DJ. Alginate Hydrogels as Biomaterials. Macromol Biosci. 2006 Aug 7;6(8):623–33.

79. Gundogdu E, Yurdasiper A. Drug transport mechanism of oral antidiabetic nanomedicines. Int J Endocrinol Metab. 2014 Jan;12(1):e8984.

80. Jain D, Bar-Shalom D. Alginate drug delivery systems: application in context of pharmaceutical and biomedical research. Drug Dev Ind Pharm. 2014 Dec;40(12):1576–84.

81. Venkatesan J, Nithya R, Sudha PN, Kim S-K. Role of alginate in bone tissue engineering. Adv Food Nutr Res. 2014;73:45–57.

82. European Wound Management Association (EWMA). Pain at wound dressing changes. London: MEP Ltd; 2002.

83. Meyer K, Palmer JW. The Polysaccharide of the Vitreous Humor. J Biol Chem. 1934 Jan 12;107(3):629–34.

84. Lee JY, Spicer AP. Hyaluronan: a multifunctional, megaDalton, stealth molecule. Curr Opin Cell Biol. 2000 Oct 1;12(5):581–6.

85. Chen L, Guo S, Ranzer MJ, DiPietro LA. Toll-like receptor 4 has an essential role in early skin wound healing. J Invest Dermatol. 2013 Jan;133(1):258–67.

86. Kaya G, Rodriguez I, Jorcano JL, Vassalli P, Stamenkovic I. Selective suppression of CD44 in keratinocytes of mice bearing an antisense CD44 transgene driven by a tissue-specific promoter disrupts hyaluronate metabolism in the skin and impairs keratinocyte proliferation. Genes Dev. 1997 Apr 15;11(8):996–1007.

87. Tolg C, Hamilton SR, Nakrieko K-A, Kooshesh F, Walton P, McCarthy JB, et al. Rhamm-/- fibroblasts are defective in CD44-mediated ERK1,2 motogenic signaling, leading to defective skin wound repair. J Cell Biol. 2006 Dec 18;175(6):1017–28.

88. Gaffney J, Matou-Nasri S, Grau-Olivares M, Slevin M. Therapeutic applications of hyaluronan. Mol Biosyst. 2010 Feb 17;6(3):437–43.

89. Coradini D, Pellizzaro C, Abolafio G, Bosco M, Scarlata I, Cantoni S, et al. Hyaluronic-acid butyric esters as promising antineoplastic agents in human lung carcinoma: A preclinical study. Invest New Drugs. 2004;22(3):207–17.

90. Pellizzaro C, Speranza A, Zorzet S, Crucil I, Sava G, Scarlata I, et al. Inhibition of human pancreatic cell line MIA PaCa2 proliferation by HA-but, a hyaluronic butyric ester: A preliminary report. Pancreas. 2008;36(4):e15–23.

91. Daniel P, Brazier M, Cerutti I, Pieri F, Tardivel I, Desmet G, et al. Pharmacokinetic study of butyric acid administered in vivo as sodium and arginine butyrate salts. Clin Chim Acta Int J Clin Chem. 1989 May 31;181(3):255–63.

92. Miller AA, Kurschel E, Osieka R, Schmidt CG. Clinical pharmacology of sodium butyrate in patients with acute leukemia. Eur J Cancer Clin Oncol. 1987 Sep;23(9):1283–7.

93. Hamer HM, Jonkers D, Venema K, Vanhoutvin S, Troost FJ, Brummer R-J. Review article: the role of butyrate on colonic function. Aliment Pharmacol Ther. 2008 Jan 15;27(2):104–19.

94. Encarnação JC, Abrantes AM, Pires AS, Botelho MF. Revisit dietary fiber on colorectal cancer: butyrate and its role on prevention and treatment. Cancer Metastasis Rev. 2015;34(3):465–78.

95. Vander Heiden MG, Cantley LC, Thompson CB. Understanding the Warburg Effect: The Metabolic Requirements of Cell Proliferation. Science. 2009 May 22;324(5930):1029–33.

96. Canani RB, Costanzo MD, Leone L, Pedata M, Meli R, Calignano A. Potential beneficial effects of butyrate in intestinal and extraintestinal diseases. World J Gastroenterol. 2011;17(12):1519–28.

97. Sossai P. Butyric acid: what is the future for this old substance? Swiss Med Wkly. 2012;142:w13596.

98. Kim S-K. Chitin and Chitosan Derivatives: Advances in Drug Discovery and Developments. CRC Press. 2013. 527 p.

99. Cheung RCF, Ng TB, Wong JH, Chan WY. Chitosan: An update on potential biomedical and pharmaceutical applications. Mar Drugs. 2015;13(8):5156–86.

100. Azuma K, Izumi R, Osaki T, Ifuku S, Morimoto M, Saimoto H, et al. Chitin, Chitosan, and Its Derivatives for Wound Healing: Old and New Materials. J Funct Biomater. 2015 Mar 13;6(1):104–42.

101. Alves NM, Mano JF. Chitosan derivatives obtained by chemical modifications for biomedical and environmental applications. Int J Biol Macromol. 2008 Dec;43(5):401–14.

102. Kubota N, Tatsumoto N, Sano T, Toya K. A simple preparation of half N-acetylated chitosan highly soluble in water and aqueous organic solvents. Carbohydr Res. 2000 Mar 10;324(4):268–74.

103. Yang T-C, Chou C-C, Li C-F. Antibacterial activity of N-alkylated disaccharide chitosan derivatives. Int J Food Microbiol. 2005 Jan 1;97(3):237–45.

104. Muzzarelli RA, Tanfani F, Emanuelli M, Pace DP, Chiurazzi E, Piani M. Sulfated N-(carboxymethyl)chitosans: novel blood anticoagulants. Carbohydr Res. 1984 Mar 15;126(2):225–31.

105. Spinelli VA, Laranjeira MCM, Fávere VT. Preparation and characterization of quaternary chitosan salt: adsorption equilibrium of chromium(VI) ion. React Funct Polym. 2004 Nov;61(3):347–52.

106. Yalpani M, Hall LD. Some chemical and analytical aspects of polysaccharide modifications. 3. Formation of branched-chain, soluble chitosan derivatives. Macromolecules. 1984;17(3):272–81.

107. Donati I, Stredanska S, Silvestrini G, Vetere A, Marcon P, Marsich E, et al. The aggregation of pig articular chondrocyte and synthesis of extracellular matrix by a lactose-modified chitosan. Biomaterials. 2005;26(9):987–98.

108. Donati I, Borgogna M, Turello E, Cesàro A, Paoletti S. Tuning Supramolecular Structuring at the Nanoscale Level: Nonstoichiometric Soluble Complexes in Dilute Mixed Solutions of Alginate and Lactose-Modified Chitosan (Chitlac). Biomacromolecules. 2007 May 1;8(5):1471–9.

109. Donati I, Haug IJ, Scarpa T, Borgogna M, Draget KI, Skjåk-Braek G, et al. Synergistic effects in semidilute mixed solutions of alginate and lactose-modified chitosan (chitlac). Biomacromolecules. 2007 Mar;8(3):957–62.

110. Marsich E, Borgogna M, Donati I, Mozetic P, Strand BL, Salvador SG, et al. Alginate/lactose-modified chitosan hydrogels: a bioactive biomaterial for chondrocyte encapsulation. J Biomed Mater Res A. 2008 Feb;84(2):364–76.

111. Cummings RD, Liu F-T. Galectins. In: Varki A, Cummings RD, Esko JD, Freeze HH, Stanley P, Bertozzi CR, et al., editors. Essentials of Glycobiology [Internet]. 2nd ed. Cold Spring Harbor (NY): Cold Spring Harbor Laboratory Press; 2009 [cited 2016 Feb 10]. Available from: http://www.ncbi.nlm.nih.gov/books/NBK1944/

112. Marcon P, Marsich E, Vetere A, Mozetic P, Campa C, Donati I, et al. The role of Galectin-1 in the interaction between chondrocytes and a lactose-modified chitosan. Biomaterials. 2005 Aug;26(24):4975–84.

113. Travan A, Marsich E, Donati I, Foulc M-P, Moritz N, Aro HT, et al. Polysaccharide-coated thermosets for orthopedic applications: from material characterization to in vivo tests. Biomacromolecules. 2012 May 14;13(5):1564–72.

114. Bowler PG, Duerden BI, Armstrong DG. Wound microbiology and associated approaches to wound management. Clin Microbiol Rev. 2001;14(2):244–69.

115. Owens CD, Stoessel K. Surgical site infections: epidemiology, microbiology and prevention. J Hosp Infect. 2008 Nov;70, Supplement 2:3–10.

116. Cohen ML. Changing patterns of infectious disease. Nature. 2000 Aug 17;406(6797):762–7.

117. Ranotkar S, Kumar P, Zutshi S, Prashanth KS, Bezbaruah B, Anand J, et al. Vancomycin-resistant enterococci: Troublemaker of the 21st century. J Glob Antimicrob Resist. 2014;2(4):205–12.

118. Rice LB. The clinical consequences of antimicrobial resistance. Curr Opin Microbiol. 2009 Oct;12(5):476–81.

119. Roe D, Karandikar B, Bonn-Savage N, Gibbins B, Roullet J-B. Antimicrobial surface functionalization of plastic catheters by silver nanoparticles. J Antimicrob Chemother. 2008 Jan 4;61(4):869–76.

120. Huh AJ, Kwon YJ. "Nanoantibiotics": A new paradigm for treating infectious diseases using nanomaterials in the antibiotics resistant era. J Controlled Release. 2011;156(2):128–45.

121. Kalhapure RS, Suleman N, Mocktar C, Seedat N, Govender T. Nanoengineered drug delivery systems for enhancing antibiotic therapy. J Pharm Sci. 2015;104(3):872–905.

122. Espinosa-Cristóbal LF, Martínez-Castañón GA, Martínez-Martínez RE, Loyola-Rodríguez JP, N. Patiño-Marín, Reyes-Macías JF, et al. Antibacterial effect of silver nanoparticles against Streptococcus mutans. Mater Lett. 2009;63(29):2603–6.

123. Pal S, Tak YK, Song JM. Does the antibacterial activity of silver nanoparticles depend on the shape of the nanoparticle? A study of the gram-negative bacterium Escherichia coli. Appl Environ Microbiol. 2007;73(6):1712–20.

124. Zhong W. Efficacy and toxicity of antibacterial agents used in wound dressings. Cutan Ocul Toxicol. 2015;34(1):61–7.

125. Marsich E, Bellomo F, Turco G, Travan A, Donati I, Paoletti S. Nano-composite scaffolds for bone tissue engineering containing silver nanoparticles: preparation, characterization and biological properties. J Mater Sci Mater Med. 2013 Jul;24(7):1799–807.

126. Nganga S, Travan A, Marsich E, Donati I, Söderling E, Moritz N, et al. In vitro antimicrobial properties of silver-polysaccharide coatings on porous fiber-reinforced composites for bone implants. J Mater Sci Mater Med. 2013 Dec;24(12):2775–85.

127. Sacco P, Travan A, Borgogna M, Paoletti S, Marsich E. Silver-containing antimicrobial membrane based on chitosan-TPP hydrogel for the treatment of wounds. J Mater Sci Mater Med. 2015 Mar;26(3):128.

128. Travan A, Marsich E, Donati I, Benincasa M, Giazzon M, Felisari L, et al. Silver-polysaccharide nanocomposite antimicrobial coatings for methacrylic thermosets. Acta Biomater. 2011;7(1):337–46.

129. Kokubo T, Kushitani H, Sakka S, Kitsugi T, Yamamuro T. Solutions able to reproduce in vivo surface-structure changes in bioactive glass-ceramic A-W3. J Biomed Mater Res. 1990 Jun 1;24(6):721–34.

130. Donati I, Feresini M, Travan A, Marsich E, Lapasin R, Paoletti S. Polysaccharide-based polyanion--polycation--polyanion ternary systems. A preliminary analysis of interpolyelectrolyte interactions in dilute solutions. Biomacromolecules. 2011 Nov 14;12(11):4044–56.

131. Geremia I, Borgogna M, Travan A, Marsich E, Paoletti S, Donati I. Determination of the composition for binary mixtures of polyanions: the case of mixed solutions of alginate and hyaluronan. Biomacromolecules. 2014 Mar 10;15(3):1069–73.

132. Barbosa I, Garcia S, Barbier-Chassefière V, Caruelle J-P, Martelly I, Papy-García D. Improved and simple micro assay for sulfated glycosaminoglycans quantification in biological extracts and its use in skin and muscle tissue studies. Glycobiology. 2003 Sep;13(9):647–53.

133. Liang C-C, Park AY, Guan J-L. In vitro scratch assay: a convenient and inexpensive method for analysis of cell migration in vitro. Nat Protoc. 2007 Feb;2(2):329–33.

134. Wolfe KL, Liu RH. Cellular Antioxidant Activity (CAA) Assay for Assessing Antioxidants, Foods, and Dietary Supplements. J Agric Food Chem. 2007 Oct 1;55(22):8896–907.

135. Yaku K, Enami Y, Kurajyo C, Matsui-Yuasa I, Konishi Y, Kojima-Yuasa A. The enhancement of phase 2 enzyme activities by sodium butyrate in normal intestinal epithelial cells is associated with Nrf2 and p53. Mol Cell Biochem. 2012 Nov;370(1-2):7–14.

136. Travan A, Fiorentino S, Grassi M, Borgogna M, Marsich E, Paoletti S, et al. Rheology of mixed alginate-hyaluronan aqueous solutions. Int J Biol Macromol. 2015 Jul;78:363–9.

137. Travan A, Scognamiglio F, Borgogna M, Marsich E, Donati I, Tarusha L, et al. Hyaluronan delivery by polymer demixing in polysaccharide-based hydrogels and membranes for biomedical applications. Carbohydrate Polymers.

138. Jang J, Seol Y-J, Kim HJ, Kundu J, Kim SW, Cho D-W. Effects of alginate hydrogel cross-linking density on mechanical and biological behaviors for tissue engineering. J Mech Behav Biomed Mater. 2014;37:69–77.

139. Coda A, Lamberti R, Martorana S. Classification of prosthetics used in hernia repair based on weight and biomaterial. Hernia. 2012;16(1):9–20.

140. Lindenhayn K, Perka C, Spitzer R, Heilmann H, Pommerening K, Mennicke J, et al. Retention of hyaluronic acid in alginate beads: aspects for in vitro cartilage engineering. J Biomed Mater Res. 1999 Feb;44(2):149–55.

141. Donati I, Gamini A, Skjåk-Braek G, Vetere A, Campa C, Coslovi A, et al. Determination of the diadic composition of alginate by means of circular dichroism: a fast and accurate improved method. Carbohydr Res. 2003 May 1;338(10):1139–42.

142. Kuo CK, Ma PX. Ionically crosslinked alginate hydrogels as scaffolds for tissue engineering: Part 1. Structure, gelation rate and mechanical properties. Biomaterials. 2001;22(6):511–21.

143. Kuo CK, Ma PX. Maintaining dimensions and mechanical properties of ionically crosslinked alginate hydrogel scaffolds in vitro. J Biomed Mater Res A. 2008 Mar 15;84(4):899–907.

144. Sikorski P, Mo F, Skjåk-Braek G, Stokke BT. Evidence for egg-box-compatible interactions in calcium-alginate gels from fiber X-ray diffraction. Biomacromolecules. 2007 Jul;8(7):2098–103.

145. Dame MK, Jiang Y, Appelman HD, Copley KD, McClintock SD, Aslam MN, et al. Human colonic crypts in culture: Segregation of immunochemical markers in normal versus adenoma-derived. Lab Invest. 2014;94(2):222–34.

146. Pedersen G. Development, validation and implementation of an in vitro model for the study of metabolic and immune function in normal and inflamed human colonic epithelium. Dan Med J. 2015;62(1):B4973.

147. Pedersen G, Saermark T, Giese B, Hansen A, Drag B, Brynskov J. A simple method to establish short-term cultures of normal human colonic epithelial cells from endoscopic biopsy specimens: Comparison of isolation methods, assessment of viability and metabolic activity. Scand J Gastroenterol. 2000;35(7):772–80.

148. Stauffer JS, Manzano LA, Balch GC, Merriman RL, Tanzer LR, Moyer MP, et al. Development and characterization of normal colonic epithelial cell lines derived from normal mucosa of patients with colon cancer. Am J Surg. 1995;169(2):190–6.

149. Tolg C, Telmer P, Turley E. Specific Sizes of Hyaluronan Oligosaccharides Stimulate Fibroblast Migration and Excisional Wound Repair. PLoS ONE [Internet]. 2014 Feb 13 [cited 2015 Feb 19];9(2). Available from: http://www.ncbi.nlm.nih.gov/pmc/articles/PMC3923781/

150. Zhu R, Wang S-C, Sun C, Tao Y, Piao H-L, Wang X-Q, et al. Hyaluronan-CD44 Interaction Promotes Growth of Decidual Stromal Cells in Human First-Trimester Pregnancy. PLoS ONE [Internet]. 2013 Sep 19 [cited 2015 Feb 20];8(9). Available from: http://www.ncbi.nlm.nih.gov/pmc/articles/PMC3777984/

151. West DC, Shaw DM, Lorenz P, Adzick NS, Longaker MT. Fibrotic healing of adult and late gestation fetal wounds correlates with increased hyaluronidase activity and removal of hyaluronan. Int J Biochem Cell Biol. 1997 Jan;29(1):201–10.

152. Fung KYC, Cosgrove L, Lockett T, Head R, Topping DL. A review of the potential mechanisms for the lowering of colorectal oncogenesis by butyrate. Br J Nutr. 2012 Sep;108(5):820–31.

153. Tailor D, Hahm E-R, Kale RK, Singh SV, Singh RP. Sodium butyrate induces DRP1-mediated mitochondrial fusion and apoptosis in human colorectal cancer cells. Mitochondrion. 2014 May;16:55–64.

154. Xiao M, Liu YG, Zou MC, Zou F. Sodium butyrate induces apoptosis of human colon cancer cells by modulating ERK and sphingosine kinase 2. Biomed Environ Sci BES. 2014 Mar;27(3):197–203.

155. Topping DL, Clifton PM. Short-Chain Fatty Acids and Human Colonic Function: Roles of Resistant Starch and Nonstarch Polysaccharides. Physiol Rev. 2001 Jul 1;81(3):1031–64.

156. Archer S, Meng S, Wu J, Johnson J, Tang R, Hodin R. Butyrate inhibits colon carcinoma cell growth through two distinct pathways. Surgery. 1998 Aug;124(2):248–53.

157. Chopin V, Toillon R-A, Jouy N, Le Bourhis X. P21(WAF1/CIP1) is dispensable for G1 arrest, but indispensable for apoptosis induced by sodium butyrate in MCF-7 breast cancer cells. Oncogene. 2004 Jan 8;23(1):21–9.

158. Hu S, Dong TS, Dalal SR, Wu F, Bissonnette M, Kwon JH, et al. The microbe-derived short chain fatty acid butyrate targets miRNA-dependent p21 gene expression in human colon cancer. PloS One. 2011;6(1):e16221.

159. Jiang W, Guo Q, Wu J, Guo B, Wang Y, Zhao S, et al. Dual effects of sodium butyrate on hepatocellular carcinoma cells. Mol Biol Rep. 2012 May;39(5):6235–42.

160. Karna E, Trojan S, Pałka JA. The mechanism of butyrate-induced collagen biosynthesis in cultured fibroblasts. Acta Pol Pharm. 2009 Jun;66(3):229–33.

161. Hinz B. Formation and Function of the Myofibroblast during Tissue Repair. J Invest Dermatol. 2007;127(3):526–37.

162. David-Raoudi M, Tranchepain F, Deschrevel B, Vincent J-C, Bogdanowicz P, Boumediene K, et al. Differential effects of hyaluronan and its fragments on fibroblasts: relation to wound healing. Wound Repair Regen Off Publ Wound Heal Soc Eur Tissue Repair Soc. 2008 Apr;16(2):274–87.

163. Franz MG, Steed DL, Robson MC. Optimizing Healing of the Acute Wound by Minimizing Complications. Curr Probl Surg. 2007 Nov;44(11):691–763.

164. Longaker MT, Whitby DJ, Adzick NS, Crombleholme TM, Langer JC, Duncan BW, et al. Studies in fetal wound healing, VI. Second and early third trimester fetal wounds demonstrate rapid collagen deposition without scar formation. J Pediatr Surg. 1990 Jan;25(1):63–8; discussion 68–9.

165. Croce MA, Dyne K, Boraldi F, Quaglino Jr D, Cetta G, Tiozzo R, et al. Hyaluronan affects protein and collagen synthesis by in vitro human skin fibroblasts. Tissue Cell. 2001 Aug;33(4):326–31.

166. Liu J, Wang F, Luo H, Liu A, Li K, Li C, et al. Protective effect of butyrate against ethanol-induced gastric ulcers in mice by promoting the anti-inflammatory, anti-oxidant and mucosal defense mechanisms. Int Immunopharmacol. 2016;30:179–87.

167. Marambio-Jones C, Hoek EMV. A review of the antibacterial effects of silver nanomaterials and potential implications for human health and the environment. J Nanoparticle Res. 2010;12(5):1531–51.

168. Johnston HJ, Hutchison G, Christensen FM, Peters S, Hankin S, Stone V. A review of the in vivo and in vitro toxicity of silver and gold particulates: particle attributes and biological mechanisms responsible for the observed toxicity. Crit Rev Toxicol. 2010 Apr;40(4):328–46.

169. Andersen T, Melvik JE, Gåserød O, Alsberg E, Christensen BE. Ionically gelled alginate foams: physical properties controlled by operational and macromolecular parameters. Biomacromolecules. 2012 Nov 12;13(11):3703–10.

170. Chen X, Schluesener HJ. Nanosilver: A nanoproduct in medical application. Toxicol Lett. 2008 Jan 4;176(1):1–12.

171. Ge L, Li Q, Wang M, Ouyang J, Li X, Xing MMQ. Nanosilver particles in medical applications: synthesis, performance, and toxicity. Int J Nanomedicine. 2014;9:2399–407.

172. Arora S, Jain J, Rajwade JM, Paknikar KM. Interactions of silver nanoparticles with primary mouse fibroblasts and liver cells. Toxicol Appl Pharmacol. 2009 May 1;236(3):310–8.

173. Hussain SM, Hess KL, Gearhart JM, Geiss KT, Schlager JJ. In vitro toxicity of nanoparticles in BRL 3A rat liver cells. Toxicol Vitro Int J Publ Assoc BIBRA. 2005 Oct;19(7):975–83.

174. Prabhu S, Poulose EK. Silver nanoparticles: mechanism of antimicrobial action, synthesis, medical applications, and toxicity effects. Int Nano Lett. 2012 Oct 29;2(1):32.

175. Travan A, Donati I, Marsich E, Bellomo F, Achanta S, Toppazzini M, et al. Surface modification and polysaccharide deposition on BisGMA/TEGDMA thermoset. Biomacromolecules. 2010 Mar 8;11(3):583–92.

176. Rayment EA, Upton Z, Shooter GK. Increased matrix metalloproteinase-9 (MMP-9) activity observed in chronic wound fluid is related to the clinical severity of the ulcer. Br J Dermatol. 2008 May;158(5):951–61.

177. Wysocki AB, Staiano-Coico L, Grinnell F. Wound fluid from chronic leg ulcers contains elevated levels of metalloproteinases MMP-2 and MMP-9. J Invest Dermatol. 1993;101(1):64–8.

178. Kim M-M, Kim S-K. Chitooligosaccharides inhibit activation and expression of matrix metalloproteinase-2 in human dermal fibroblasts. FEBS Lett. 2006 May 15;580(11):2661–6.

179. Walker M, Bowler PG, Cochrane CA. In vitro studies to show sequestration of matrix metalloproteinases by silver-containing wound care products. Ostomy Wound Manage. 2007 Sep;53(9):18–25.

180. HINMAN CD, MAIBACH H. Effect of Air Exposure and Occlusion on Experimental Human Skin Wounds. Nature. 1963 Oct 26;200(4904):377–8.

181. Ito Y, Correll K, Schiel JA, Finigan JH, Prekeris R, Mason RJ. Lung fibroblasts accelerate wound closure in human alveolar epithelial cells through hepatocyte growth factor/c-Met signaling. Am J Physiol Lung Cell Mol Physiol. 2014 Jul 1;307(1):L94–105.

182. Nunan R, Harding KG, Martin P. Clinical challenges of chronic wounds: searching for an optimal animal model to recapitulate their complexity. Dis Model Mech. 2014 Nov;7(11):1205–13.